FREE SPACE CHARGE DOMINATED INSTABILITIES AND RESONANCES IN SYNCHROTRONS

By

Michael A. Balcewicz

A DISSERTATION

Submitted to
Michigan State University
in partial fulfillment of the requirements
for the degree of

2023

ABSTRACT

FREE SPACE CHARGE DOMINATED INSTABILITIES AND RESONANCES IN SYNCHROTRONS

By

Michael A. Balcewicz

A Multiple Loop Square Well Model has been developed to simulate coherent motion in synchrotron machines, while including space charge and wakefields. The model builds upon previous single-well work by Blaskiewicz[?] and Burov[?] to allow the approximation of arbitrary potentials via the superposition of multiple square wells. Model predictions and experimental confirmation are discussed. In particular the convective instability is simulated and compared with experimental results showing good agreement between the two.

Please note that figures are still in work. References and Bibliography still need to be provided.

TABLE OF CONTENTS

0.1 Preface

The main body of this dissertation is divided into five chapters, with some additional material contained in Appendices. This dissertation discusses the development of a Multiple Loop Square Well (MLSW) model to simulate beam stability in high intensity synchrotron machines including synchro-betatron coupling, as well as model predictions and experimental confirmation.

Chapter 1 is primarily concerned with establishing the background for subsequent sections. This will act as the minimum baseline to understand collective effects and beam instabilities, including sideband generation, coherent space charge tune shift, and wakefields. This chapter concludes with a brief survey of coherent instabilities and modeling efforts.

Chapter 2 contains the detailed mathematical derivation of the Multiple Loop Square Well model, although some of the more tedious portions of the derivation were relegated to Appendix **??** to improve readability and flow. This model is a description of bunch evolution in the presence of significant space charge tune shift and is a generalization of previous work by Blaskiewicz [**?**] and Burov [**?**]. This model generalizes the longitudinal dynamics as an arbitrary system of square potential wells, generating new physical results. The final sections of the chapter describe the implementation of the MLSW model in a C++ code with python wrapper.

Chapter 3 focuses on the predictions of this model, beginning with demonstrating that this new MLSW matches the well established results from the limiting case of Blaskiewicz's Square Well Model. From there, we move on to study the implications of more complex longitudinal dynamics, such as approximating arbitrary particle distributions, nonlinear chromaticity, along with the convective instability[**?**] and coupled bunch modes over extended

time periods.

Chapter 4 is focused on an experimental study of mode coupling instabilities at the Fermilab Recycler to confirm aspects of the MLSW model. Initial work was concentrated on studying existing data sets from the Waker experiment which uses a kicker to artificially simulate wakeforces. This culminated in a dedicated February 2023 experiment where the convective instability was observed using the Waker.

In Chapter 5 we end with a study of Periodic Resonances in the AGS. These resonances are driven by synchro-betatron coupling at significant space charge tune shifts and are therefore complementary to the main body of work.

Chapter 1

Collective Effects and Instabilities

Particle accelerators have gone through many generations of evolution in the past century, growing from small tabletop experiments to larger Van de Graaff machines and cyclotrons, and so on to modern day linear accelerators, Free Electron Lasers, and kilometer scale synchrotrons. The applications of these accelerators have expanded from pure physics to other applications including materials and biology research from light-sources to medical isotopes and treatment. Over time, the accelerators have evolved to higher and higher energies and intensities.

Conventional non-wakefield acceleration is limited by breakdown. If electric fields are too strong, small imperfections and residual gas will cause an arc between high and low potentials and reduce the electric field. This makes it less economical to build a high energy accelerator out of a linear set of voltage gaps once the single particle energy becomes too high. A more efficient new circular geometry must be adopted. In such an accelerator particles will pass the same magnets and the same cavities over and over making it possible to get a much higher final energy than achievable with a linear configuration. The cavity fields sinusoidal, operating at an harmonic of the time it takes a particle to complete one revolution. Therefore particles will be accelerated each and every turn. The sinusoidal form of the cavity fields also provide longitudinal confinement of the bunch, as particles along the length of the bunch will observe slightly different fields, the proper choice of which will give

linear focusing for a small offset from the central synchronous particle.

Higher intensity is needed to provide good statistics as the number of events observed scales linearly with beam intensity. While high intensity is needed, the beam quality must also be considered, to ensure the particles are where you actually want them, as quantified by figures of merit like luminosity and bightness. There are several ways to increase intensity, but there are essentially two options: increase the number of bunches, or put more particles within each bunch. It is possible to transport the same number of bunches as the harmonic number of the accelerating cavity, but this may not be practical due to tight timing constraints and interactions between the nearby bunches. Each particle bunch interacts with the accelerating structures it passes, generating wakefields which may interfere with the propagation of multiple bunches. These interactions will decay over time, but additional bunches too soon after the initial bunch can create a feedback loop and disrupt transport. Wakefields will be discussed in more detail in section ??

Adding more particles to a single bunch will increase the free space charge of the bunch. Like any charged particle distribution it will generate fields which will interact with other particles in the field. Since all particles within the bunch have the same charge, the coulomb forces are defocusing, and without external fields from the accelerator will lead to loss. The interaction of the space charge and wakefields generated by the bunch itself also creates feedback within the bunch, making it possible to drive particle loss–known as collective instability–inside the bunch.

It could be said that the final fate of a synchrotron is to become the injector for a next generation accelerator. Because of this, old machines will often have to transport a higher current than they were designed for. This can mean that assumptions break down and new sources of loss can be introduced. A thorough understanding of collective instabilities is

necessary to adjust these old accelerators, as well as to design new higher current machines.

1.1 Frame of Reference and Coordinates

1.1.1 Accelerator 'Tune' and 'Time Like' Coordinates

A particle going through any lattice with optics will oscillate in the transverse planes. This is known as betatron oscillation. We can think of this as a phase advance that increases along the optics. For a regular structure that will be traversed repeatedly, the total phase advance will be the sum of the individual phase advances. A synchrotron is a good example of a regular structure (the phase advance can change over the ramp, but this is slow). The total number of oscillations in a revolution around a synchrotron is known as the tune. There is a tune for each transverse direction Q_x, Q_y as well as the longitudinal direction Q_s.

A bunch in a synchrotron stays centered around the synchronous particle with small position and velocity offsets from it. Since synchrotrons are relativistic, the velocity of the synchonous particle is nearly constant. This means that there is a direct correspondence between the position of the central particle s, the azimuthal angle around the synchrotron θ and time t. The relation between these for a synchrotron with circumference C is:

$$\beta ct = s = C\theta \tag{1.1}$$

This will lead to some artifacts depending on which time like variable is used. For example, dx/ds is often used instead of dx/dt as a transverse velocity. In this work, all three of these time like variables (t, s, θ) will be used.

1.1.2   The Beam Frame of Reference

The normal coordinate system for accelerators is known as the Ferret Serret[**?**] coordinate system. The coordinate system is defined with a travelling and rotating origin following the reference orbit of a synchronous particle. By defining the system this way, we essentially make a transformation to the bunch's frame of reference. The time like vector along the bunch is $\vec{s} = \beta c t \hat{z}$. Small position offsets in the direction of motion are a displacement z from this synchronous particle. The z dimension is often known as the longitudinal or synchrotron direction.

The other spatial dimensions x and y are known as the transverse or betatron directions. $\hat{x}$ is in the radial direction for a rotating synchronous particle. That is, for a synchronous particle undergoing rotation about an axis in the $\hat{y}$ direction passing through point $\vec{p}(s)$, $\hat{x}$ is oriented in the direction of the vector from the center of rotation to the origin of the synchronous particle. Synchrotrons are circular machines and therefore the direction of motion of the origin must undergo some rotation to be periodic. Technically this rotation can be arbitrary as long as it is periodic over one circumference, but generally rotations are constrained to a single plane. In straight sections of the synchrotron the Ferret Serret vectors for $\hat{x}$ and $\hat{y}$ are multiply defined, but this can be fixed by treating the straight section as having an infinitesimal curvature in the direction of one's choice.

1.1.3   Small Phase Advance Optics

To maintain bunch shape and position in an accelerator, constraining forces must are applied. In order to simplify construction and to enable focusing in both trasnverse planes, focusing is split into discrete elements along the accelerator. Transverse (betatron) focusing is provided
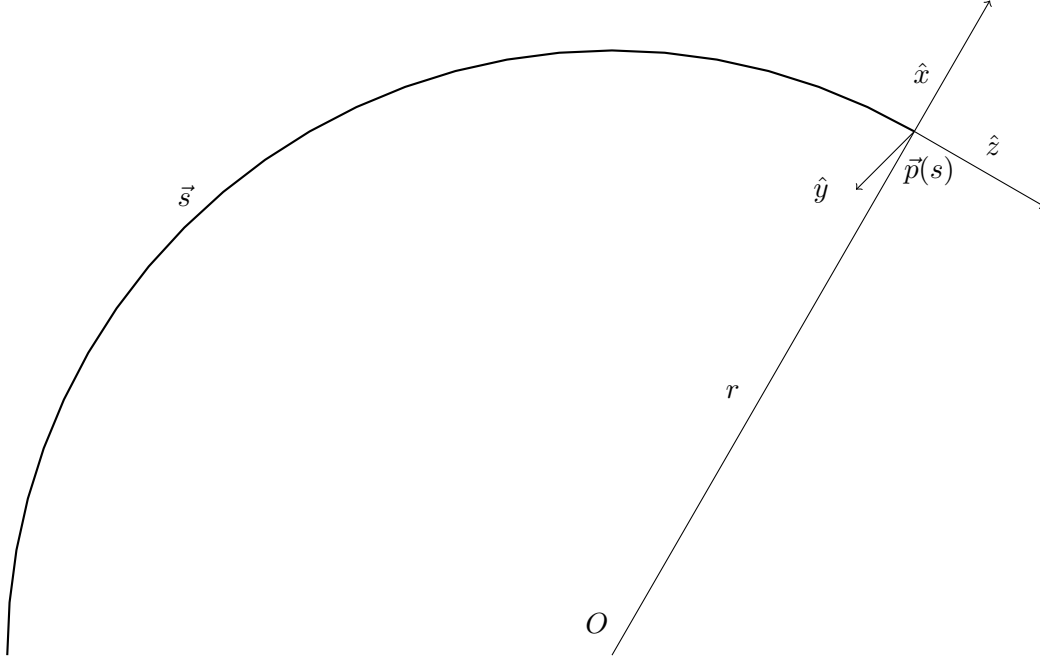
Figure 1.1: Diagram of the Frenet-Serret coordinate system.

by magnetic and electrostatic elements that are slowly varied with beam energy. Longitudinal (synchrotron) focusing and acceleration are generally performed by RF cavities.

Longitudinal focusing tends to be much slower than transverse due to several factors. Longitudinal focusing occurs with net acceleration from RF potential gaps. Since the bunch is moving relativistically in the longitudinal direction, kicks provided by RF are comparatively small compared to the transverse dimensions perpendicular to the relativistic motion.

Since accelerator elements are separated into discrete along s we can define the focusing strength along the accelerator as a focusing strength $K(s)$ which varies as it passes individual elements giving Hill's Equation:

$$x'' + K(s)y = 0 \tag{1.2}$$

This for elements with a constant value K within them, the solution can be represented as a

$\hat{x}$

| 1/2 Focusing Quad | Drift | Defocusing Quad | Drift | 1/2 Focusing Quad |
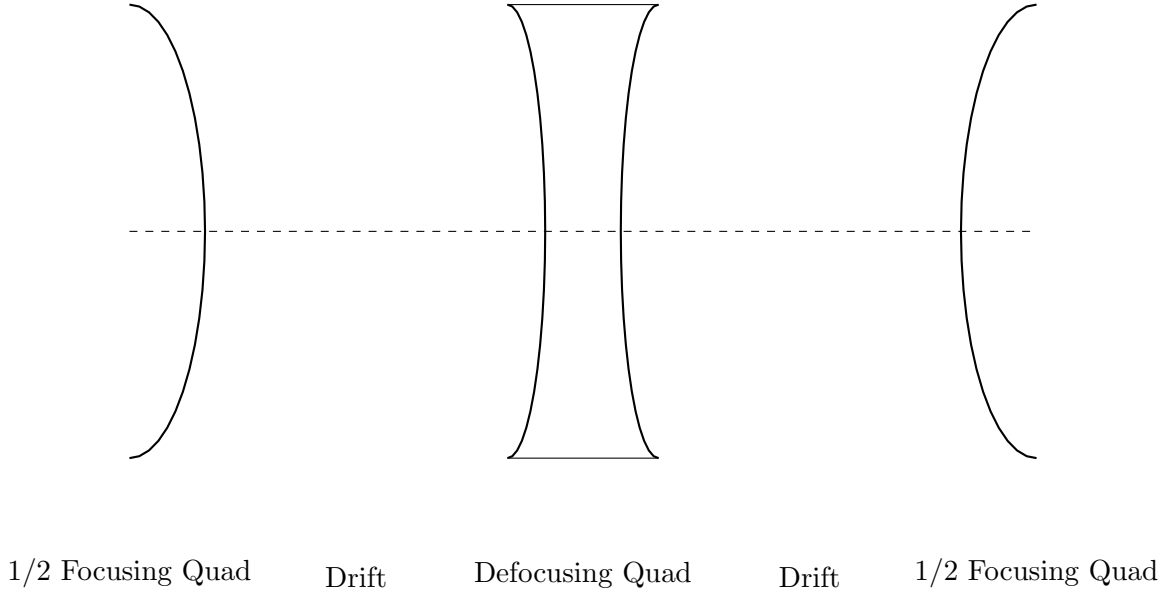
Figure 1.2: Diagram of a FODO cell. For symmetry the focusing quad is split into two half elements.

transfer matrix evaluated at the edge of the bunch and making beam transport along a line of linear elements matrix multiplication. However, under certain conditions Hill's Equation and the corresponding Matrices simplify down to simple harmonic motion.

Let us consider with a FODO (Focusing Drift Defocusing Drift) cell of length ℓ and focal length f in both transverse directions. This transfer matrix has the form:

$$\begin{pmatrix} x \\ x' \end{pmatrix}_{s+\ell} = \begin{pmatrix} 1 - \frac{\ell^2}{8f^2} & \ell(1 + \frac{\ell}{4f}) \\ -\frac{\ell}{4f^2}(1 - \frac{\ell}{4f}) & 1 - \frac{\ell^2}{8f^2} \end{pmatrix} \begin{pmatrix} x \\ x' \end{pmatrix}_s$$

The transfer matrix M_{FODO} can be thought of as a solution to a differential equation at $s+\ell$ given certain initial conditions at s. Assuming the cell is small, we take the differential to get the differential equations of motion.

$$\frac{d}{ds}\begin{pmatrix} x \\ x' \end{pmatrix}_s \approx \frac{\Delta}{\Delta s}\begin{pmatrix} x \\ x' \end{pmatrix}_s = \frac{1}{\ell}(M_{FODO} - I)\begin{pmatrix} x \\ x' \end{pmatrix}_s$$

These matrices correspond to equations of motion:

$$x' = -x\frac{\ell}{8f^2} + x'(1 + \frac{\ell}{4f}) \tag{1.3}$$

$$x'' = -x\frac{1}{4f}(1 - \frac{\ell}{4f}) - x'\frac{\ell}{8f^2} \tag{1.4}$$

Both ℓ and $1/f$ are small and can be ignored at $O(\ell^2)$, $O(\ell f^{-1})$, $O(f^{-2})$, and above.

$$x' = x' + O(2) \tag{1.5}$$

$$x'' = -x\frac{1}{4f}(1 - \frac{l}{4f}) + O(3) \tag{1.6}$$

Which is just the harmonic oscillator in spatial units. The conversion to time yields a harmonic oscillator with $\omega = \frac{\beta c}{2\sqrt{f}}\sqrt{1 - \frac{l}{4f}}$.

If a particle is not moving at the design velocity, there is a slight correction to the single particle tune due to the longitudinal momentum offset. This is normally defined in terms of $\delta \equiv \Delta p/p$, but our choice of canonical variable $\dot{z}$ works as well. Chromaticity is defined in the following way: $\frac{\Delta Q_x}{\Delta \dot{z}} = \xi(\dot{z})$.

1.2 Sideband Modes

In the simplest case, an oscillator can be thought of as an object experiencing a 'spring like' force, oscillating at a rate which is dependent on the force and object itself. The addition of another spring force orthogonal to the original force generates coherent frequencies offset by multiples of the second oscillator's frequency.

In a charged particle bunch, the particles themselves are a system of coupled (and possibly nonlinear) oscillators. For a synchrotron, the bunch is constrained in all three spatial dimensions so we should expect to observe sidebands due to coupling between these modes. This is not the only source of sidebands, as even a single spatial dimension can have multiple orthogonal modes with corresponding sidebands.

With the multiplicity of different modes describing the bunch, it may seem difficult to fully analyze them all. Thankfully, this is not necessary. Each sideband mode is orthogonal to one another so it becomes possible to decompose the bunch into these modes and limit our view to those which are the most physically interesting.

1.2.1 Betatron Distribution Sidebands

Phase space modes of a beam have effective frequencies contingent on the rotational symmetry of the mode. An arbitrary one dimensional distribution is comprised of a sum of these modes. The zero mode, also known as the equilibrium distribution[**?**], is the fundamental and has a zero frequency corresponding to a distribution that does not vary in time. Higher order modes have sidebands given by their mode number m. Consider a phase space ρ that

can be expressed in terms of action angle coordinates (J, φ) along with mode number.

$$\rho(J, \varphi) = R(J)cos(m\varphi) = \frac{R(J)}{2}(e^{im\varphi} + e^{-im\varphi}) \tag{1.7}$$

Where $R(J)$ is a function of action. For a harmonic oscillator $\dot{\varphi}$ (the frequency) is a constant, leading to a constant phase advance along the bunch. In this case the motion has two interfering oscillatory components, the forward and backward propagating elements. These two frequencies for each mode m are considered sidebands. In the transverse direction these are known as betatron sidebands, and in the longitudinal direction synchrotron sidebands. Sidebands are generally symmetrically offset around a fundamental frequency.

A similar argument can be made using a one turn map. The initial phase space distribution has an equivalent definition as Eq. 1.7. The phase advance does not need to be constant over the entire lattice period, only that the map M, defined as $M^n\vec{q}_0 = \vec{q}_n$ must be linear. For the mth mode the system will oscillate with a constant phase advance for every application of the map. This map has the same oscillatory properties where it is comprised of both a positive and negative rotating term.

Experimentally it is necessary to constrain our solutions to positive frequencies as oscilloscopes and analyzers only provide positive frequencies[?]. Only positive frequencies are necessary to describe the system due to the properties of complex numbers. For mth sideband with a coherent frequency ΔQ which is observed, the pickup signal has the form:

$$Ae^{-2\pi ni(mQ-\Delta Q)} = A^*e^{2\pi ni(mQ-\Delta Q)} \tag{1.8}$$

making it possible to reflect negative sidebands across the origin. Each sideband mode will

have a different contribution to the total motion of the bunch. For dipole instabilities, the upper sideband $+1Q$ is often considered to be the dominant term in a possible instability. To make the upper sideband physically relevant without its conjugate, modifciations may be necessary.

1.2.2 Synchro-Betatron Sideband Generation

Synchrotrons are circular accelerators where the beam propagates through the same elements many times. Multiple transverse focusing elements are needed to generate a net focusing effect on the bunch in both directions with many oscillations per revolution. The large number of betatron oscillations along with superperiodicity are necessary (but not sufficient) for stability from space charge effects. There are fewer longitudinal cavities which are located near to one another, and so multiple turns are needed to complete a synchorotron oscillation. Thus it can safely be assumed that $Q_x > 1 > Q_s$; $Q_x >> Q_s$.

Every individual particle will oscillate with their own amplitude and phase, but with a well defined wave velocity which is quite interestingly the synchrotron tune Q_s where $Q_s = \Delta\varphi_s/\Delta\theta$. θ corresponds to the angle around the accelerator which is a time coordinate; φ_s is the synchrotron phase along the bunch which is a spatial coordinate. For simplicity, let us assume that the phase advance per element along the accelerator is small and consistent enough to be well approximated by a linear oscillator. Effectively this means that individual particles and waves propagate around the bunch at a rate related to the synchrotron tune.

This system consists of simple uncoupled oscillators, but variations in the spatial distribution of the particle ensemble can be decomposed into orthogonal terms in Fourier space coupling them together and generating sidebands.

Collective effects and chromaticity have explicit longitudinal dependence which shift the

sideband modes generated by the variations in particle distribution. This explicit synchro-beta coupling is naturally expressed in terms of conjugate variables z and $\dot{z}$ rather than with phase terms φ_s and J_s, complicating the solutions. The difficulty of including coupling with sidebands is one of the main driving forces for approximate PDE methods such as the Square Well Model [?]. The exact PDE treatment is given in Chapter ??

Coupling between variations in the ensemble can be seen in the first order moment $\overline{x}$ of the transverse dimension:

$$\overline{x}(\theta, \psi_s) = \cos(Q_x\theta) \sum_{n=0}^{\infty} A_n \cos(n(Q_s\theta - \varphi_s)) \tag{1.9}$$

The transverse moment of a bunch varies along the synchrotron phase with the variations represented by the Fourier series. Variations can come from many sources including Schottky noise[?]. Each Fourier term is trapped in the same potential, so while they have different spatial content, they all travel along the bunch at the same rate and undergo a full oscillation in $1/Q_s$ revolutions. Individual Fourier modes can be restated as synchrotron sidebands using angle addition.

$$x_n(\theta, \psi_s) = A_n cos(Q_x\theta)cos(n(Q_s\theta - \varphi_s)) \tag{1.10}$$

$$= \frac{A_n}{2}[cos(Q_x\theta + n(Q_s\theta - \varphi_s)) + cos(Q_x\theta - n(Q_s\theta - \varphi_s))] \tag{1.11}$$

This makes the total bunch motion the sum of all modes $\overline{x}$

$$\overline{x}(\theta, \psi_s) = \sum_{n=0}^{\infty} = \frac{A_n}{2}[cos(Q_x\theta + n(Q_s\theta - \varphi_s)) + cos(Q_x\theta - n(Q_s\theta - \varphi_s))] \tag{1.12}$$

It is expected that lower n modes will tend to have larger Fourier components varying

bunch by bunch. It is sufficient to only study sideband modes near to the fundamental in most cases. Wakes with sufficiently rapid oscillation frequencies compared to the bunch may drive higher order components.

Although the system has been approximated as harmonic oscillators, nonlinearity can be understood qualitatively. If the nonlinearity is sufficiently small, it can be treated by splitting the bunch into multiple ensembles with each detuned slightly. Nonlinearity in the transverse dimension (red lines in fig. **??**) will spread out all the tunes but preserve the spacing between them. Linear synchro-betatron coupling shifts the sidebands, while coupling synchrotron tune adds tune spread that increases for higher n sidebands (blue lines in fig. **??**).

So far, bunches have only been looked at in terms of coupling from the longitudinal dimension to the transverse. This tends to be dominant because the action of the longitudinal direction is much larger than that of the transverse plane. Although the inverse is possible, where betatron motion couples to create sidebands in synchrotron oscillations, such coupling can be neglected. Since $Q_x >> Q_s$ this will produce sidebands that are essentially nonphysical. This can be visualized as follows: synchro-betatron coupling creates small changes in frequency due to small and slow oscillations coupling into a betatron dimension, wearas in the converse, the frequency change due to a rapid oscillation will average out over the synchrotron oscillation.

1.2.3 Head Tail Phase

So far we have limited the scope of our discussions to coupling due to the shape of the synchrotron bunch distribution, but chromatic effects cannot be ignored. Small variations in longitudinal momentum (δ) or velocity ($\dot{z}$) cause particles to spend differing amounts of

.png

Figure 1.3: Diagram of sideband modes.

time in accelerator elements effectively detuning them from the synchronous tune. For linear chormaticity, particles are over-focused for one half of the synchrotron period and under-focused in the other. This leads to an overall mismatch in phase φ_β over the half synchrotron period. and ξ is the chromaticity.

$$\varphi_\beta = \int \xi \dot{z} d\psi_s \tag{1.13}$$

Where ξ is the linearized chromaticity in term of $\dot{z}$. Although over a complete synchrotron period the betatron phase difference resolves itself, there is a phase shift from the front to the back of the bunch. This is known as the head tail phase shift χ. For a linear chromaticity one obtains a total head tail phase shift of:

$$\chi = \xi \int_0^\pi sin(\varphi_s) d\varphi_s \tag{1.14}$$

This phase difference can be treated as a wave that accumulates and fades away along the synchrotron oscillation.

1.3 Free Space Charge

1.3.1 Fields From Moments

For the general case, analytic solutions for particle motion with self fields only exist for specific pathologic distributions[?]. Rather than limit ourselves to these distributions (many of which have been studied extensively[?]) or simply simulate the problem (which can be noise dominated in certain regimes) we will look at how to approximate this space charge

effect.

Space charge derives from the total effect of all particles in the beam distribution. Imagine a distribution of charged particles f comprising a bunch. The electric field will be a convolution of the electric field of an infantesimal charge and the distribution itself. The field can then be calculated at an arbitrary point, and be Taylor expanded to a specific order (unlike that of a single particle, which cannot be Taylor expanded due to its singular nature). This field can then be separated into linear and nonlinear components. For a sufficiently small excursion about the center of the expansion, linear components remain the dominant contribution to the field.

A particle in this linear regime will observe a springlike defocusing force proportional to its displacement. Over a small time period, it may be adequate to treat this as an external force but this becomes less accurate as the distribution deforms.

Another similar but more preferred approach is to express the forces in terms of basis functions of the distribution rather than Taylor expanding them after the fact. In this case, the basis functions of the expansion may cross couple to one another. However, due to the peaked nature of the distribution, only limited orders of the Taylor expansion are necessary.

1.3.2 Coherent Tune Shift

To begin with, let us consider the linear order space charge force. As noted earlier, this is a linear force which acts with a spring like force centered around the center of momentum, and will have the same effect on the moments of bunch distribution as well. Since these forces correspond to basis functions of the distribution itself, the bunch distribution will oscillate with a space charge contribution shifting the frequency.

Because the space charge effect varies along the distribution, the average space charge

detuning for particles at two specific sets of initial conditions are not necessarily the same. But as coherent space charge is a linear force on particles in the bunch, one might naively assume that coherent mode is purely a function of $\lambda(z)$ the linear charge density ($\Delta Q_x = \sqrt{Q_x^2 - C_{sc}\lambda(z)} - Q_x$). While this can be approximately correct in certain cases, it is not actually true in general, especially when sidebands are included.

Consider a particle with position x only experiencing constant linear focusing and a coherent space charge force proportional to the displacement from the center of the bunch $x - \overline{x}$.

$$\ddot{x} = -Q_x^2 x + C_{sc}(x - \overline{x}) \tag{1.15}$$

Since all particles within the bunch oscillate linearly one expects that motion of a single particle and the total bunch moment are interrelated. As a result, there is no longer a constant offset or a simple driving harmonic. It will average out to an effective tune shift over a complete synchrotron period. The exact interrelation between these modes will depend upon the sidebands of the system[?].

1.3.3 Incoherent Tune Spread

The problem fundamentally changes when nonlinearity is no longer neglected. Nonlinearity can come from either the bare lattice optics or the Taylor expanded nonlinear portion of the space charge forces. The space charge force assumes a basis set of distributions that shift and evolve along the distribution with the distribution itself shifting along the bunch.

A central difference for the nonlinear motion is due to amplitude dependent tune (frequency) shifts. This means that particles no longer oscillate in phase with one another.

Therefore, rather than a single coherent tune shift, the tunes spread out into an incoherent continuum of transverse frequencies. This is not necessarily a bad thing, as incoherent tune spread over the driving frequency is central for Landau damping. This will mostly be beyond the scope of this thesis but will be touched on briefly in chapter 3.

1.3.4   Coherent Mode Splitting

When examining a bunch distribution, it is important to understand the continuity and boundary conditions of the system. Let us consider an infinitesimally thin 'loop' of current in longitudinal phase space. This airbag of current has a synchrotron period and exhibits transverse waves along the length of the bunch that corresponds to synchro-betatron sidebands. Each wave must be continuous over the longitudinal extent of the bunch and has a characteristic frequency associated with its sideband.

Any arbitrary longitudinal phase space distribution can be treated as an infinite collection of infinitesimal loops of current each of which can interact through space charge and other collective forces and must simultaneously satisfy their own boundary conditions. These loops provide sufficient degrees of freedom in frequency domain for multiple valid tunes to exist that satisfy all the boundary conditions for a given sideband mode. The valid tunes originate from the same sideband before splitting off from one another.

These split modes can intermittently couple to other modes and become degenerate. Such degenerate modes correspond to imaginary frequencies (growth and decay modes) and are lightly unstable examples of the collective instability which will be covered in more detail later in this work.

Functionally it can be difficult to split a sideband into coherent modes. Such interactions between loops of current can be difficult to drive, setting a functional limit on how many

coherent modes can be identified. An example of coherent mode splitting for the MLSW model is shown in Fig. 1.4 and can also be found in [**?**]

1.4 Transverse Collective Instabilities

The combination of single particle and collective effects are nontrivial. It is not sufficient to model these collective forces as simple focusing elements.

Interactions between particles and the environment can make the beam catastrophically unstable, with significant particle loss following. There are many avenues for loss with their own characteristic dynamics and a functional 'threshold' where the beam transfers between a stable and unstable state. Knowing the physics behind a given instability makes it possible to find a regime where the beam is stable.

Most collective instabilities have strong intensity dependence. The justification to this is that one expects to regain stable motion if the bunch intensity is decreased sufficiently, given that single particle motion is stable.

1.4.1 Head Tail Instability

In the presence of wakefields head-tail phase can drive beam instability. Over many periods the head tail phase shift and the wakes that drive it give rise to comparatively slow growth over time. This growth however is difficult to naturally damp.

1.4.2 Transverse Mode Coupling Instability

Although sometimes called the Fast Head Tail Instability[**?**], the Transverse Mode Coupling Instability (TMCI) has a separate instability mechanism from Head Tail Instability. Instead,

.png
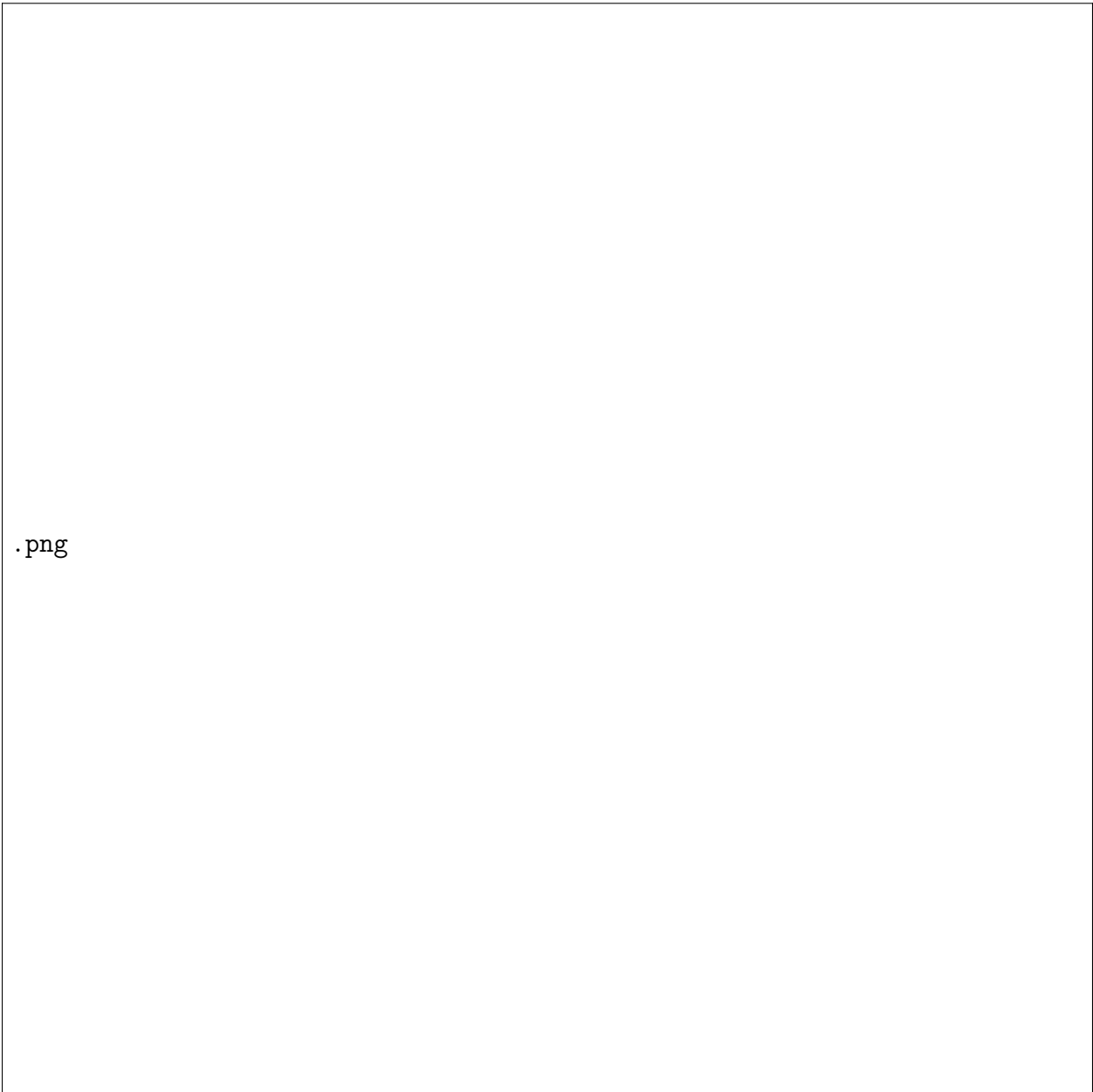
Figure 1.4

TMCI occurs when two synchrotron sideband modes are shifted together by wakes and become degenerate.

It can be unclear what this physically corresponds to, so a two macro particle description will be used to obtain a simplified model. This method is similar to that in [?], but has a few different assumptions. These macroparticles oscillate in transverse and longitudinal dimensions with transverse wakeforces generated by the head particle witnessed by the tail particle. Every half synchrotron period the macroparticles exchange positions and the head particle moves to the tail and vice versa. Instability will occur when the interchange between particles leads to sustained and uncontrollable growth in bunch (dipole) position.

Let us consider the following inhomogeneous harmonic oscillators along the synchrotron period. The integer n is the number of synchrotron oscillations, w is the wake strength and subscripts denote the macroparticle.

$$\ddot{x}_1 + Q_x^2 x_1 = \begin{cases} 0 & \text{for } 2\pi n < Q_s\theta < \pi(2n+1) \\ \\ wx_2 & \text{for } \pi(2n+1) < Q_s\theta < 2\pi(n+1) \end{cases} \tag{1.16}$$

$$\ddot{x}_2 + Q_x^2 x_2 = \begin{cases} wx_1 & \text{for } 2\pi n < Q_s\theta < \pi(2n+1) \\ \\ 0 & \text{for } \pi(2n+1) < Q_s\theta < 2\pi(n+1) \end{cases} \tag{1.17}$$

This can also be given as a set matrix of linear differential equations as of the form:

$$
\frac{d}{d\theta}
\begin{pmatrix} x_1 \\ \dot{x}_1 \\ x_2 \\ \dot{x}_2 \end{pmatrix}
=
\begin{pmatrix}
0 & 1 & 0 & 0 \\
-Q_x^2 & 0 & 0 & 0 \\
0 & 0 & 0 & 1 \\
w & 0 & -Q_x^2 & 0
\end{pmatrix}
\begin{pmatrix} x_1 \\ \dot{x}_1 \\ x_2 \\ \dot{x}_2 \end{pmatrix}
\Bigg|_{2\pi n < Q_s\theta < \pi(2n+1)}
\tag{1.18}
$$

$$
\frac{d}{d\theta}
\begin{pmatrix} x_1 \\ \dot{x}_1 \\ x_2 \\ \dot{x}_2 \end{pmatrix}
=
\begin{pmatrix}
0 & 1 & 0 & 0 \\
-Q_x^2 & 0 & w & 0 \\
0 & 0 & 0 & 1 \\
0 & 0 & -Q_x^2 & 0
\end{pmatrix}
\begin{pmatrix} x_1 \\ \dot{x}_1 \\ x_2 \\ \dot{x}_2 \end{pmatrix}
\Bigg|_{\pi(2n+1) < Q_s\theta < 2\pi(n+1)}
\tag{1.19}
$$

From here it is simple enough to simulate this two particle model in order to determine thresholds. But that is not particularly physically meaningful. Other methods are given in [?] and [?]. Let us consider two adjacent (one odd, one even) synchro-betatron modes along the bunch. The total motion of the two bunches can be redefined in terms of the even sum mode $x_+ = \frac{1}{2}(x_1 + x_2)$ and the odd difference mode $x_- = \frac{1}{2}(x_1 - x_2)$. Normally each mode in a bunch would be driven by small dipole moments along the length of the bunch where each mode is unique and separately driven. With only two particles only such sum and difference modes exist. Making a change of variables to sum and difference modes we obtain:

$$
\frac{d}{d\theta}
\begin{pmatrix} x_+ \\ \dot{x}_+ \\ x_- \\ \dot{x}_- \end{pmatrix}
=
\begin{pmatrix}
0 & 1 & 0 & 0 \\
-Q_x^2 + \frac{w}{2} & 0 & \frac{w}{2} & 0 \\
0 & 0 & 0 & 1 \\
-\frac{w}{2} & 0 & -Q_x^2 - \frac{w}{2} & 0
\end{pmatrix}
\begin{pmatrix} x_+ \\ \dot{x}_+ \\ x_- \\ \dot{x}_- \end{pmatrix}
\Bigg|_{2\pi n < Q_s\theta < \pi(2n+1)}
\tag{1.20}
$$

$$
\frac{d}{d\theta}
\begin{pmatrix} x_+ \\ \dot{x}_+ \\ x_- \\ \dot{x}_- \end{pmatrix}
=
\begin{pmatrix}
0 & 1 & 0 & 0 \\
-Q_x^2 + \frac{w}{2} & 0 & -\frac{w}{2} & 0 \\
0 & 0 & 0 & 1 \\
\frac{w}{2} & 0 & -Q_x^2 - \frac{w}{2} & 0
\end{pmatrix}
\begin{pmatrix} x_+ \\ \dot{x}_+ \\ x_- \\ \dot{x}_- \end{pmatrix}
\Bigg|_{\pi(2n+1) < Q_s\theta < 2\pi(n+1)}
\tag{1.21}
$$

With the change of variables, a few phenomena become obvious. The sum mode observes a defocusing wake in the first half period and a focusing mode in the second half period. This can be thought of as a physical explanation why beams are not necessarily unstable to TMCI even while the tail particle is unstable. Since this change is periodic in time, it is straightforward to combine the equations of motion for the entire domain.

$$
F(\theta) =
\begin{cases}
-\frac{w}{2} & \text{for } 2\pi n < Q_s\theta < \pi(2n+1) \\[2mm]
\frac{w}{2} & \text{for } \pi(2n+1) < Q_s\theta < 2\pi(n+1)
\end{cases}
\tag{1.22}
$$

The inhomogenous portion of the equation is periodic (with a period $2\pi/Q_s$) and can

therefore be treated as a sum of individual Fourier driving terms.

$$F(\theta) = \sum_{i=1}^{\infty} b_n sin(nQ_s\theta) \qquad (1.23)$$

$$
\begin{aligned}
b_n &= \frac{2Q_s}{2\pi} \int_0^{\frac{2\pi}{Q_s}} F(\theta)sin(nQ_s\theta)d\theta \\
&= \frac{wQ_s}{\pi} \left[\int_0^{\frac{\pi}{Q_s}} (-1/2)sin(nQ_s\theta)d\theta + \int_{\frac{\pi}{Q_s}}^{\frac{2\pi}{Q_s}} (1/2)sin(nQ_s\theta)d\theta \right] \\
&= \frac{w}{2n\pi} \left[cos(nQ_s\theta)|_0^{\frac{\pi}{Q_s}} - cos(nQ_s\theta)|_{\frac{\pi}{Q_s}}^{\frac{2\pi}{Q_s}} \right]
\end{aligned}
\qquad (1.24)
$$

$b_n = \frac{2w}{n\pi}$ for odd values of n and $b_n = 0$ for even n. The new basis is constructed of two symmetric coupled differential equations:

$$\ddot{x}_+ = (-Q_x^2 + \frac{w}{2})x_+ + \frac{2w}{\pi}x_- \sum_{i=1}^{\infty} \frac{sin((2n-1)Q_s\theta)}{(2n-1)} \qquad (1.25)$$

$$\ddot{x}_- = (-Q_x^2 - \frac{w}{2})x_- - \frac{2w}{\pi}x_+ \sum_{i=1}^{\infty} \frac{sin((2n-1)Q_s\theta)}{(2n-1)} \qquad (1.26)$$

Here we reach a conundrum. Although the equations have been simplified, a clean solution of the system is not obvious. Perturbative solutions are available, but do not exhibit a clear threshold due to the truncated solution. Two methods show promise: guessing a solution to the differential equation with synchrobetatron modes, or further simplifying the differential equations into a more tractable form. This second method is what we shall attempt.

The sum and difference differential equations are similar in form to one another save for two aspects. First, the wake drives a small frequency detuning from the transverse fre-

quency. The magnitude of this detuning is small compared to the total oscillation magnitude. Secondly, the coupling terms have the opposite sign of the wake force due to macroparticle interchange. Thus, if the detuning is vanishingly small the two equations will retain a constant phase difference and any growth will be slow compared to the speed of transverse oscillations. If a set of initial conditions can be chosen such that the $x_+ = -x_x$ this problem simplifies to the form:

$$\ddot{x}_+ = (-Q_x^2 + \frac{w}{2})x_+ - \frac{2w}{\pi}x_+ \sum_{n=1}^{\infty} \frac{sin((2n-1)Q_s\theta)}{(2n-1)} \tag{1.27}$$

$$\ddot{x}_- = (-Q_x^2 - \frac{w}{2})x_- + \frac{2w}{\pi}x_- \sum_{n=1}^{\infty} \frac{sin((2n-1)Q_s\theta)}{(2n-1)} \tag{1.28}$$

Both sums are of a similar form, with a small frequency offset that will eventually cause dephasing of the solution. We shall neglect this dephasing as it occurs slowly compared to the speed of instability growth.

The Fourier sum term is formed due to particle interchange of the two macroparticles. Under one half synchrotron period the sum mode is driven while in the other half period the difference mode is driven instead. In order to make this into a solvable form it becomes necessary to determine if any of the Fourier terms dominate. If so, it may be possible to neglect minor terms to arrive at a usable solution.

But is this actually the case? One may expect that harmonics will not drive instabilities as strongly as that of the fundamental tune. The exact form of such resonances are difficult to characterize as these harmonics are not independent. The higher order terms aren't suppressed either. The Fourier constants are of the form $b_n \approx 1/(2n-1)$, so higher order terms will have less of a contribution, but the scaling alone is divergent. Therefore, we cannot justify a simplification to only include a single frequency.

Instead of finding a justification for simplifying the system any further, we can find an analogous head tail system instead. Such a system must have an odd wake force and must be positive in the first half synchrotron period, and negative in the second half. The expression $sin(Q_s\theta)$ satisfies both criteria. The analogous form has the differential equation:

$$\ddot{x}_+ \approx -Q_x^2 x_+ - \frac{2w}{\pi} x_+ sin(Q_s\theta) \tag{1.29}$$

This differential equation is a statement of the Matteiu Equation[?], but it needs to be massaged slightly to obtain the correct final form. We make a change of variables from the azimuthal angle θ to τ to retrieve a conventional Mattieu form. Here we define $2\tau_s\theta$ where $\frac{d}{d\theta} = \frac{Q_s}{2}\frac{d}{d\tau}$.

$$\frac{d^2 x_+}{d\tau^2} + [a + 2q sin(2\tau)]x_+ \approx 0 \tag{1.30}$$
$$a = (\frac{2Q_x}{Q_s})^2; q = \frac{4w}{\pi Q_s^2}$$

This equation has a solution of form $[c_1 e^{i\mu\tau} - c_2 e^{-i\mu\tau}]\Phi(\tau)$ where Φ is a periodic function. If the characteristic exponent μ becomes complex the system is unstable making it possible to determine the TMCI threshold[?]. Calculating this threshold by hand is unnecessary as the characteristic exponent is included in many standard libraries[?]. The instability threshold of such a model is shown in Fig. ?? in terms of the wake strength w.

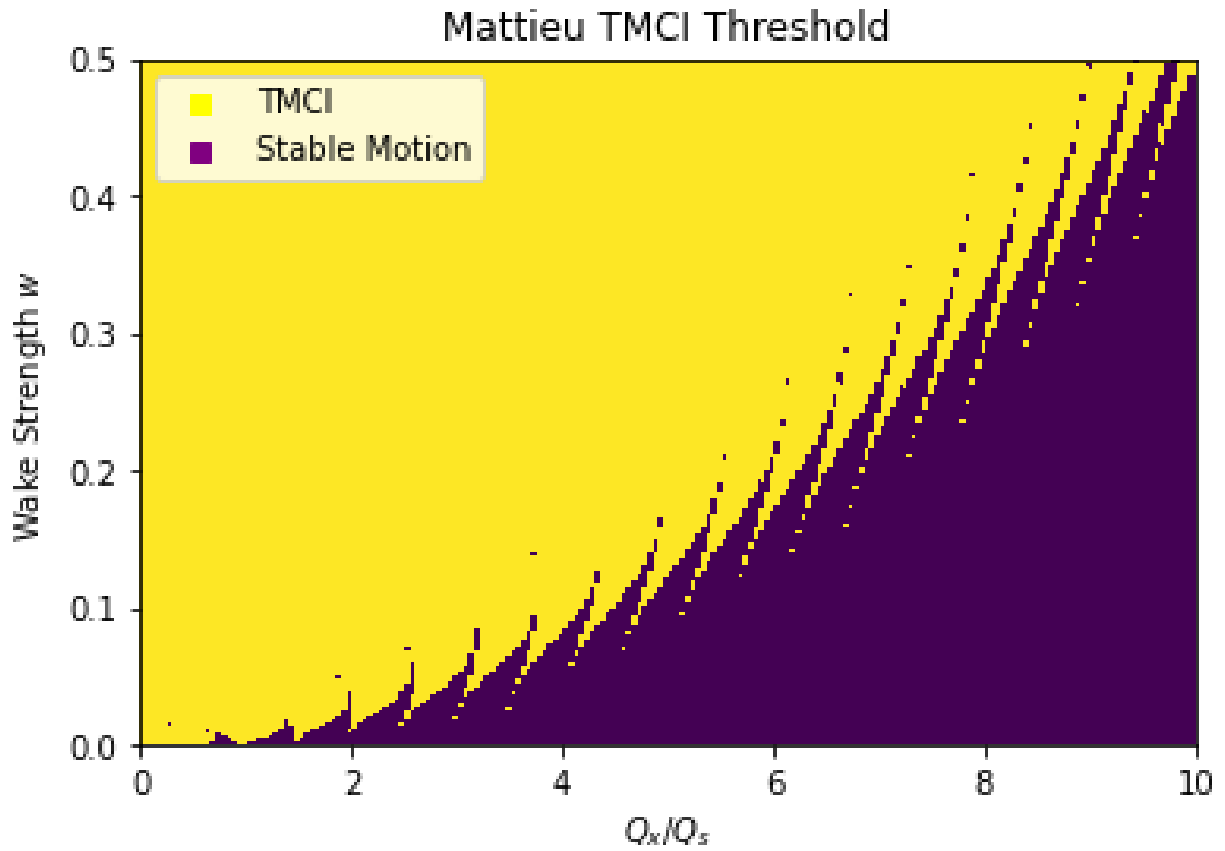Figure 1.5: TMCI threshold shown. The system becomes unstable when the characteristic exponent of the solution becomes complex. Note the distinctive parabolic form of TMCI threshold.

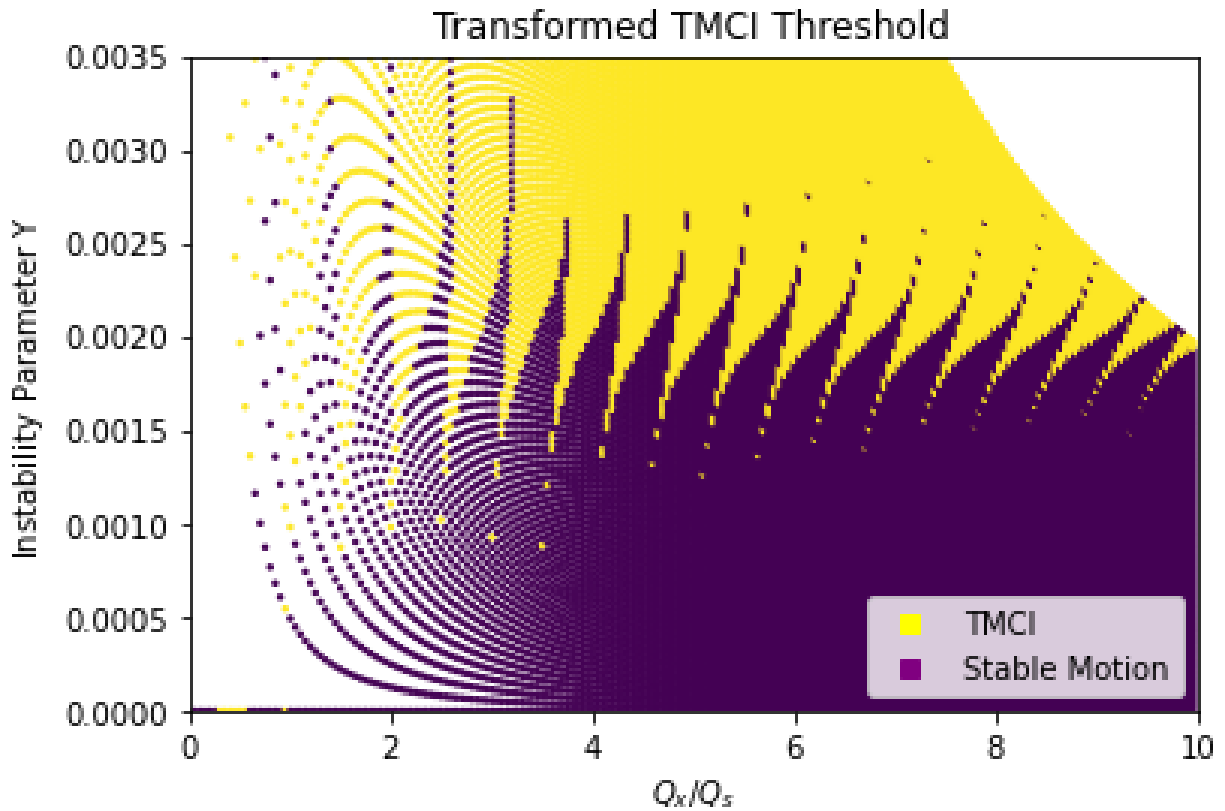Figure 1.6: TMCI threshold in terms of stability criterion Υ which becomes unstable above a certain value. This graph shows a similar form to that given in Dr. Chao's text[**?**], although the functional forms of the two are somewhat different.

1.4.3 TMCI Models

Perhaps the best known model for TMCI is the two particle model given in Dr. Chao's text on collective effects[**?**]. Unfortunately this model is not the most precise in a realistic case. To get quantitative results other models need to be applied.

Strong instabilities can be well modeled by Particle in Cell (PiC) codes with full collective effects from wakefields and space charge. These are attractive methods due to the their obvious applicability to real machines. However, PiC codes can have significant shot noise and are slow to run [**?**]. One can think of PiC codes as multidimensional numerical differential equations evolving in time with both single particle and ensemble effects. The smaller the timestep, the lower the error. This numerical error will accumulate to some degree over long runtimes, potentially muddying the results. As more particles are added, this becomes more computationally intensive. As particles propagate within the bunch, its space charge forces and wakes generated need to be correspondingly updated for correct collective motion.

Analytical models are another common method to understand TMCI. TMCI is not analytically solvable with both an arbitrary distribution and space charge so significant simplifications must be made to arrive at a solvable model. One of the largest difficulties in creating a solvable model are realistic collective effects. Although relatively simple models can generate necessary wake modes, transverse space charge is effectively 'pancaked' at highly relativistic velocities making its effects short ranged along the bunch length and very sensitive to distribution shape compared to low frequency wakefields.

Good examples of this are the Square Well Model (SWM)[**?**] and the Airbag Square Well (ABS) [**?**]. These models simplify the longitudinal dynamics to a continuum of current in a square potential well, the average motion of which can be solved as a system of linear ODEs.

Although solvable, the unrealistic phase space shape is a significant detriment, making it most useful for its qualitative dynamics.

A derivation of the SWM/ABS is given in chapter **??** as it gives strong physical intuition for TMCI and will act as the starting point for the main thrust of this work.

1.4.4 Space Charge and TMCI

The two particle approach gives insight into the onset and prevention of Mode coupling instabilities. Changing the ratio of coupling tunes and decreasing wake impedance are obvious solutions to move below instability threshold. A feedback system, an artificial wake designed to counteract natural wakes in the system is also a viable solution to such a problem.

Due to simplifications in the two particle model (specifically the fact that it is just a two particle model) space charge effects cannot be included in a well justified way. Other methods and models will have to be used to derive the functional form of space charge effects. With that said, a qualitative understanding can be arrived at without a space charge model.

As shown in the previous section, TMCI is driven by mode degeneracy. Two previously stable modes combine together into a new set of unstable tunes with long term growth in θ the time-like coordinate. Space charge slows the oscillation of the coherent motion shifting all the modes of the system. If this shift prevents modes from becoming degenerate, collective motion will not become unstable.

1.4.5 Circulant Matrix Models and BimBim

Later comparisons in sections **??** will compare results with the simulation code BimBim [**?**]. This is what is known as a Circulant Matrix Model (CMM). For CMM, longitudinal phase

space is decomposed into radial and azimuthal sections, with each section having a definite geometric size, shape, and density. Because these are directly sampled from the distribution, rather than constructed from macroparticles the system is not susceptible to Schottky noise, making it possible to attain relevant results with fewer model elements.

Each section of longitudinal phase space is assumed to evolve as a single quantity $x_{\rho,\phi}$ in transverse dimensions. These terms are projected onto the z axis before undergoing transport and collective forces between $x_{\rho,\phi}$s. Transport and collective effects of this form can be represented by a Circulant Matrix and are therefore solvable.

It should be noted that BimBim does not have fully self consistent space charge kicks. Instead, the space charge is a small correction on the bare lattice path of the beam. In cases where this correction is small (such as weak space charge or small step size) this is sufficient. Step size can be varied, but will lead to increased computation time.

1.4.6   Convective Instabilities without TMCI

If wakes continue to be increased but the system remains absolutely temporally stable[?] due to space charge forces the saturated solution will not grow in time. In such a case oscillation frequencies shift but do not grow or decay. Unfortunately, stability in time is not sufficient to prevent beam loss. Head-tail amplification–transverse beam growth along the length of the bunch–can cause the bunch to reach a maximum transverse displacement near the tail. If the maximum position is larger than the beam pipe, particles will hit the wall and be lost.

Head Tail amplification can be thought of as unstable growth along the bunch and is the genesis for the somewhat confusing name of the convective instability. The convective instability does not need to undergo 'convection', that is motion to short ranged kinetic interactions. The 'convective' in convective instability is actually due to an unstable term

$\dot{z}\frac{\partial}{\partial z}$ in the total derivative $\frac{d}{dt}$. This total derivative is sometimes known as the 'convective' derivative[?] leading to the name and the confusion.

Coherent space charge itself can effectively be thought of as a retarding/defocusing force, slowing the oscillation speed of coherent modes. Let us consider some wake driven by an initial transverse bunch offset. If the wake drives significant motion from the head to the tail of the bunch, the bunch is convective. Unlike true instabilities, convective motion does not have a threshold; as long as head-tail amplification is small enough and the beam pipe large enough, particles will not be lost.

Normally this class of instability is characterized using Burov's ABS model[?]. However other analytic models also reproduce convective behavior. An example of such a model is given below.

According to linear small phase advance optics bunches are constructed of multiple coherent modes, with a small wake that does not heavily impact the tune of the system. Each of these modes has the form $x_n(t) \propto cos((Q_x\omega_0 t + \Delta Q(\omega_0 t - \psi_s))$. There are potentially multiple coherent modes for each sideband, leading to a large set of valid tune shifts ΔQ_x. All particles flow cyclically around in synchrotron phase space, therefore there is a constant phase where $\Delta Q(\omega_0 t - \psi_s) = 0$. The phase contribution $\dot{z} = v_p(z)$ is the phase velocity of a wave of particles along the length of the bunch. Thus $\phi_s \equiv \int_0^z \frac{dz'}{vp(z')}$. The beginning differential equation has the following form:

$$[\frac{d^2}{dt^2} + (Q_x + \Delta Q_x)]x = F(t, z) + O(\epsilon) \tag{1.31}$$

$$F(t, z) = \int_0^z f(z - z')\lambda(z')x(t, z')dz'$$

Since $F(t, z)$ is small it would be tempting to consider it a perturbation and obtain a

solution for a short time scale. However this will only be valid over short times, and we are looking for a more general solution. In fact, we know that for small wakes the system remains stable and bounded (which is necessary for accelerators everywhere). Instead we will look at the spatial dependence of the system. The wake is the convolution of average particle position and the wake function $f(z - z')$. Because of the form of the wake, we can expect an oscillatory solution in time and phase with varying amplitude along the bunch length due to the wake forces. There are multiple other coherent frequencies which interact through their wake forces, but these are not expected to have a significant contribution due to poor coupling.

The wake force is a convolution of the wake function and the transverse moment $\lambda(z)x(t, z)$. We can then take the spatial derivative of Eq. 1.32 and obtain the following:

$$\frac{d}{dz}(\frac{d^2}{dt^2} + (Q_x + \Delta Q_x))x = \frac{d}{dz}\int_0^z f(z - z')\lambda(z')x(t, z')dz' \qquad (1.32)$$

$$(\frac{d^2}{dt^2} + (Q_x + \Delta Q_x))\frac{d}{dz}x = f(0)\lambda(z)x - f(z)\lambda(0)x(0)$$

We can see that the wake force will add a small detuning to the system $\frac{d^2}{dt^2} = -(Q_x + \Delta Q_x + \Delta Q_w)^2$. With this in mind we guess a solution to the differential equation.

$$x(t, z) = b(z)cos(Q_x\omega_0 t + (\Delta Q_x + \Delta Q_w)(\omega_0 t - \int_0^z \frac{dz'}{v_p(z')}))$$

$$\frac{dx}{dz} = b'(z)cos(Q_x\omega_0 t + (\Delta Q_x + \Delta Q_w)(\omega_0 t - \int_0^z \frac{dz'}{v_p(z')})) \,(1.33)$$

$$+b(z)(\Delta Q_x + \Delta Q_w)(\frac{1}{v_p(z)} - \frac{1}{v_p(0)})sin(Q_x\omega_0 t + (\Delta Q_x + \Delta Q_w)(\omega_0 t - \int_0^z \frac{dz'}{v_p(z')}))$$

If we assume that the phase velocity is approximately constant, then $v_p(z), \lambda(z), f(z)$ are constant. This simplifies the system a bit. Including the approximation and substituting

34

into the differential equation yields:

$$f(0)\lambda(z)x(z) - f(z)\lambda(0)x(0) = -2\Delta Q_w(Q_x + \Delta Q_x + \Delta Q_w/2)\frac{b'(z)}{b(z)}x(z)$$

$$1 - \frac{x(0)}{x(z)} = -\frac{2\Delta Q_w}{f(0)\lambda(0)}(Q_x + \Delta Q_x + \Delta Q_w/2)\frac{b'(z)}{b(z)}$$

$$\int(1 - \frac{x(0)}{x(z)})dz = -\frac{2\Delta Q_w}{f(0)\lambda(0)}(Q_x + \Delta Q_x + \Delta Q_w/2)\int\frac{b'(z)}{b(z)}dz \qquad (1.34)$$

$$z - \int(\frac{x(0)}{x(z)})dz = -\frac{2\Delta Q_w}{f(0)\lambda(0)}(Q_x + \Delta Q_x + \Delta Q_w/2)ln(b(z))$$

$$b(z) = e^{-(Q_x + \Delta Q_x + \Delta Q_w/2)\frac{f(0)\lambda(0)}{2\Delta Q_w}(z - \int(\frac{x(0)}{x(z)})dz)}$$

One might be mistaken in assuming that this is a decay rather than growth of the beam along the length of the bunch. However, $\Delta Q_w < 0$ and $|\Delta Q_w| \sim Q_s$ meaning that instead of a negative term in the argument of the exponential, it is instead highly positive. This also simplifies the integral in b(z); $x(z) \propto b(z)$ so we can expect that the contribution from the integral $\int\frac{x(0)}{x(z)}dz$ contributies a multiplicative factor for a rapidly amplifying beam. Therefore the the solution for convective motion is:

$$x(t, z) = b(z)cos(Q_x\omega_0 t + (\Delta Q_x + \Delta Q_w)(\omega_0 t - \int_0^z\frac{dz'}{v_p(z')})) \qquad (1.35)$$

$$b(z) \approx Ae^{zf(0)\lambda(0)\frac{(Q_x + \Delta Q_x + \Delta Q_w/2)}{2|\Delta Q_w|}}$$

Chapter 2

Multiple Loop Square Well

It is clear that including space charge effects may have a significant effect on the instability threshold. However, at this point many analytic methods for studying instabilities break down. The structure of the beam itself is necessary to include space charge, leading to more general systems where self forces are included. One such system, the Square Well Model[**?**] includes space charge and arbitrary wake functions. In the intervening years since its invention, this model has appeared in several different forms including the Airbag Square Well (ABS)[**?**] and Core Halo Models[**?**].

In order to make both space charge and wakes solvable in such a system, it is necessary to heavily simplify the longitudinal dynamics. In the case of the SWM it is simplified into a single longitudinal energy trapped in a square potential well. However, by splitting the longitudinal dynamics into a series of discrete steps, it is possible to turn the system into a series of loops of current, each with a different energy and different synchrotron tunes. This model we shall call the Multiple Loop Square Well (MLSW).

We shall derive the equations which govern the MLSW prior to discussing the limiting cases of SWM and ABS to give physical intuition and context.

2.1 The Vlasov Equation and Transverse Moments

To begin this derivation shall define a continuity equation in three dimensions:

$$\frac{\partial f}{\partial t} + \sum_{i=1}^{3} (\dot{q}_i \frac{\partial f}{\partial q_i} + \dot{p}_i \frac{\partial f}{\partial p_i}) = \frac{df}{dt} = 0 \tag{2.1}$$

Eq. 2.1 is also known as the Vlasov equation. Particle flux is not created or destroyed, but it can flow in all three dimensions. The transverse dimensions are (x, p_x, y, p_y) whereas the coordinates for the synchrotron direction are $(z, \dot{z})$ with z being the position along the bunch and $\dot{z}$ as the momentum coordinate to make the physical meaning of the longitudinal motion clear. The time dependence can also be represented by other time-like variables as necessary while $\dot{z}$ can be expressed in terms of δ (see sections **??** and **??**). For a decoupled system, this can be simplified into a pair of two dimensional Vlasov equations, one for each transverse dimension. Such a distribution is collisionless but has electromagnetic interactions within the ensemble.

Due to the collective effects and external optics, the Vlasov equation becomes a mixture of single particle and collective motion. The collective forces are constructed of moments as in section **??**. The moments of the bunch distribution f are the following:

$$M^{j,k} \equiv \int_{-\infty}^{\infty} dx x^j \int dp_x p_x^k f \tag{2.2}$$

For the rest of this section, the bounds of all integrals are $-\infty$ to ∞. The zeroth (0th) and the normalized first (1st) order moments of x will be most important and will therefore be

given their own definitions:

$$\psi \equiv M^{0,0} = \int dx \int dp_x f$$

$$\psi X \equiv M^{1,0} = \int dx\, x \int dp_x f \qquad (2.3)$$

$$\psi P \equiv M^{0,1} = \int dx \int dp_x\, p_x f$$

Normalizing the 1st order moments means that X and P will correspond to the average position and momenta.

2.1.1 Derivatives of Moments

Applying the total derivative of the Vlasov equation it is possible to define equations of motion for the the various moments of the system. These moments are physically meaningful as TMCI is a dipole instability–which is to say driven by first order moments. Furthermore, the Vlasov equation makes certain simplifications possible. But first a few identities must be obtained by integrating the Vlasov equation.

$$\int dx \int dp_x \frac{df}{dt} = \int dx \int dp_x [\frac{\partial f}{\partial t} + \sum_{i=1}^{3}(\dot{q_i}\frac{\partial f}{\partial q_i} + \dot{p_i}\frac{\partial f}{\partial p_i})] = 0 \qquad (2.4)$$

As these are a proper set of canonical coordinates, Hamilton's equations can be substituted for $\dot{q_i} = \partial H/\partial p_i$ and $\dot{p_i} = -\partial H/\partial q_i$, and further where $\dot{q_i} = p_i$ and $\dot{p_z} = -\frac{U(t,z,\dot{z})}{dz}$ and not a function of p_i.

$$\int dq_x \int dp_x \dot{q_x}\frac{\partial f}{\partial q_x} = \int dq_x \frac{\partial f}{\partial q_x}\int dp_x p_x \qquad (2.5)$$

$$\int_{-\infty}^{\infty}\frac{\partial f}{\partial q_x} = f|_{-\infty}^{\infty} = 0$$

38

$$\int dq_x \int dp_x \dot{p}_x \frac{\partial f}{\partial p_x} = \int dq_x \frac{dU_i}{dq_x} \int dp_x \frac{\partial f}{\partial p_x} \tag{2.6}$$

$$\int_{-\infty}^{\infty} \frac{\partial f}{\partial p_x} = f|_{-\infty}^{\infty} = 0$$

This allows us to eliminate the transverse dependence of the integral:

$$\int dx \int dp_x \frac{df}{dt} = \int dx \int dp_x [\frac{\partial f}{\partial t} + \sum_{i \neq x} (\dot{q}_i \frac{\partial f}{\partial q_i} + \dot{p}_i \frac{\partial f}{\partial p_i})] = 0 \tag{2.7}$$

If the transverse motion is oscillatory and is much faster than the synchrotron motion its net effect averages to zero. Therefore, the longitudinal Hamilton's equations will not contain transverse coupling terms. In order to get the equations of motion of the moments themselves we must compute their derivatives. The derivation of these moments is rather long and involved and has been moved to appendix **??** to facilitate readability.

2.2 Collective Equations of Motion

Since Mode Coupling is a linear phenomenon it is sufficient to quantify the first order dipole moments. Higher order transverse terms may have some effect on this dipole motion, but can be neglected. The differential equations of the first order moment calculated in Appendix **??** are given below:

$$\dot{X} = \sum_{i=1}^{12} T_i = P - F_y \frac{\partial X}{\partial p_y} + \int dx x F_y \int dp_x f$$

$F_y \equiv \dot{p}_y$ is the transverse force in the y direction. There is an equivalent term F_x for the other transverse direction. Taking the derivative and rearranging, we get:

$$\ddot{X} + F_y \frac{d}{dt} \frac{\partial X}{\partial p_y} - \frac{d}{dt} \int dx x F_y \int dp_x f = \dot{P} \tag{2.8}$$

$$\dot{P} = \sum_{i=13}^{24} T_i = -g_0 \psi - g_1 X - \int (F_x - g_0 - g_1 x) dx \int f dp_x$$
$$+ \frac{\partial}{\partial p_y} \int dx F_y \int dp_x p_x f - F_y \frac{\partial P}{\partial p_y}$$

Combining these equations yields:

$$\ddot{X} + g_0 \psi + g_1 X + \int (F_x - g_0 - g_1 x) dx \int f dp_x = \tag{2.9}$$
$$-F_y \frac{d}{dt} \frac{\partial X}{\partial p_y} + \frac{d}{dt} \int dx x F_y \int dp_x f + \frac{\partial}{\partial p_y} \int dx F_y \int dp_x p_x f - F_y \frac{\partial P}{\partial p_y}$$

Note that this equation of motion neglects the effects of nonlinear optics and higher order space charge terms. Transverse forces of a given nonlinear order generate coupling to moments of that order and below. If only coherent motion is included, however, this simplifies into a more elegant relation. For now, we shall narrow our scope to this linearized system of differential equations:

$$\dot{X} \approx P$$

$$\dot{P} \approx -g_0 \psi - g_1 X$$

$$\ddot{X} + g_0 \psi + g_1 X \approx 0 \tag{2.10}$$

For the simplified differential equation, the two transverse dimensions are decoupled, making the dynamics a set of two simpler Vlasov equations.

2.2.1 Transverse Force F_x

It is necessary that we determine g_0 and g_1 before Eq. 2.10 can be solved. These are from the Taylor series of F_x. (Since $F_x \equiv \frac{dp_x}{dt} = -\frac{\partial H}{\partial x}$ is one of Hamilton's equations) it would be tempting to define a single particle Hamiltonian and go from there, but this isn't necessary). We have previously defined the components of this force in Chapter 1 (Sections **??**, **??**, and **??**) and can build terms g_0 and g_1, out of bare optics (including chromaticity), coherent space charge, and diffuse wakes.

One main caveat should be noted however. The collective moments of the transverse equations become independent from one another when the axes of the beam distribution and optics are aligned. The space charge effects from a properly rotated bunch will satisfy this condition. This independence may be violated if the input beam is offset from the beam optics, although that may not be significant if the offset angle is small.

Including wakes, space charge and optics to the linear order g_0 and g_1 (from the Appendix **??**) we arrive at the following form:

$$g_0(t,z)\omega_0^{-2} = -2Q_x\Delta Q'_{sc}\lambda(z)\overline{X}(t,z) + \int_0^z W(z-z')\lambda(z')\overline{X}(t,z') \tag{2.11}$$

$$g_1(z,\dot{z})\omega_0^{-2} = -Q_x^2 + 2Q_x(\Delta Q'_{sc}\lambda(z) - \xi(\dot{z})) \tag{2.12}$$

Where $\overline{X} \equiv \int_{-\infty}^{\infty} \psi X d\dot{z} / \int_{-\infty}^{\infty} \psi d\dot{z}$ and the line density $\lambda(z) = \int_{-\infty}^{\infty} \psi d\dot{z}$. Even after all that simplifying, we can see this system is still a second-order PDE of three separate variables. Thankfully, it is possible to simplify the system into one that is more tractable.

The next few sections will focus on this process. These sections parallel that of [**?**], which is in preparation.

2.2.2 Upper Betatron Sideband Approximation

The total distribution of particles will have moments generated by the order of the betatron sideband. The ± 1 betatron sidebands (normal betatron oscillations) are primary oscillation frequencies that generate first-order moments. By assuming that the tune is primarily due to this sideband, we can assume a form for X and reduce the order of the differential equation. In this case we assume X is made up of a slowly varying term $\tilde{X}$ and a fast oscillation at the upper betatron sideband tune:

$$X \equiv Re(\tilde{X}e^{-iQx\omega_0 t}) \tag{2.13}$$

$$P = Re((\dot{\tilde{X}} - iQ_x\omega_0\tilde{X})e^{-iQx\omega_0 t})$$

$$\frac{d^2}{dt^2}(\tilde{X}e^{-iQx\omega_0 t}) = (\ddot{\tilde{X}} - 2iQ_x \quad \omega_0\dot{\tilde{X}} - Q_x^2\omega_0^2\tilde{X})e^{-iQx\omega_0 t}$$

Since the $\tilde{X}$ is slowly varying compared to the betatron tune it is not a significant contribution to the solution ($\ddot{\tilde{X}} = 0$). Thus, when substituting into Eq. 2.10 we obtain a first order differential equation.

$$\frac{2Q_x}{i\omega_0}\dot{\tilde{X}} = \tilde{X}(Q_x^2 + g_1(z, \dot{z})) + e^{iQx\omega_0 t}g_2(t, z) \tag{2.14}$$

The total time derivative can be divided into explicit and implied components $\frac{d}{dt} = \frac{\partial}{\partial t} + \sum_{i=1}^{3}(\dot{q}_i \frac{\partial}{\partial q_i} + \dot{p}_i \frac{\partial}{\partial p_i})$. Since the transverse dependence has either been integrated out or is independent, this is equivalent to the one-dimensional total derivative. $\frac{d}{dt_l} = \frac{\partial}{\partial t} + \dot{z}\frac{\partial}{\partial z} + \frac{dU}{dz}\frac{\partial}{\partial \dot{z}}$. $U(z)$ is a scaled potential from section **??** such that it is in the proper relativistic frame with mass taken out. Substituting this into the collective equation of motion yields the following:

$$\frac{\partial X}{\partial t} + \dot{z}\frac{\partial X}{\partial z} - \frac{1}{m}\frac{dU}{dz}\frac{\partial X}{\partial \dot{z}} = \frac{i\omega_0}{2Q_x}[\tilde{X}(Q_x^2 + g_1(z, \dot{z})) + e^{iQ_x\omega_0 t}g_2(t, z)] \tag{2.15}$$

With the current form of the partial differential equation, the solution is not obvious. Even if a solution could be found, it would likely only be solvable in special cases. However, if the system can be simplified to a system of linear ODEs, the problem will become solvable. Therefore, we shall attempt to make the system one dimensional in z only, as well as linearize it such that the problem has the form $M\vec{\nu} - \Lambda\vec{\nu} = 0$ where M is the matrix of differential equations, $\vec{\nu}$ is an eigenvector constructed of basis functions, and Λ is the eigenvalue.

2.2.3 Betatron Tune Shift ΔQ_x

In a coherent system like this, the motion is governed by a sum of oscillation frequencies. It is therefore reasonable to assume a solution where $\partial/\partial t = -i\Delta Q_x\omega_0$. Although there are ways to calculate what this tune shift must be for a given system, it is not necessary as it can be easily determined using an error minimization scheme. (See section **??**)

$$\frac{\partial X}{\partial z} = \frac{i\omega_0}{2Q_x\dot{z}}[\tilde{X}(Q_x^2 + g_1(z, \dot{z})) + e^{iQ_x\omega_0 t}g_0(t, z) + 2Q_x\Delta Q_x] + \frac{1}{\dot{z}}\frac{dU}{dz}\frac{\partial X}{\partial \dot{z}} \tag{2.16}$$

43

2.2.4 Wake Forces

The wake force integral is the last major hurdle that needs to be defined. Specifically, the wake force must be a basis function (or set of basis functions) of the system of differential equations in order to be solvable in such a manner.

$$F \equiv e^{-iQx\omega_0 t} \int_0^z W(z - z')\lambda(z')\overline{X}(z') \tag{2.17}$$

Where W is the wake function, λ is the line density, and the line density is the projection of the distribution function f onto the z axis. The differential equation for F follows the Liebniz Integral Rule:

$$\frac{dF}{dz}e^{iQx\omega_0 t} = \frac{d}{dz}\int_0^z W(z - z')\lambda(z')\overline{X}(z') \tag{2.18}$$
$$= W(z - z)\lambda(z)\overline{X}(z)\frac{d}{dz}z - W(z - 0)\lambda(0)\overline{X}(0)\frac{d}{dz}0$$
$$+ \int_0^z \frac{\partial}{\partial z}W(z - z')\lambda(z')\overline{X}(z')$$

$$\frac{dF}{dz}e^{iQx\omega_0 t} = W(0)\lambda(0)\overline{X}(z) + \int_0^z \frac{\partial}{\partial z}W(z - z')\lambda(z')\overline{X}(z') \tag{2.19}$$

If the wake force is a sum of κ exponential terms rather than an arbitrary function of the form $W(z - z') = \sum_{k=1}^{\kappa} w_k e^{-\alpha_k(z-z')}$, then it becomes

$$\frac{dF}{dz}e^{iQx\omega_0 t} = W(0)\lambda(0)\overline{X}(z) - \alpha_k \sum_{k=1}^{\kappa} \int_0^z w_k e^{-\alpha_k(z-z')}\lambda(z')\overline{X}(z') \tag{2.20}$$

w_k and α_k are chosen to approximate the actual wake function. If the wake function decays before the next bunch arrives, it can be approximated by the Fourier set. That being said, it

is often considered sufficient to model the wake with only a few exponential terms. $w_k > 0$ corresponds to a 'natural' wake–wake a that creates forces in the same direction as the offset while a negative $w_k < 0$ corresponds to a damping kicker creating forces in the opposite direction as the offset that generated it making it a common choice to tamp down collective motion. Each of these individual terms k will be a basis function in the system of linear ODEs. For ease of identification, all basis functions will have a hat, therefore we shall define the wake force basis vectors as $\hat{F}_k \equiv e^{-iQx\omega_0 t} w_k \int_0^z e^{-\alpha_k(z-z')}\lambda(z')\overline{X}(z')$.

$$F = \sum_{k=1}^{\kappa} \hat{F}_k \tag{2.21}$$

$$\frac{d\hat{F}_k}{dz} = w_k \lambda(0) e^{-iQx\omega_0 t}\overline{X}(z) - \alpha_k e^{iQx\omega_0 t}\int_0^z w_k e^{-\alpha_k(z-z')}\lambda(z')\overline{X}(z')$$

$$\frac{d\hat{F}_k}{dz} = w_k \lambda(0)\tilde{\overline{X}}(z) - \alpha_k \hat{F}_k \tag{2.22}$$

Collecting terms and redefining:

$$h_0 \equiv \frac{g_0(t,z)}{2Q_x} e^{iQx\omega_0 t} g_2(t,z) \tag{2.23}$$

$$= -\Delta Q'_{sc}\lambda(z)\tilde{\overline{X}}(t,z) + e^{iQx\omega_0 t}\frac{1}{2Q_x}\int_0^z W(z-z')\lambda(z')\overline{X}(t,z') \tag{2.24}$$

$$h_1 \equiv \frac{Q_x^2 \Delta Q_x + 2Q_x \Delta Q_x + g_1(z,\dot{z})}{2Q_x} \tag{2.25}$$

$$= (\Delta Q_x + \Delta Q'_{sc}\lambda(z) - \xi(\dot{z})) \tag{2.26}$$

$$\frac{\partial X}{\partial z} = \frac{i\omega_0}{\dot{z}}[(h_1(z,\dot{z}))\tilde{X} + h_2(t,z)] + \frac{1}{\dot{z}}\frac{dU}{dz}\frac{\partial X}{\partial \dot{z}} \qquad (2.27)$$

2.3   Longitudinal Dynamics

Up to this point, we haven't made any statement as to the form of the longitudinal phase space and constraining potential, other than it is an equilibrium distribution and it couples to the transverse dynamics, while the effect of transverse dynamics on it averages to zero. Because of this lack of coupling, the tune in the longitudinal dimension is:

$$Q_s \equiv \frac{\tau\omega_0}{2\pi} = \frac{\omega_0}{2\pi}\oint \frac{dz}{\dot{z}} \qquad (2.28)$$

τ is the period of the synchrotron oscillation and $\dot{z} \equiv \pm\sqrt{2(E_0 - U(z))}$. To obtain the ODE form must eliminate the term $\frac{1}{\dot{z}}\frac{dU}{dz}\frac{\partial X}{\partial \dot{z}} \to 0$ from the differential equations of motion Eq. 2.15. Therefore $U(z)$ must be constant, and form a loop in phase space. Such a system is only satisfied with a square potential well–or a series of finite height square potential wells. Longitudinal particle velocity is constant and transverse motion is defined by a system of ordinary linear differential equations between the edges.

The following sections will define the notation and machinery to model nested square wells.

2.3.1   Approximating Longitudinal Potentials

Assume that we have a singly peaked potential $U(z)$ that we wish to approximate with N square potential wells bounded by $2N$ edges. Only N of the edges need to be defined–the others will be conjugate equipotentials. Ordering the edges along z we define them in order as

z_n where z_0 is the head of the bunch and z_{2N-1} is the tail. Since this system is periodic over the bunch train, the head of the next bunch (possibly the same bunch on a subsequent turn) can be defined as z_{2N} to include multi-bunch wake forces. However, if wakes decay quickly compared to the distance between bunchs or have some other multiscale characteristic, it may not be necessary to define z_{2N}. For simplicity, we have so far assumed that $z_0 = 0$ and $z_{2N-1} = l_b$ (the total length of the bunch), but this can be adjusted to accommodate for any singly peaked potential. These edges split the domain into a set of $2N$ subdomains where subdomain n lies between z_{n-1} and z_n. There are no particles trapped in the final subdomain.

It should be noted that we cannot know a priori the optimum choice of edges for a given system. The choices must capture the relevant physics in the bunch, and sufficiently sample the state space. The choice of edges need not be perfect, but should be chosen according to the main features of the physics.

After discretiztion, many of the functions will be discontinuous (or discontinuous in the derivative) at the edges z_n but continuous within each subdomain. As such it becomes useful to define these terms in the following way:

$$f(z) \equiv f^n(z) \text{ for } z_{n-1} < z < z_n \tag{2.29}$$

Where f(z) is an arbitrary function that may be discontinuous at edges z_n. The longitudinal potential can be discretized in this form. It should be noted that the range for the potential of each subdomain is the average $\overline{U}(z)$ where:

$$\overline{U}^m \equiv \begin{cases} \dfrac{\int_{z_{n-1}}^{z_n} U(z)dz + \int_{z_{2N-n-1}}^{z_{2N-n}} U(z)dz}{(z_n - z_{n-1}) + (z_{2N-n} - z_{2N-n-1})} & \text{for } n \neq N \\[12pt] \dfrac{\int_{z_{n-1}}^{z_n} U(z)dz}{(z_n - z_{n-1})} & \text{for } n = N \end{cases} \tag{2.30}$$

$$m \equiv N - |N - n| \tag{2.31}$$

Terms such as linear density, longitudinal velocity, and the averaged potential $\overline{U}(z)$ will be symmetric around the central well, yielding the form $f^m(z)$.

2.3.2 Continuity of Current in Airbag Loops

Now that the potential has been approximated, it becomes necessary to discretize the phase space to reduce the number of equations of motion to a finite set and to generate realistic synchrotron tunes. Each finite square well traps a continuous ring of energy levels spanning multiple subdomains. Without discretization, each energy level would contribute another set of coupled ODEs. Also, due to the stepwise structure of the square potential wells, some of these energy levels would have unrealistic tunes.

We must further discretize each of these ring surfaces of current into a monoenergetic 'loop' of current (also known as airbag distributions), with a single loop of current trapped by each square potential well. The currents of individual loops are constant so the line density will vary with the velocity of the bunch. For the loop of current trapped by the jth square well, the continuity between slices n and o has the following form:

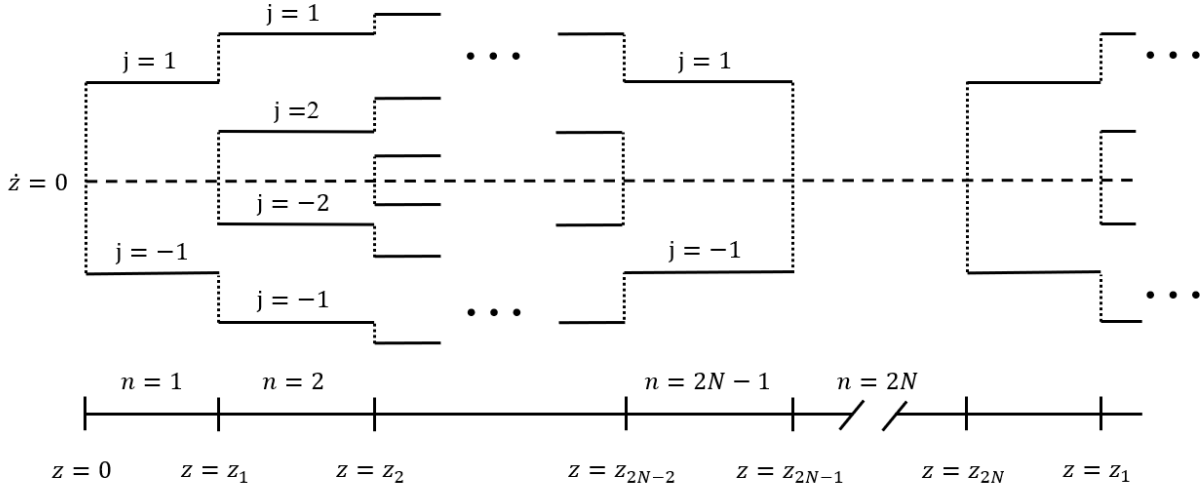$$\dot{z}_j^n \lambda_j^n = \dot{z}_j^o \lambda_j^o \tag{2.32}$$

Figure 2.1: An annotated example phase space portrait of multiple loops of current trapped in a discretized potential.

Each loop of current can be divided into two half loops with the opposing velocities ($\dot{z}_{-j} = -\dot{z}_j$). Fig. **??** shows the loops of current in phase space.

2.3.3 Determining Q_s for Current Loops

Each current loop has a tune Q_s which will decrease monotonically with the total energy of the loop. The choice of a proper Q_s is necessary as mode coupling is heavily dependent on the synchrotron tune. Since it is monotonic, there is only one corresponding velocity for a given target tune. The expression for the synchrotron tune of the nth current loop is:

From here it is possible to either invert $Q_s(E)$ or perform a concentration series to bound the necessary energy. The expression for the synchrotron tune of the jth well is:

$$Q_{s,j}(E_j) = \frac{\omega_0}{2\pi} \oint \frac{dz}{\dot{z}} = \frac{\omega}{\pi} \sum_{n=j}^{2N-j} \frac{z_n - z_{n-1}}{\dot{z}_j^m(E_j)} \tag{2.33}$$

$$\dot{z}_j^m = \sqrt{2(E_j - \overline{U}^m)} \tag{2.34}$$

What is the proper tune for a loop of current? If the loop of current is undergoing linear focusing, there is only one tune and the solution is trivial. But when nonlinear terms are present, the synchrotron tune of the original 'true' potential will vary with energy. Therefore, particles trapped within a loop of current will not have a single tune. For maximum accuracy, one can calculate the average tune of the portion of the 'true' distribution trapped in a given potential well (by using a procedure similar to section 2.3.4). Or with enough subdomains, the differences in tune within that loop of current become small and we can use the method in section 2.3.4 directly.

2.3.4   Sculpting Phase Space

Just like the potential, we must bin the particle density into individual subdomains. Because of current continuity the line density λ will be the average value of of the true linear density $\lambda_{true}(z)$.

$$\lambda = \lambda^m \equiv \begin{cases} \dfrac{\int_{z_{n-1}}^{z_n} \lambda_{true}(z)dz + \int_{z_{2N-n-1}}^{z_{2N-n}} \lambda_{true}(z)dz}{(z_n - z_{n-1}) + (z_{2N-n} - z_{2N-n-1})} & \text{for n} \neq N \\ \dfrac{\int_{z_{n-1}}^{z_n} \lambda_{true}(z)dz}{(z_n - z_{n-1})} & \text{for } n = N \end{cases} \tag{2.35}$$

Since multiple loops of current contribute to the total line density of the system, we can treat this as a sum of the form:

$$\lambda = \lambda^m = 2 \sum_{j=1}^{m} \lambda_j^m \tag{2.36}$$

50

At the edges of the distribution, there is only a single loop of current making the line density simple to determine ($\lambda^1 = 2\lambda_1^1$). Using the continuity of current for a single loop of current it is possible to determine the complete λ_1^m. This in turn makes it possible to calculate the contribution from the next (loop $j = 2$) loop. This procedure is repeated until the system is completely defined.

2.3.5   Generalized Equations of Motion

Now that the longitudinal dynamics are fully determined for the MLSW model we can come up with the final system of equations. Since the velocity of particles in a subdomain are constant, we can evaluate Eq. 2.27 at each longitudinal velocity $\dot{z}_j^n$. Doing this gives the following basis differential equations:

$$\frac{d\hat{F}_k^n}{dz} = w_k \sum_{j=1}^{m} \lambda_j^n (\hat{X}_j^n + \hat{X}_{-j}^n) - \alpha_k \hat{F}_k^n \tag{2.37}$$

$$\frac{d\hat{X}_j^n}{dz} = \frac{i\omega_0}{\dot{z}_j^n}[h_1(z, \dot{z}_j^n)\hat{X}_j^n + h_0(t, z)] \text{ if } \dot{z}_j^n \text{ is real} \tag{2.38}$$

$$\frac{d\hat{X}_j^n}{dz} = \epsilon \hat{X}_j^n \text{ if } \dot{z}_j^n \text{ is imaginary, } \epsilon << 1 \tag{2.39}$$

$$h_0(z) = -\Delta Q_{sc}' \sum_{j=1}^{m} \lambda_j^n (\hat{X}_j^n + \hat{X}_{-j}^n) + \frac{1}{2Q_x} \sum_{k=1}^{\kappa} \hat{F}_k^n \tag{2.40}$$

51

$$h_1(z, \dot{z}_j^n) = \xi_1 \dot{z}_j^n + \Delta Q'_{sc} \sum_{j=1}^{m} \lambda_j^n + \Delta Q_x \qquad (2.41)$$

Special notice should be given to Eq. 2.39, if $\dot{z}_j^n$ is imaginary, this loop of current has been trapped by a previous square potential well and is therefore not present in this subdomain. It is possible to change the size of the matrix at each subdomain (as is done in the code itself for performance), but this is unnecessary from a notation perspective. Ideally, the matrices in each subdomain have the same order to facilitate matrix multiplication down the line. It is valid to extend the smaller matrices with the addition of diagonal elements with vanishingly small value ϵ. This allows us to match the equations at the boundaries of the bunch (z_0 and z_{2N}) rather than matching them one by one as the size of the matrix changes and loops of current are trapped by progressive square wells. The differential equations for each subdomain can be expressed with the following matrix:

$$\frac{d\vec{V^n}}{dz} = M^n \vec{V^n} \qquad (2.42)$$

$$\vec{V}^n = \begin{pmatrix} \hat{F}_1^n \\ \vdots \\ \hat{F}_\kappa^n \\ \hat{X}_1^n \\ \hat{X}_{-1}^n \\ \vdots \\ \hat{X}_N^n \\ \hat{X}_{-N}^n \end{pmatrix} \tag{2.43}$$

This matrix form has solutions that are an eigensystem with eigenvalues Λ and eigenvectors $\vec{\nu}$.

$$(M^n - \Lambda)\vec{\nu} = 0 \tag{2.44}$$

Each eigenvector propagates with its given eigenvalue such that $\vec{\nu}_a(z) = \vec{\nu}_a(z_{n-1})e^{\Lambda_a^n(z-z_{n-1})}$. Λ_i is the ith eigenvalue while $\vec{\nu}_i$ is the corresponding eigenvector. This makes the propagation of the individual basis function $\vec{V}$:

$$\vec{V}^n(z) = \sum_{a=1}^{\kappa+2N} (\nu^n)_{ca}^{-1} E_{aa}^n(z)\nu_{ab}^n \vec{V}^n(z_{n-1}) \tag{2.45}$$

The diagonal matrix $E_{aa} \equiv e^{\Lambda_a(z-z_{n-1})}$. ν_{ab} is a matrix made up of row vectors $\vec{\nu}$ that translates from the basis of basis functions $\vec{V}$ to the basis of eigenvectors $\vec{\nu}$. We are essentially translating the initial conditions at the edge of a subdomain z_{n-1} into a sum of eigenvectors

before propagating the eigenvectors and then translating back to the initial basis.

2.3.6   Continuity and Boundary Conditions

The motion of the bunch is now well defined in a single subdomian for all basis functions. Wake forces $\hat{F}_k$ and the average position $\hat{X}_{\pm j}$ of the bunch are continuous along the length of the bunch where $\vec{V}_j^n(z_n) = \vec{V}_j^{n+1}(z_n)$. Therefore, the propagation of all basis functions has the form:

$$\vec{V}(z) = \sum_{e=1}^{\kappa+2N} (\nu^{-1})_{he} E_{ee}(z) \nu_{eg} \prod_{d=1}^{n-1} [\sum_{a=1}^{\kappa+2N} (\nu^d)_{ca}^{-1} E_{aa}(z_d) \nu_{ab}^d] \vec{V}^1(z_0) \tag{2.46}$$

$$\text{for } z_{n-1} < z < z_n$$

$$\vec{V}(z_{2N}) \equiv \mathcal{M} \vec{V}(z_0) \tag{2.47}$$

Now that we can propagate the system to an arbitrary position within the bunch while maintaining continuity, we can define a vector of boundary conditions that must be satisfied. First is the boundary condition for the wakes f_k, which defines continuity of wakes between bunches (z_0 and z_{2N}). Bunches may be out of phase with one another which will add a complex multiplicative factor. This will often be a pure rotation as is the case in coupled bunch modes, but may vary for specific cases.

At the same time, the upper and lower half loops of current $\hat{X}_j$ and $\hat{X}_{-j}$ must have the same value at their edges $\hat{X}_j(z_{j-1}) = \hat{X}_{-j}(z_{j-1})$, $\hat{X}_j(z_{2N-j}) = \hat{X}_{-j}(z_{2N-j})$. We shall consider the boundary condition at the head portion of the loop to be a_n and the tail of the loop as b_n. This seems to suggest that our boundary conditions are a system of $\kappa + 2N$ equations with the same number of unknowns. This is however not actually the case. Instead the head of the outermost loop must be offset from the center of the beampipe by some small

amount–this is because our betatron sideband is nonzero. We may arbitrarily set this initial

offset to 1 as we do not know the true offset of an input beam. Because of this it is not

possible to satisfy all boundary conditions simultaneously except in special cases. Therefore,

there will be a small error e that must be accounted for on its own. This error could be

included anywhere, but calculations are simplified if the error is accounted for at the tail of

the initial loop. The initial and final boundary conditions $\vec{V}(z_0)$ and $\vec{V}(z_{2N})$ are:

$$
\vec{V}(z_0) = \begin{pmatrix} f_1 e^{-2\pi i \frac{B}{T} - \mathcal{D}} \\ \vdots \\ f_\kappa e^{-2\pi i \frac{B}{T} - \mathcal{D}} \\ 1 \\ 1 \\ a_2 \\ a_2 \\ \vdots \\ a_N \\ a_N \end{pmatrix} , \vec{V}(z_{2N}) = \begin{pmatrix} f_1 \\ \vdots \\ f_\kappa \\ b_1 + e \\ b_1 \\ b_2 \\ b_2 \\ \vdots \\ b_N \\ b_N \end{pmatrix} \tag{2.48}
$$

Where B is the coupled bunch mode number, T is the total number of equally spaced

bunches, and $\mathcal{D}$ is a decay factor from the multiscale system. We can represent both of these

vectors of the initial and final conditions in terms of a vector of constraints $\vec{q}$ and the vector

of the initial offset of the bunch $\vec{c}$:

$$\vec{q} = \begin{pmatrix} f_1 \\ \vdots \\ f_\kappa \\ e \\ b_1 \\ a_2 \\ b_2 \\ \vdots \\ a_N \\ b_N \end{pmatrix} , \vec{c} = \begin{pmatrix} 0 \\ \vdots \\ 0 \\ 1 \\ 1 \\ 0 \\ 0 \\ \vdots \\ 0 \\ 0 \end{pmatrix} \tag{2.49}$$

Where $\vec{V}_0 - \vec{c} \equiv R_i \vec{q}$ and $\vec{V}_{2N} \equiv R_f \vec{q}$. Therefore,

$$
R_i =
\begin{pmatrix}
e^{-2\pi i \frac{B}{T} - \mathcal{D}} & & & & & & & & & \\
& \ddots & & & & & & \text{\Large 0} & & \\
& & e^{-2\pi i \frac{B}{T} - \mathcal{D}} & & & & & & & \\
& & & 0 & 0 & & & & & \\
& & & 0 & 0 & & & & & \\
& & & & & 1 & 0 & & & \\
& & & & & 1 & 0 & & & \\
& \text{\Large 0} & & & & & & \ddots & & \\
& & & & & & & & 1 & 0 \\
& & & & & & & & 1 & 0
\end{pmatrix}
\tag{2.50}
$$

$$
R_f =
\begin{pmatrix}
1 & & & & & & & & & \\
& \ddots & & & & & & \text{\Large 0} & & \\
& & 1 & & & & & & & \\
& & & 1 & 1 & & & & & \\
& & & 0 & 1 & & & & & \\
& & & & & 0 & 1 & & & \\
& & & & & 0 & 1 & & & \\
& \text{\Large 0} & & & & & & \ddots & & \\
& & & & & & & & 0 & 1 \\
& & & & & & & & 0 & 1
\end{pmatrix}
\tag{2.51}
$$

With this it becomes possible to use matrix methods to determine the boundary conditions:

$$\vec{V}(z_{2N}) = \mathcal{M}\vec{V}(z_{2N})$$

$$R_f\vec{q} = \mathcal{M}(R_i\vec{q} + \vec{c})$$

$$\mathcal{M}^{-1}R_f\vec{q} = R_i\vec{q} + \vec{c}$$

$$(\mathcal{M}^{-1}R_f - R_i)\vec{q} = \vec{c}$$

$$\vec{q} = (\mathcal{M}^{-1}R_f - R_i)^{-1}\vec{c} \qquad (2.52)$$

This vector of constraints/initial conditions is only physical when the error boundary condition $e = 0$. This is the $\kappa + 1$ constraint. Since the matrix $\mathcal{M}$ changes with the input tune shift ΔQ_x we can therefore find a choice of tune shift that brings the error to zero.

2.3.7 Determining ΔQ_x

As we can see, the entire bunch is defined within an error term concentrated at the tail of the bunch. A real solution will have this error go to zero and satisfy all of the boundary conditions. This will only occur at certain values of the parameter ΔQ_x, which we can vary to find proper solutions. We shall minimize this error e using a gradient descent method [?].

For every initial choice of tune shift $\Delta Q_{x,i}$ there is a complex valued error e. By choosing slight offset tune shifts $\Delta Q_{x,i} + d\Omega$ and $\Delta Q_{x,i} + id\Omega$ we can then calculate the derivatives for the real and imaginary errors. $d\Omega$ is a small change to the initial tune shift used to calculate

the numerical derivative.

$$
\begin{pmatrix} Re(e) \\ Im(e) \end{pmatrix} = \begin{pmatrix} \frac{dRe(e)}{dRe(\Omega)} & \frac{dRe(e)}{dIm(\Omega)} \\ \frac{dIm(e)}{dRe(\Omega)} & \frac{dIm(e)}{dIm(\Omega)} \end{pmatrix} \begin{pmatrix} Re(\Omega) \\ Im(\Omega) \end{pmatrix} \tag{2.53}
$$

Ω is the change to the tune shift necessary to minimize error if the error is completely linear. With this in mind we can define a new initial tune shift and iterate the solution as necessary until the error is below some arbitrary threshold. It can be useful to place an upper limit on the stepsize in order to not jump toward a more strongly attracting tune solution.

$$
\begin{pmatrix} \frac{dRe(e)}{dRe(\Omega)} & \frac{dRe(e)}{dIm(\Omega)} \\ \frac{dIm(e)}{dRe(\Omega)} & \frac{dIm(e)}{dIm(\Omega)} \end{pmatrix}^{-1} \begin{pmatrix} Re(e) \\ Im(e) \end{pmatrix} = \begin{pmatrix} Re(\Omega) \\ Im(\Omega) \end{pmatrix} \tag{2.54}
$$

$$
\Delta Q_{x,f} = \Delta Q_{x,i} - \Omega \tag{2.55}
$$

Interestingly, it turns out that this method for calculating tune shifts is very robust for the system we are studying. It continues to function even with a large number of square potential wells, as long as a sufficient number of initial starting points near to the coherent modes are selected.

2.3.8 Physical Interpretation of MLSW

What we have spent most of this chapter solving is the slowly varying portion of the dipole moments. Since all basis functions oscillate at the same tune $(Q_x + \Delta Q_x))$, the total dipole motion of a coherent mode is:

$$\overline{\hat{X}} = \frac{\sum_j^m \lambda_j^n (\hat{x}_j^n + \hat{\bar{x}}_j^n)}{2 \sum_j^m \lambda_j^n} \tag{2.56}$$

Therefore the average position of particles oscillating at a specific tune shift will be:

$$\overline{X} = Re(\frac{\sum_j^m = 1 \lambda_j^n (\hat{x}_j^n + \hat{\bar{x}}_j^n)}{\sum_j^m = 1 \lambda_j^n} e^{-2\pi i \omega t (Q_x + \Delta Q_x)}) \tag{2.57}$$

The weighted sum of all valid tune shift modes will give the complete solution.

This is the steady-state solution for the coherent bunch motion. Wakes will grow and bunches deform until this system arrives at these coherent modes. Because of this, it may take several synchrotron periods in order for the system to reach this final steady and state crossing the parameter space as it does so. If this path towards the steady state crosses an instability threshold (shown in Fig. **??**) it may experience this instability even if the steady state itself is stable.

2.3.9 Solving the MLSW with Codes

It should be obvious that although this is an exactly solvable problem, boundary condition matching for such a system is an iterative process. A code and accompanying wrapper have been developed to discretize a beam, translate it into the square well method then calculate the coherent modes of the system.

The Python wrapper discretizes the input potential and generates a set of input files with longitudinal dynamics and transverse parameters (sections **??-??**). This is then read by the main C++ code which uses the matrix solver Eigen[**?**] to satisfy boundary conditions

??-??). The coherent tune shift and the shape of the bunch modes along with the bunch shape are then saved as output files that can be read and visualized by the wrapper.

The python[**?**] wrapper for the MLSW code has the following form. It begins with an input potential which it discretizes into a set of square potential wells (section **??**) and bins the line particle density. From there the tune of the trapped particles is calculated and an energy level assigned to give the approximating airbag the correct tune (section **??**). Particle densities are meted out to the individual loops before being combined with transverse bunch information (section **??**). The wrapper then saves an input file for each individual setting which can be used by the main C++ calculation code.

The C++ code is a multi-threaded code that uses the matrix solver Eigen[**?**] to perform the individual matrix calculations. Each input file is read by one of the threads which are then translated into two sets of matrices. The first matrix is the total system with no tune shift term $M|_{\Delta Q_x=0}$. The second matrix is R, the matrix of constants and prefactors for the tune shift, where $R \equiv (M - M|_{\Delta Q_x=0})/\Delta Q_x$. This way it is possible to evaluate the total matrix M quickly since $M = M|_{\Delta Q_x=0} + \Delta Q_x R$. Then the error minimization can be performed to satisfy boundary conditions. With boundary conditions satisfied, the individual coherent modes and the spatial functions are then saved to a file where they can be visualized by the python wrapper.

Chapter 3

MLSW Results

The generalized Multiple Loop Square Well model is only useful insofar as they tell us more about the system then the limiting cases. Therefore we shall begin with a comparison of the MLSW model with the SWM and ABS (sections **??** and **??**). A systematic study of multiloop phenomena is then performed from the normal case (section **??**). After that, we use the MLSW to analyze certain systems such as nonlinear chromaticity (section 3.4), oscillating wakes (section **??**), nonlinear longitudinal potentials (section **??**), and methods for damping instabilities (section **??**).

3.1 SWM Comparisons with MLSW

In the limit of a single square well, the Multiple Loop Square Well reduces to the Square Well Model[**?**]. In this section we will demonstrate that the MLSW match the SWM results in this limiting case. We will survey these results to give physical intuition and offer a comparison point for more complex dynamics of multiple square wells and loops of current.

For a single square well, the velocity can be easily defined in terms of tune:

$$Q_s = \frac{\omega_0}{2\pi} \left(\int_0^{l_b} \frac{dz}{v_s} + \int_{l_b}^0 \frac{dz}{-v_s} \right)$$

$$v_s = \frac{\omega_0 l_b}{\pi Q_s} \tag{3.1}$$

A single loop of current will have longitudinal velocity $\pm v_s$ and the corresponding two equations of motion–one for the forward propagating and one for the backward propagating portion of the bunch. Since this bunch has a non-infinitesimal amount of particles oscillating at a given tune, the loops of current in this distribution have a density in phase space of $\lambda \delta(\dot{z} \pm v_s)/2$ where δ is the Dirac Delta Function. This has the added effect of making the the particle density $\lambda(z)$ constant within the square potential well and zero everywhere else. Evaluating this gives the set basis of differential equations $\hat{X}_+, \hat{X}_-$ completing the set of basis vectors for the system of linear ordinary differential equations.

$$\frac{d\hat{X}_+}{dz} = \frac{i\pi Q_s}{l_b}[(\Delta Q_x + \frac{\chi \omega_0}{\pi Q_s})X_+ + \frac{\lambda}{2}\Delta Q'_{sc}(\hat{X}_+ - \hat{X}_-) + \frac{1}{2Q_x}\sum_{k=1}^{\kappa}\hat{F}_k)] \tag{3.2}$$

$$\frac{d\hat{X}_-}{dz} = -\frac{i\pi Q_s}{l_b}[(\Delta Q_x - \frac{\chi \omega_0}{\pi Q_s})X_- + \frac{\lambda}{2}\Delta Q'_{sc}(\hat{X}_- - \hat{X}_+) + \frac{1}{2Q_x}\sum_{k=1}^{\kappa}\hat{F}_k)] \tag{3.3}$$

$$\frac{d\hat{F}_k}{dz} = w_k\lambda(\hat{X}_+ + \hat{X}_-) - \alpha_k\hat{F}_k \tag{3.4}$$

Because the system only has particles at mirrored velocities, the chromatic term can only be meaningfully defined in terms of the head tail phase shift χ or the linear order of ξ ($\chi = \xi l_b$) as even components of the expansion will just lead to a small frequency detuning. The boundary conditions for a bunch with quickly decaying wakes are:

$$\hat{X}_+(0) = \hat{X}_-(0) \equiv 1 \tag{3.5}$$

$$\hat{X}_+(l_b) = \hat{X}_-(l_b) \equiv b \tag{3.6}$$

3.1.1 SWM Beam Instabilities

When a valid tune solution ΔQ_x has a negative imaginary component, $Im(\Delta Q_x) < 0$, the system becomes unstable and the bunch oscillations will grow exponentially until some mechanism stabilizes the beam. The most trivial example of this is particle loss, where loss will decrease the strength of the wake force, the main source of instability in our case. At a sufficient distance from the center of the optics nonlinear forces become stronger and we may exit the linear regime. Even if nonlinearity prevents direct particle loss there will still be a significant decrease in beam quality.

Many instability result from modes combining together and becoming degenerate as in TMCI. But there are exceptions, as the Head Tail instability does not exhibit this behavior.

3.1.2 SWM and TMCI Threshold Under Constant Wake

All tune solutions ΔQ_x for a stable system will reside on the real line ($Im(\Delta_x = 0)$), making each solution oscillate at an offset from the fundamental betatron tune. If two modes shift together on the real line they will become degenerate and create an instability. Since the distance between sideband modes without collective effects is Q_s, a wake must shift a sideband $\sim Q_s$ in order to drive this instability.

For the simplest possible wake, where $\alpha_1 = 0$ known as a constant wake or a step wake.

This is not technically a possible wake because transverse wakes must satisfy $\int_0^\infty W(z)dz = 0$ But it is possible to have a wake which only valid for the interval of interest.

When $\alpha_1 = 0$ there is no natural oscillation, and the wake will best couple to the zero mode. Thus it is possible to define the approximate tune shift generated by a step wake of this form known as the Rigid Mode tune shift ΔQ_w. $\Delta Q_w \equiv \frac{w_k}{4Q_x}$ for a bunch with a total bunch intensity of N. $\Delta Q_x = -\Delta Q_w$ while w_k is sufficiently small, effectively when the wake force does not heavily perturb the modes of the solution. However as the wake strength increases, this shifting of other modes becomes more significant and must not be discounted–leading to the shape of the instability diagram shown in Fig. 3.1. These other modes can be driven into instability as well, but only become the dominant unstable term in specific cases.

The TMCI threshold for a constant wake and no space charge is:

$$\frac{w_1}{4Q_x Q_s} \propto \frac{w_1}{4\omega_x \omega_s} > 2 \tag{3.7}$$

This has the very good agreement between the two macroparticle model with [?] with the same functional form and constant factors. However. Since the SWM is a macroparticel model approximately the same functional dependence as [?] the two macroparticle model from section ??, but lacking synchro-betatron resonances due to the continuous particle distribution.
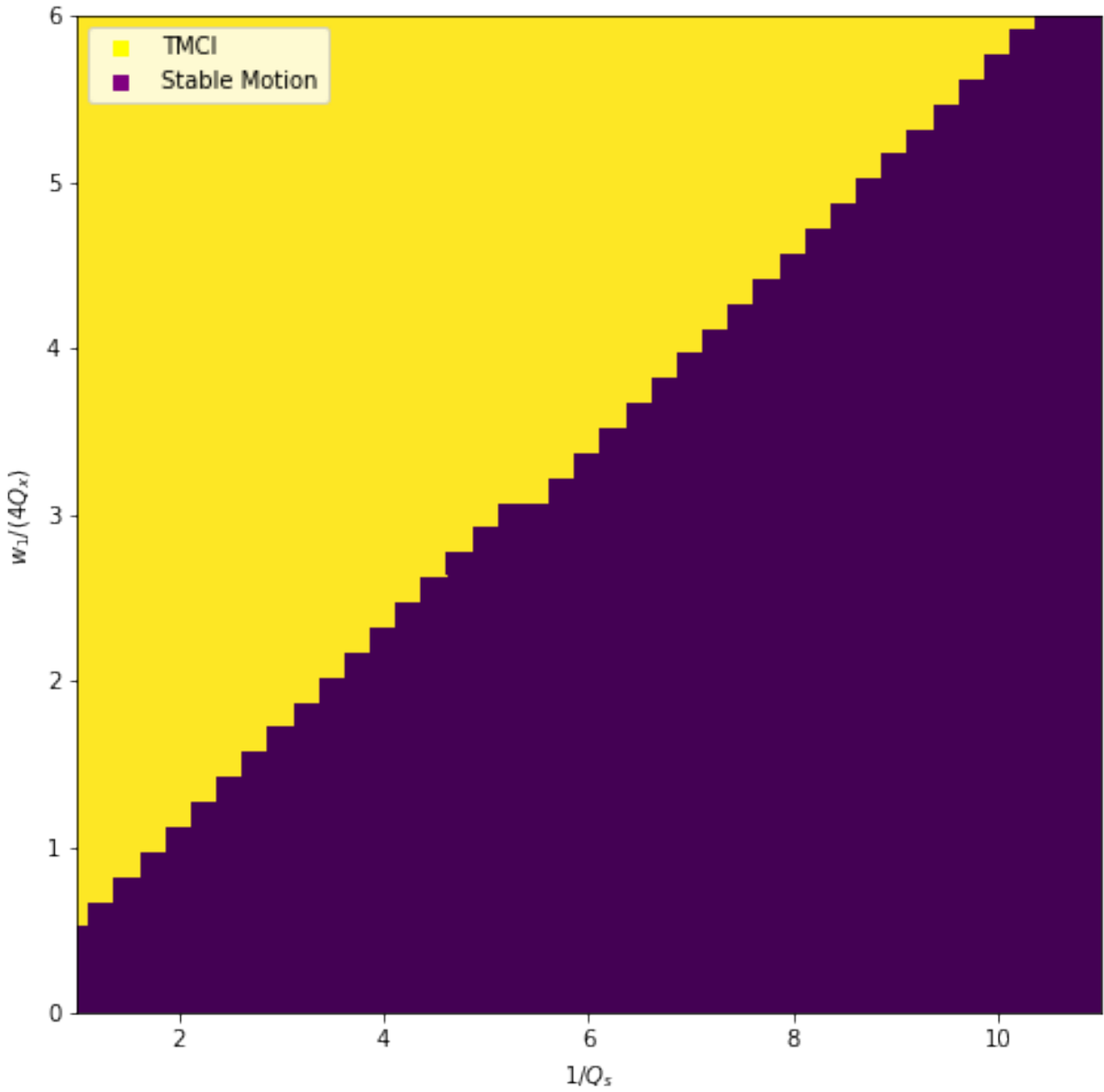
Figure 3.1: The TMCI threshold simulated using the SWM. Note the lack of resonance lines characteristic of macroparticle methods such as those shown in section ??
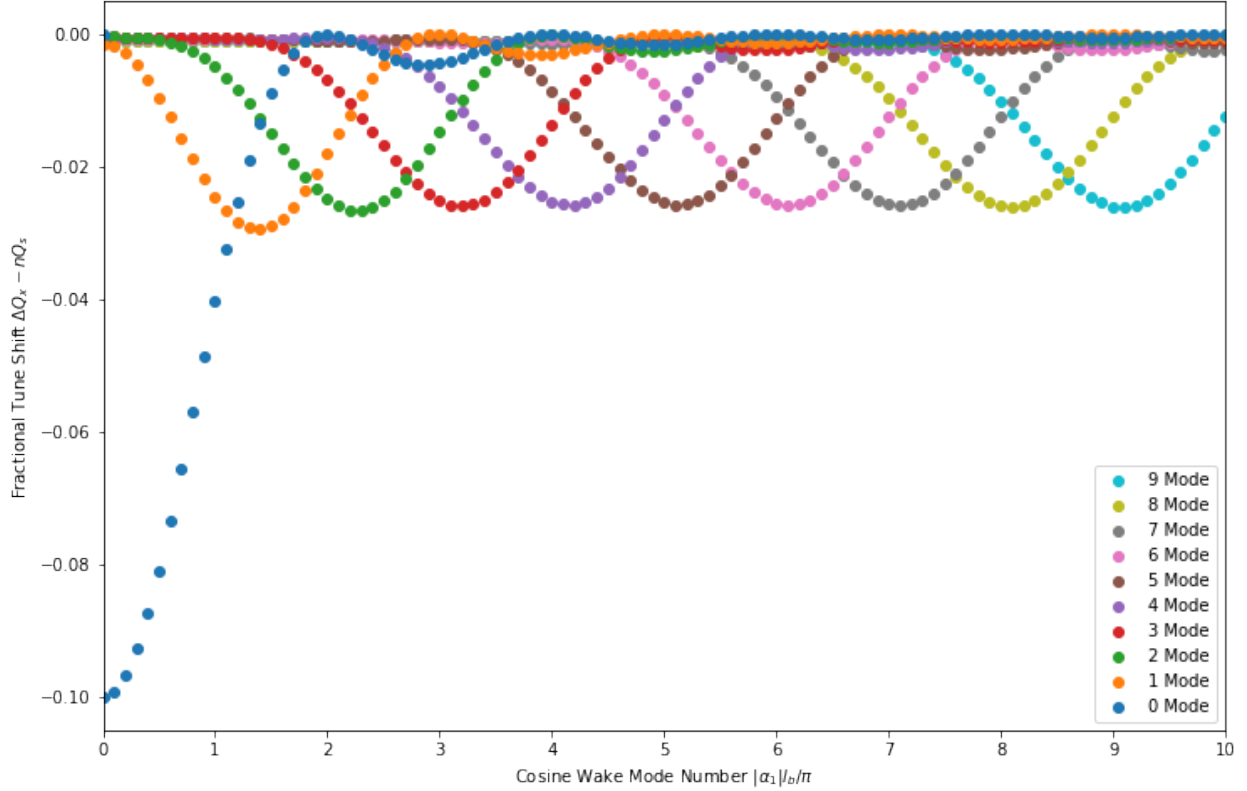
Figure 3.2: This figure shows the corresponding tune shifts of an oscillating wake frequency. The tune shift response for input the wake function is an even function of $\mathcal{N}$ ($\mathcal{N} = |\alpha_k| l_b/\pi$)while the tune kick is small. The zero mode is more strongly driven by wakes, making it easier to drive into an unstable regime compared to other wakes.

3.1.3 SWM and MLSW Mode Responses for Varying Wake Frequency

Rather than assuming a constant wake function, let us also consider wakes generated by an oscillatory wake function of the form $\alpha_k = i\pi\mathcal{N}/l_b$. The parameter $\mathcal{N}$, which we shall call the cosine wake mode number is a continuous parameter that will drive a combination of coherent modes. When $\mathcal{N}$ is in resonance–slightly above the integer due to interaction with other modes, it has the same natural frequency as a sideband mode, exciting a tune shift in the beam, as is shown in Fig. 3.2. For the single well version of this, the fundamental mode is easier to drive than the offset modes.
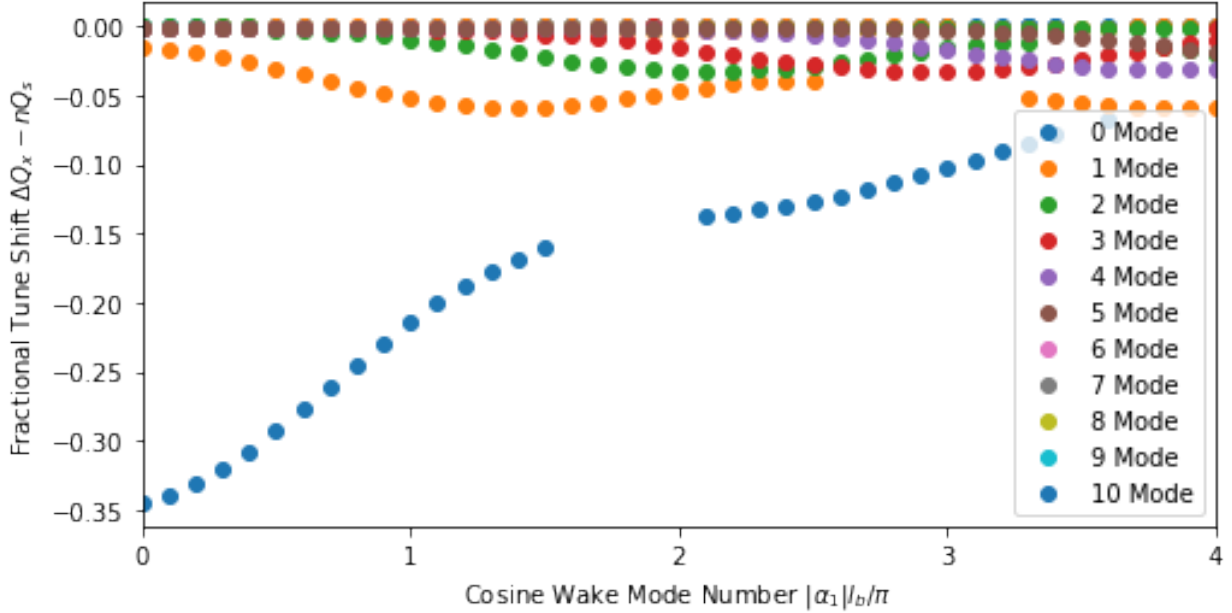
Figure 3.3: MLSW with three loops of current driven by an oscillating wake function. The tune shifts of an oscillating drive tune shifts in a combination of modes. As with the single well, this response is an even function of $\mathcal{N}$, where $\mathcal{N} = |\alpha_k| l_b / \pi$. The error minimization algorithm does not always resolve all coherent modes of interest, leading a few missing datapoints such as in the 0 mode.

Taking the same approach with three potential wells and measuring the responses we obtain Fig. 3.3 which has the same rigid fundamental mode, but a decreasing response from the sidebands. Since the bunch is no longer flat, modes are no longer solely driven by the ratio of the wake α_k to the length of the bunch l_b as the bunch shape itself has its own resonances. Therefore, we should expect this to vary with the exact distribution shape.

3.1.4 TMCI with Space Charge

In the single well limit, free space charge effects shift all modes except for the fundamental ($n = 0$) correspondingly lower, effectively slowing the oscillation speed of the bunch. The fundamental mode doesn't shift and space charge alone cannot cause mode coupling, the positive sideband modes will asymptotically approach the fundamental mode from above

while the negative sideband will continue to decrease linearly with $\Delta Q_{sc}/2$. For a real machine however, the intensity along the bunch varies longitudinally making the tune vary along with it.

With a natural wake ($w_k > 0$) space charge is a stabilizing effect. The distance between the $n = 0$ and the $n = -1$ modes will be approximately $Q_s + \Delta Q_{sc}/2$ making the total tune shift necessary to couple between such modes larger than in the absence of space charge. But this is a double edged sword. At strong space charge, damper wakes can induce instability by driving mode coupling between the modes where $n \geq 0$. This instability is shown in Fig. 3.4

Perhaps the most important prediction is that certain beams (below the red line in Fig. 3.4) cannot become unstable to TMCI no matter how high the particle intensity is. This suggests that for SWM beams it is not needed to limit the beam intensity when $2Q_x w_l/\Delta Q_{sc} > 2$).

But a slight caveat. While TMCI from the zero and one modes may be damped by sufficient space charge, other modes may not necessarily be damped in the same way. Therefore one should be aware that higher order terms may become problems at very high intensity even if space charge dampens the main instability.

When we move on to a multiple loop case this system changes significantly. Although the same modes exist in Fig. 3.5 (albeit with their frequencies adjusted slightly), other modes dominate at high intensity. These features are due to mode splitting in the coherent modes and will be talked about in section 3.2.5. Therefore at high intensity there is a strong upper current limit.
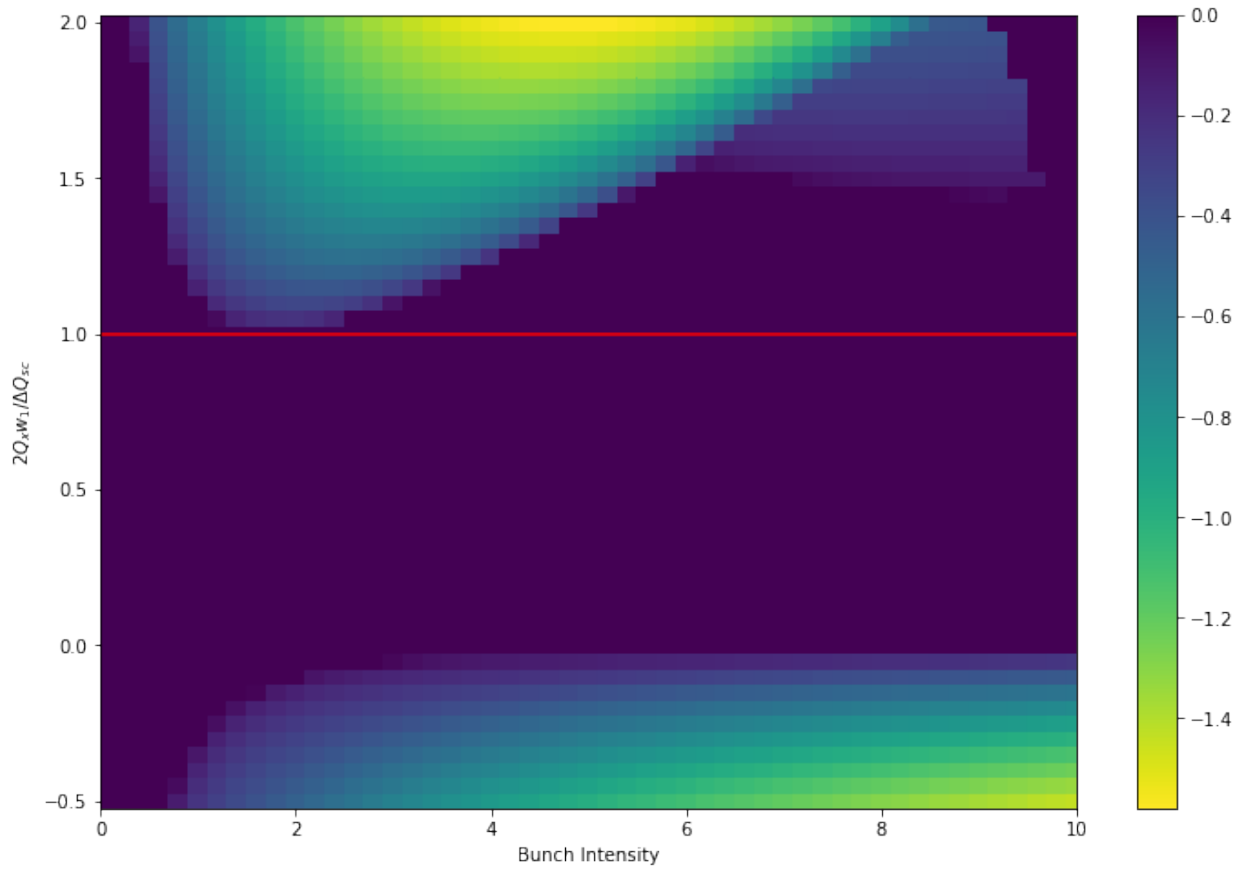
Figure 3.4: Colormap of instability magnitude for the SWM. As bunch intensity increases, so do both the rigid mode tune shift ($4Q_x w_1$) and the space charge tune shift ($\Delta Q_s c$). If the ratio the rigid mode and space charge is less than one but still greater than zero the beam will be stable for any intensity. TMCI at the top left is from modes -1 and 0, the one at the bottom is 0 and 1, while the final mode is much weaker and at the top right and is the 2 and 1 modes.
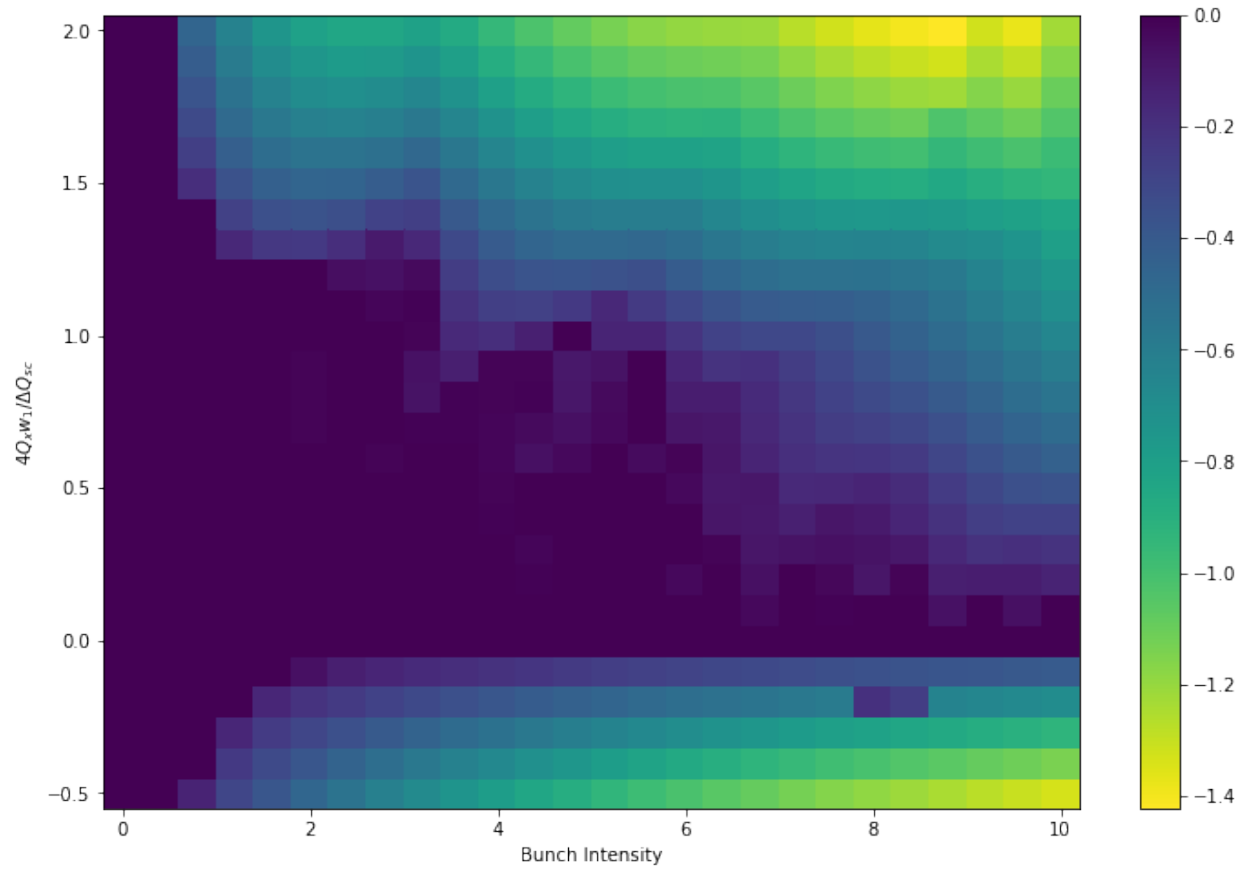
Figure 3.5: Colormap of instability magnitude for $N = 3$ mulitloop. This bunch has a worse resolution in order to save computation time so structures are not as well resolved. Note the spike like nature of some of the instabilities, these are due to orthogonal modes crossing one another briefly without fully coupling. and are only degenerate over short time in the parameter space.

3.1.5 Head-Tail Instability with Linear Chromaticity

Unlike TMCI, the head-tail instability doesn't require mode degeneracy in order to become unstable. Instead, the head-tail phase shift χ causes a small mismatch between the phase of the forward and backward propagating loops of current. Without wakes, the phase offset will satisfy boundary conditions as $cos(n\pi + \chi) = cos(n\pi - \chi)$. In the presence of wakes the tune must be complex to satisfy the boundary conditions. A diagram of this mode structure for the SWM is shown in Fig. 3.6. Since mode coupling does not occur in this case there is only one complex mode for each sideband, which may be stable or unstable depending on specific conditions.

This chromatic effect has a theoretical relationship to the growth rate of the TMCI threshold as well[**?**]. As Head Tail modes are already unstable, it can be difficult for head tail modes to couple properly into TMCI. Because of this, chromaticity is sometimes suggested as a method to damp such instabilities.

For systems where the number of loops of current $N > 1$, chromatic effects will differ due to the more complex phase space and will treated in section 3.4.

3.2 MLSW Phenomena

3.2.1 Bunch Shaping and RF

So far we have taken an overview of the MLSW model, focusing on general aspects of bunch performance. This survey used simple peaked multiwells and linear RF forces to make the results widely applicable.

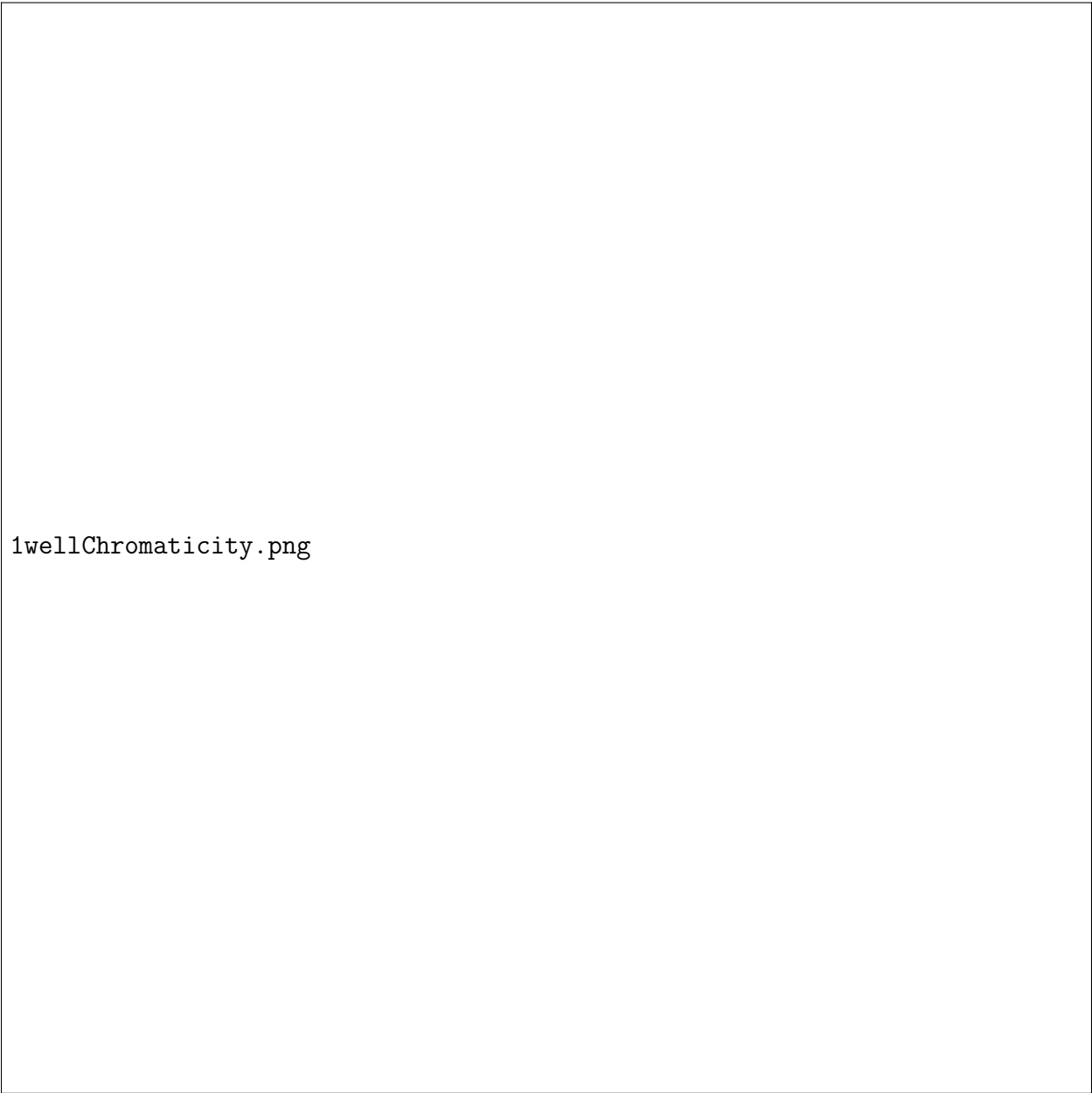As more square wells and loops of current are added the exact shape of a distribution

Figure 3.6: A plot of the most unstable modes due linear chromatic effects. Though we use nonstandard definitions for chromaticity, *chi* should remain unchanged. As has been noted before, the No comparison with MLSW will be shown here, as that will need to be discussed in more detail in section 3.4.

beomes more important. The longitudinal RF potential defines the tune of each individual loop of current while the particle distribution populates each loop with current. Many beams are approximately Gaussian in form, but any equilibrium distribution with a singly peaked potential can be approximated by the superposition of multipile square wells. It is useful to think about some special cases, which show interesting results.

3.2.2   Hollow Beams and Beams with weak Collective Effects

Let us begin by thinking about a loop of current. This is essentially a single airbag trapped in multiple square wells, and with enough loops potential wells this approximately becomes a hollow distribution, shown in Fig. 3.7. In the limit without collective effects, a bunch is made up of multiple hollow distributions evolving independently.

This gives us an interesting thought experiment. If we imagine that we have an input beam without any collective effects mediating between loops of current, this will lead to the each loop of current being oscillating based on their initial offsets. Each loop will have its own individual sidebands that propagate separately from the others.

What happens when coupling is included? As soon as there are forces propagating between the multiple loops of current, the system is fully defined and each loop of current will eventually shift to toward the system's coherent modes. Before the system saturates, each mode will shift to the final oscillation frequency. For these weak collective effects the external current loops essentially cancel the contributions of other modes while the system is dominated by the outermost loop of current. This is why the coherent tune has the synchrotron sidebands of the outermost loop as the coupling strength between loops of current goes to zero.

However, when mode bifurcation occurs these new coherent modes will be some hybrid of
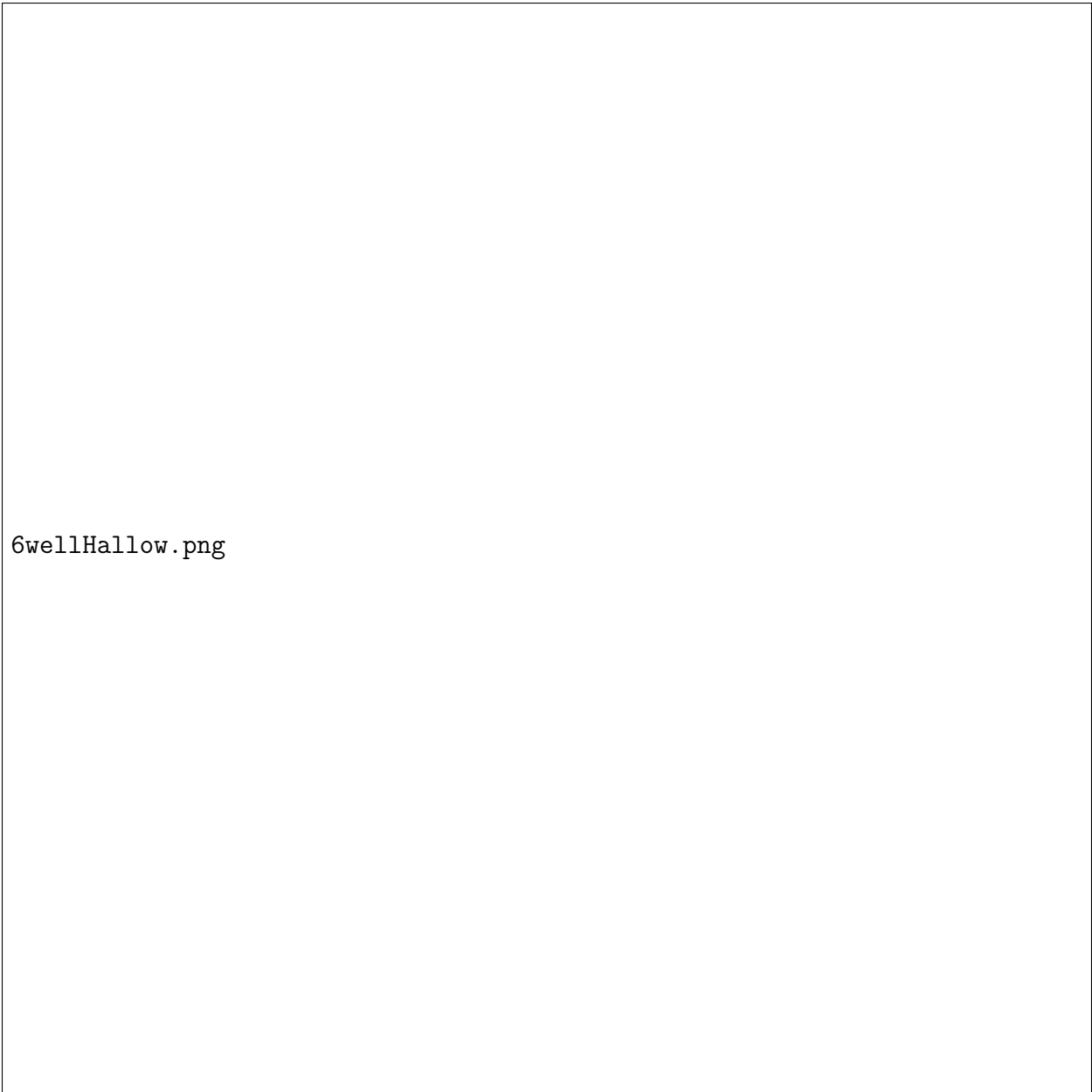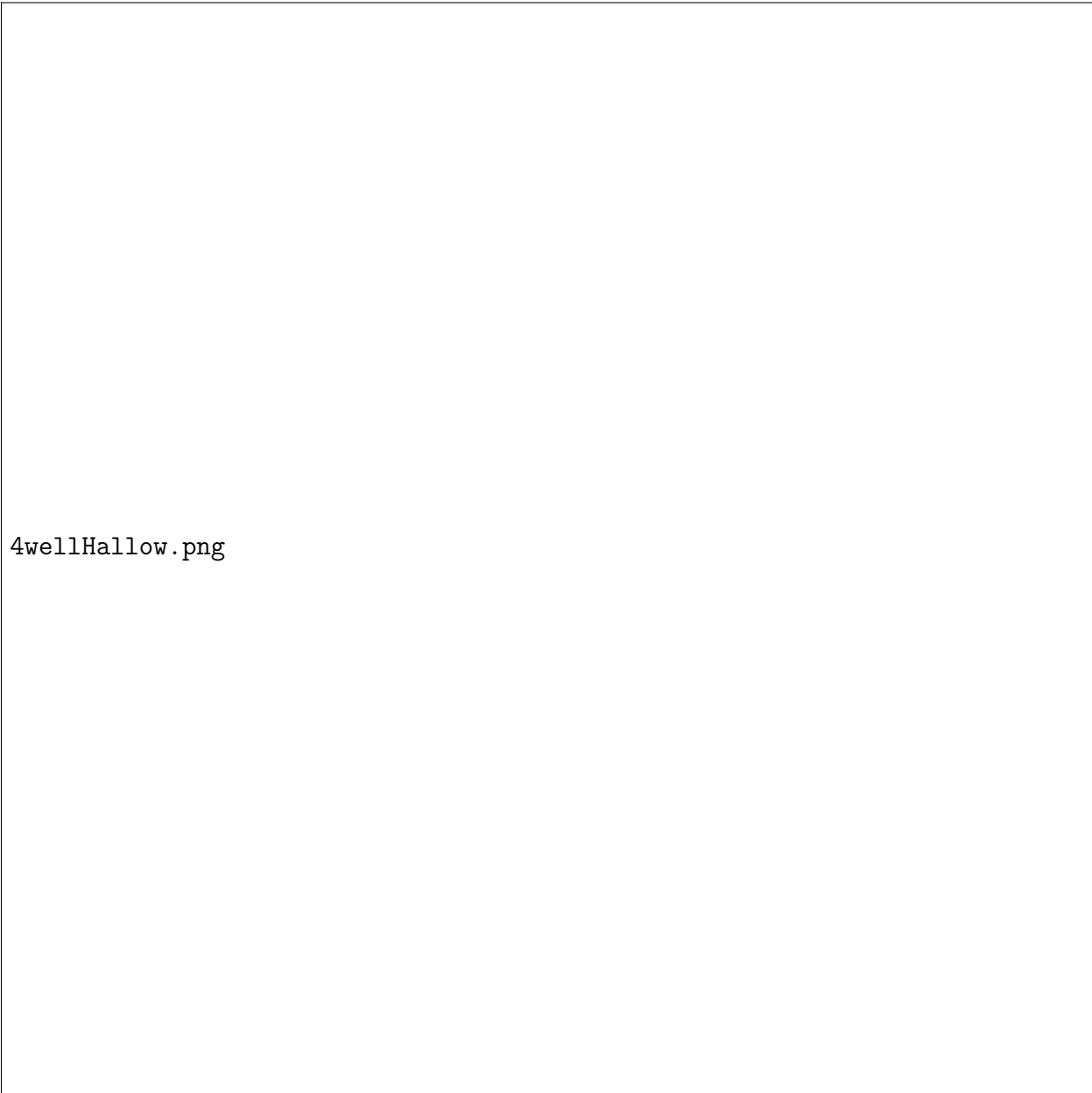
Figure 3.7: The longitudinal distribution of single airbag bunch trapped by nested square potential wells.

Figure 3.8: Instability modes for a single loop of current trapped in a series of potential wells. Note that there is no mode bifurcation as there is only a single degree of freedom in this case. The space charge tune will vary along with bunch with λ but over an oscillation will average to a single mode per sideband.

the outermost loop of current and some of inner ones that propagate slightly differently. That being said, if particles are only in a single loop of current, the bunch will regain the hollow distribution unperturbed by other loops of current and will not have bifurcating modes (Fig. 3.8).

3.2.3   The Gaussian Distribution

Gaussian beams, and others with slow decay at their edges can be difficult to model the bunch with square wells without needing to artificially cut off those particles with a large excursion from the center of the bunch. This is because it is important to have a sufficient number of particles in each loop of current. This is particularly important because the outermost loop is the one which includes the initial offset boundary condition. And therefore, if there are significantly fewer particles in this loop, it is equivalent to a smaller initial offset for the bunch overall, and will weaken the total response.

We can expect that many beams will have a Gaussian like shape, so this distribution will act as a good baseline for determining TMCI thresholds 3.9 for a normal beam. And interestingly, the space charge-less case has a similar TMCI threshold to other distributions such as those from Fig 3.8. This is because the zero mode is essentially constant, making the total rigid mode tune shift an integral of the distribution over the length of the bunch–which equals the total charge of the bunch. What is different is that this beam has significantly different space charge forces between the center and the edges of the bunch, which allows coherent modes to split quite readily from one another another.
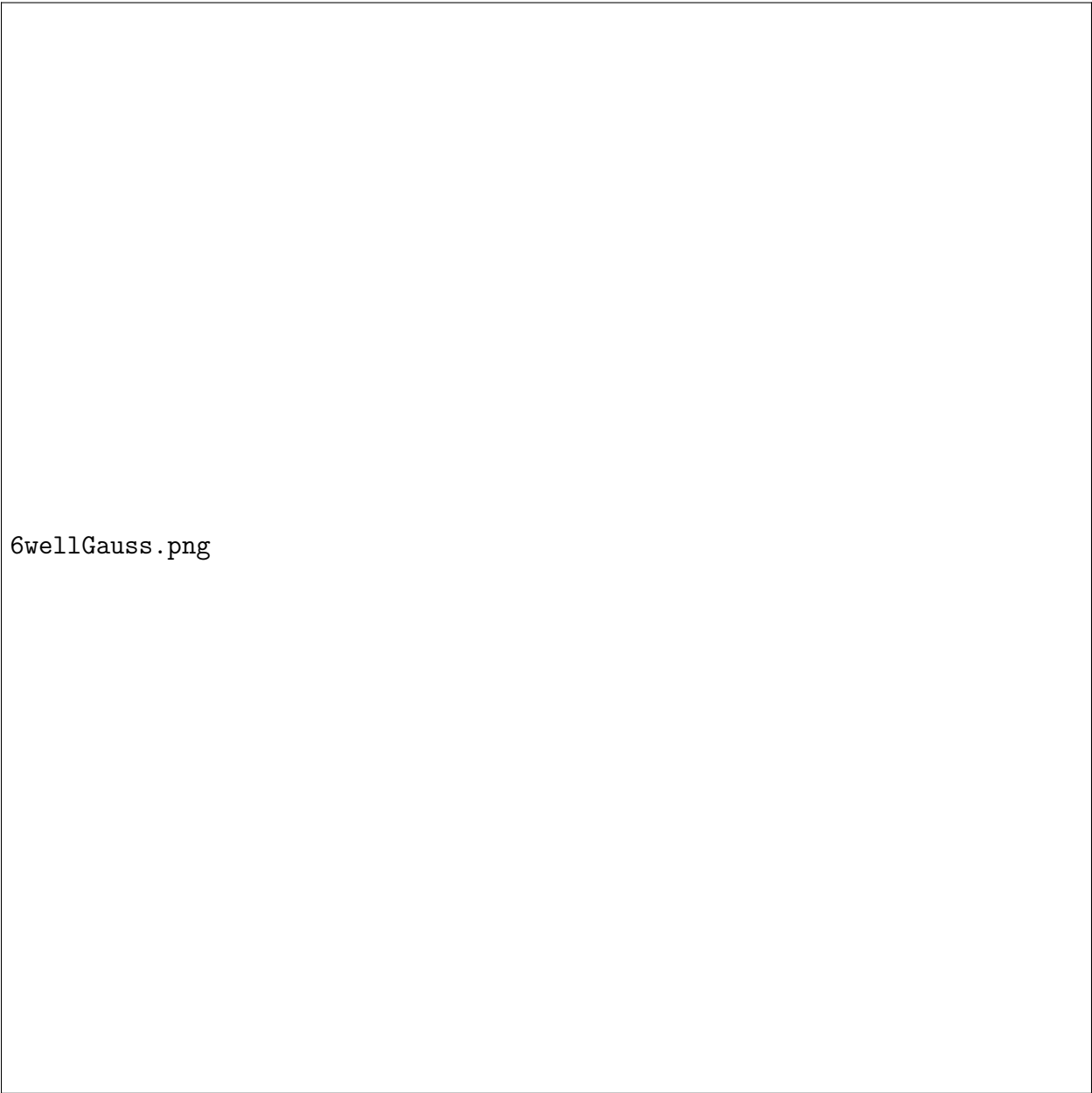
Figure 3.9: Coherent modes for an approximated Gaussian distribution with 6 loops of current. Perhaps most interestingly, it seems that that space charge-less TMCI threshold for both this and the other models are approximately the same, while space charge forces differ greatly between them.

3.2.4 TMCI Threshold Convergence

When approximating a given distribution, increasing the number of square wells (and loops of current) should improve the resolution of the approximation. For a reasonable choice of square potential wells, increasing the well number should allow the solution to converge toward the true value of such a distribution. If this does not converge or remain constrained to a small boundary, this approximation method is suspect.

To demonstrate the convergence of this method we will consider a Gaussian distribution approximated by a number N square potential well and linear RF. All loops of current will have approximately the same synchrotron tune and particle number. This will be shown in two ways, first an instability will be driven using a rigid wake which is whown in Fig. 3.10, after that is completed and instability observed, space charge will effectively dampen the instability as in Fig. 3.11. In the multiple loop cases, instabilities may also occur after TMCI is initially damped. These are due to mode splitting, the subject of the next section.

3.2.5 Bifurcating Instability Modes

Each of the N loops of current contributes a degree of freedom to bunch itself. These degrees of freedom, make it possible for multiple modes to split off from an original coherent mode as in section **??** by the physics of the system. This is perhaps most obvious when considering space charge effects where multiple loops of current can be offset to satisfy boundary conditions. These offset modes begin at the synchro-betatron sidebands. More loops of current correspond to more degrees of freedom that can be excited, which turn a sparse mode structure into a more dense one. It should be noted that these modes are still
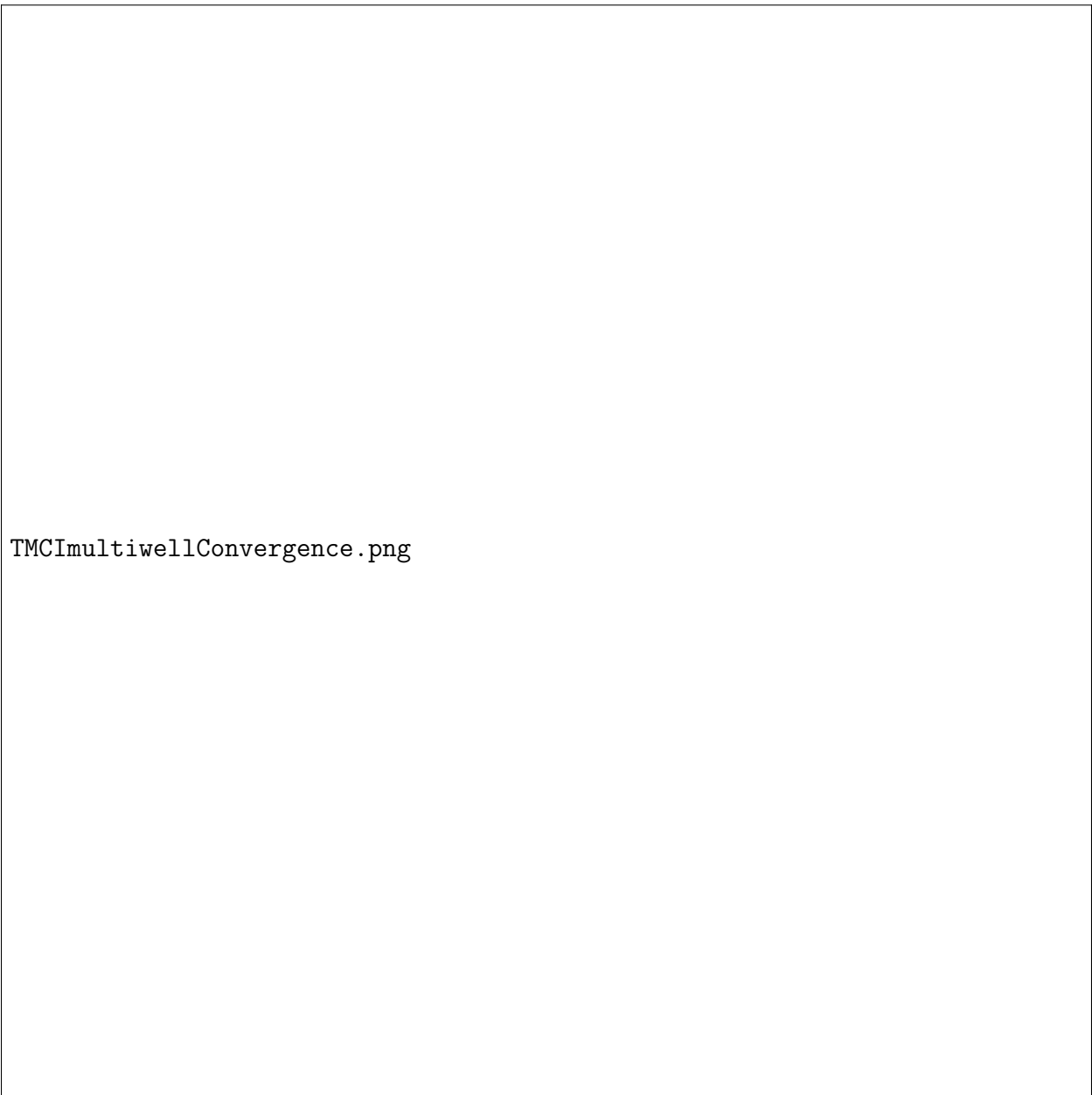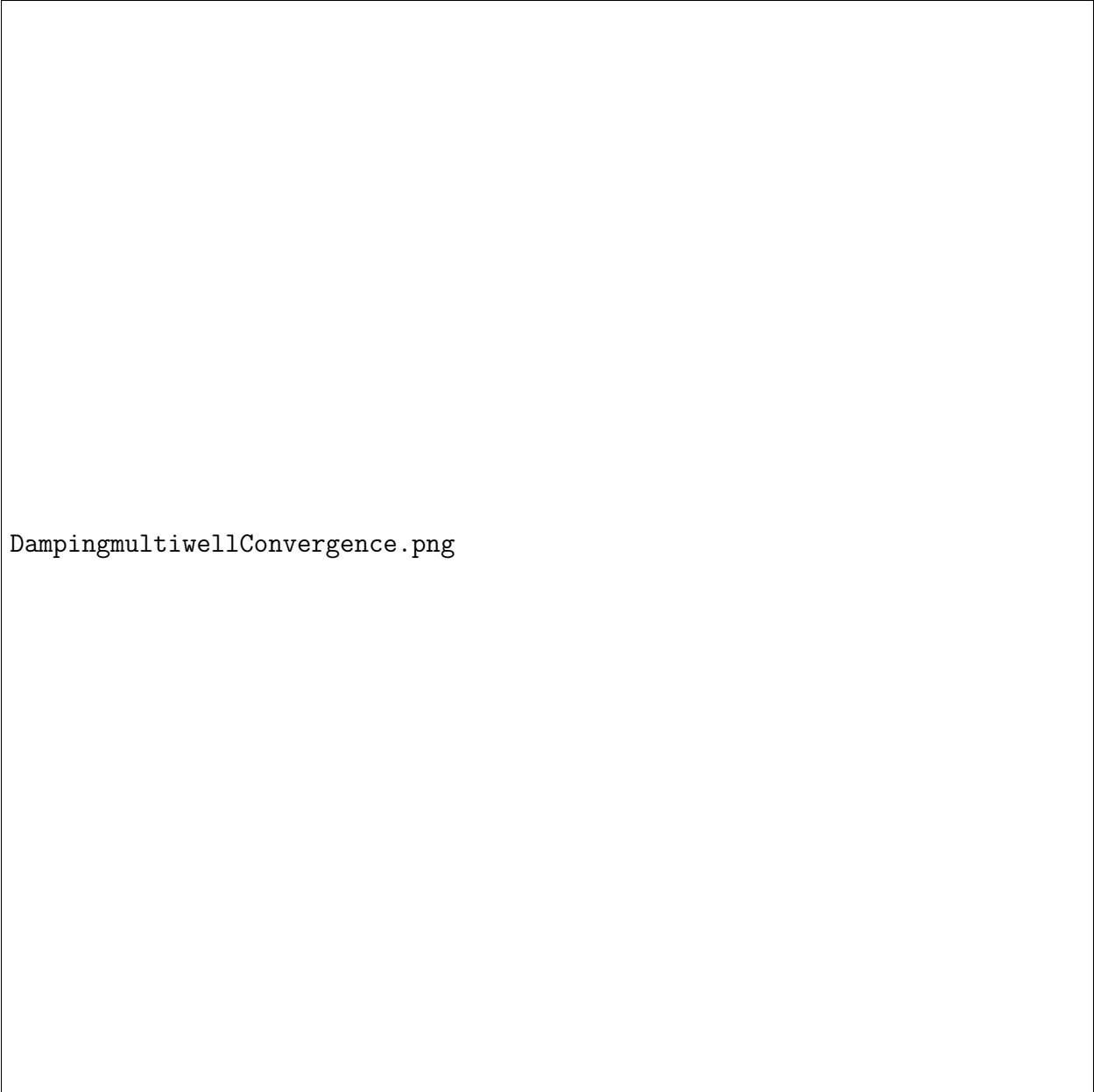
Figure 3.10: TMCI growth rate of the rigid mode of a Gaussian bunch. The threshold for mode coupling occurs when the 0 and the -1 synchrotron sidebands couple into one another generating an exponentially growth rate $-\omega_0 Im(\Delta Q_x)$. Converging threshold is observed at $\frac{w_l}{2Q_x} \approx$

Figure 3.11: The damping of TMCI with space charge with a rigid mode tune shift of $\frac{w_I}{2Q_x} = 1$, around twice the TMCI threshold. The space charge tune shift needed to dampen this instability for a large number of wells is $\Delta Q_{sc} \approx$

81

discrete and do not represent a continuum.

This has a few clear implications for the motion of the system. Space charge effects will be split into multiple degrees of freedom with each observing different average tune shifts. Thus particles dominated by the center of the beam motion can be expected to have a larger tune shift compared to a mode dominated particles at the edge of the bunches.

Each of these modes can by themselves drive mode coupling with other sidebands, but they do so in a different way due to the degrees of freedom. Modes that are from the same degree of freedom couple normally as discussed in the SWM, but if two orthogonal modes cross in tune space they will still become briefly degenerate. Such brief degeneracy of modes will cause some beam loss for the system.

It is worth noting that increasing space charge normally dampens instabilities for a single degree of freedom, but in systems with multiple orthogonal modes space charge can briefly drive mode coupling from these orthogonal modes such as is shown in Fig. 3.13. Since such modes are only briefly degenerate, with correspondingly smaller growth rates. However, as the intensity of the bunch increases we can expect these orthogonal modes to continue crossing one another making the beam likely to be unstable at high intensity.

3.2.6   Space Charge Self Effect

Additional loops of current distribute the charge among the loops. For the single well case half of the particles are in the upper filament and the other half are in the lower. Since there are no self forces, this is why the SWM has the prefactor of $1/2$ in front of ΔQ_{sc} for Eqs. 3.2 and 3.3. As more loops of current are added, this corrects itself as each filament has a relatively smaller contribution and the lack of self effect becomes comparatively less. This makes it more difficult to drive TMCI between the 0 and -1 modes of a multiloop than the
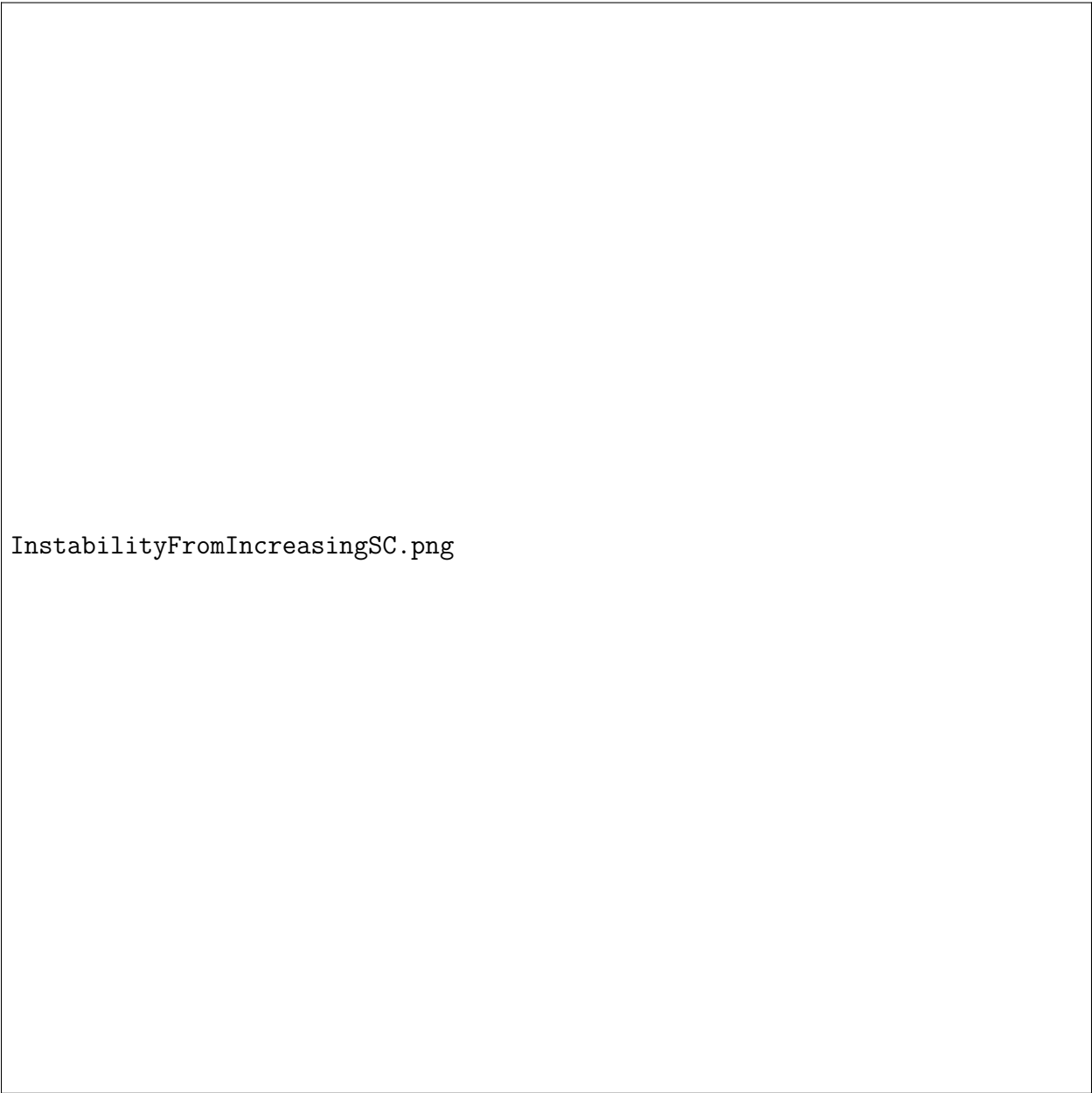
Figure 3.12: Mode structure of coherent modes at high space charge intensity without wake-fields. The real components of ΔQ_x shown in blue. Unstable modes will accompanying red dots offset by their imaginary components. The degeneracy of orthogonal modes makes this system unstable to to TMCI, which becomes worse as the intensity increases.

Figure 3.13: TMCI Threshold Portrait of a three well Gaussian distribution and single well under a varying wake strength w_l and a space charge tune shift of $\Delta Q_{sc} = 2Q_s$. Because of the lack of self effect, the single well has a lower threshold than the multiwell Gaussian.

single loop case. This can be observed in Fig. **??** which has the same scale as in Figs. 3.4 and 3.5.

Perhaps surprisingly, the negative TMCI modes are still very much the same form as the single well case. In the strong space charge regime, negative (damping) kicks can quickly drive instability.

3.3 Convective Instabilities

3.3.1 Airbag Square Well

In recent years Burov [**?**] has further expanded upon Square Well Model with his so called Airbag Square Well Model (ABS Model). This model differs from the SWM in two main ways. First of all, the model eliminates chromatic effects to make certain solutions simpler and more elegant. Secondly, it has more of a focus on the eigenfunctions of the system to derive the actual evolution and shape of the forward and backward propagating beams.

3.3.2 Spatial Modes

Since the MLSW model is a system of linear ODEs that propagate along the length of the bunch, the individual solutions are a sum of exponential solutions with complex growth rates. This means that in general this system is a combination of decay, growth, and oscillatory motion, constrined to match boundary conditions. Every subdomain of a multiwell will have different propagation making the total motion of the bunch less obvious. However just as in

the single well case it is still possible that spatial modes could drive the convective instability.

3.3.3 ABS Convective Instability

There is significant physics in the strong space charge regime where the system is stable to TMCI, but particle loss and beam quality degradation may still occur. These areas of beam degradation are due to the same convective instability that was shown in section **??**. At a high intensity, but below the TMCI threshold, the tune shift eigenvalues will be real while the bunch shape eigenvectors correspond to extreme amplification from the head of the bunch to the tail. This amplification can move the portions of the bunch outside of the dynamic aperture where particles will be lost.

The scaling for head tail amplification for modes with $n \geq 0$ is shown below. Unlike the model in the previous chapter, only those moments become convective.

It should be noted that there are two separate kinds of convective instabilities identified in [**?**], the saturating convective instability (SCI) and the absolute convective instability (ACI). The saturating convective instability will experience growth in the rear of the bunch until the system fully saturates, at which point the bunch will stop growing and become stable. If the bunch is still within the aperture, it may be transported without loss. On the other hand, if this amplification is able to drive an instability within the bunch due to head tail feedback, this system can become absolutely unstable instead.

Interestingly, there is a relatively simple way to identify whether the instability is saturating or absolute. The stroboscopic plot of the transverse centroid (plotting several turns along z) will have nodes if saturating and waists if absolute. Examples of the saturating and absolute instabilities are shown in Fig. 3.14 These are artifacts of the order of the synchro-betatron sidebands inherent in the system.
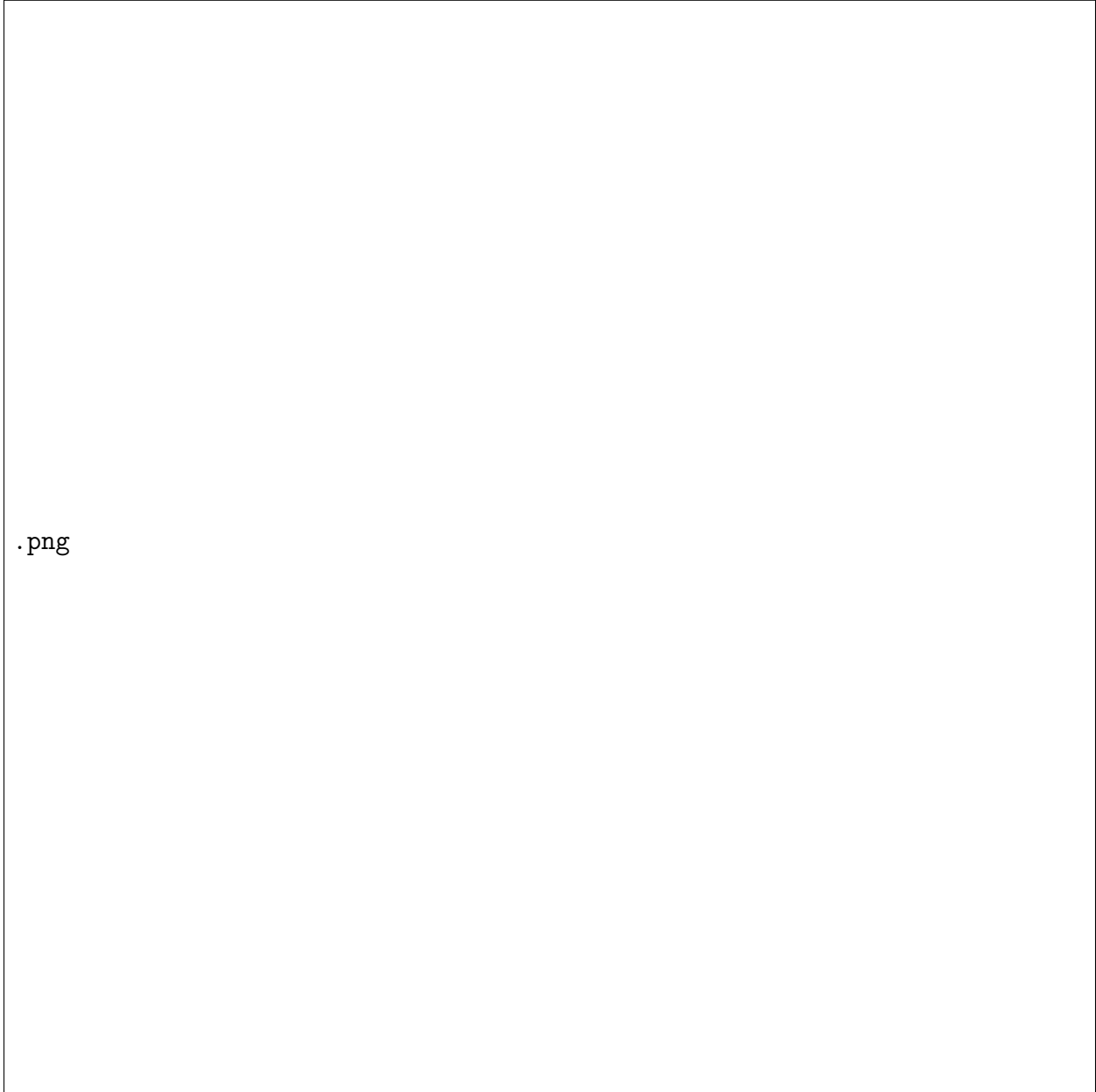
.png

Figure 3.14: The top figure shows the saturating convective instability over 20 turns. The bottom figure shows the absolute instability for the same parameters, save for tail-head feedback from including multi-turn wakefields.

3.3.4 MLSW Convective Modes

Since the initial offset of bunch particles has been set to 1 the head tail amplification is the maximum amplitude of the spatial modes. We can expect this maximum to be near the tail of the bunch as the wake will accumulate over the bunch length.

The amount of amplification that will contribute to loss depends upon the initial offset of the bunch as well as the size of the beam pipe. This makes it difficult to come calcuate a threshold for when convective modes begin to drive particle loss. So instead, we shall consider a mode as convective when head-tail amplification becomes exponential.

There are two main regions that are of interest. First is convective motion at very weak wakes and strong space charge. This region is not unstable to TMCI, but may be decidedly unstable to convective motion if growth becomes exponential. If convective motion becomes significant before the the TMCI threshold, it suggests that there is a further constraint placed on the TMCI thresholds

3.4 Chromatic Effects in the MLSW model

If there is chromaticity in a bunch, each loop of current will have a difference in the phase of the upper and lower halves of the loop. These will couple into the outermost loop to produce the total head tail phase shift χ for the bunch. In the presence of wakes, this phase shift will mismatch the boundary conditions which will need to be satisfied by the imaginary portion of the tune shift $Im(\Delta Q_x)$. If the imaginary term is a growth mode where $Im(\Delta Q_x) < 0$ the mode is unstable to the Head Tail Instability.

In the single loop case it was only possible to include a linear chromatic effect, but the more realistic longitudinal phase space in the MLSW makes it possible to observe higher

order chromatic modes.

3.4.1 Chromatically Dominated Beams

The Head Tail instability can occur below the TMCI threshold, however if the bunch is above the TMCI threshold, chromatic effects can heavily dampen the growth rate compared to that without TMCI. In the Fig. **??** we can see the strength of the TMCI alone (zero chromaticity) is near maximum instability strength.

Because there are multiple degrees of freedom within a bunch, we cannot expect to find ourselves in a region where none of the modes are unstable. However a strong chromatic effect may weaken the instability. Furthermore, it should be possible to damp these instabilities with a damping kicker[**?**].

As a benchmark to this, let us examine a hollow beam with a single loop of current. With a single degree of freedom, there should only be one set of modes for the Head Tail Instability, making it the structure simpler. We can compare this solution to Fig. 3 in [**?**] where we see good agreement.

3.4.2 Nonlinear Chromaticity

Now that we have a more complex phase space model, we shall attempt to characterize higher order chromatic effects, specifically quadratic terms of $\dot{z}$. This will make all of the loops symmetric, except the innermost and outermost loops. Because of this the inner loop will only have limited chromatic effects while the outer loop will be the most excited. In the Fig. 3.17
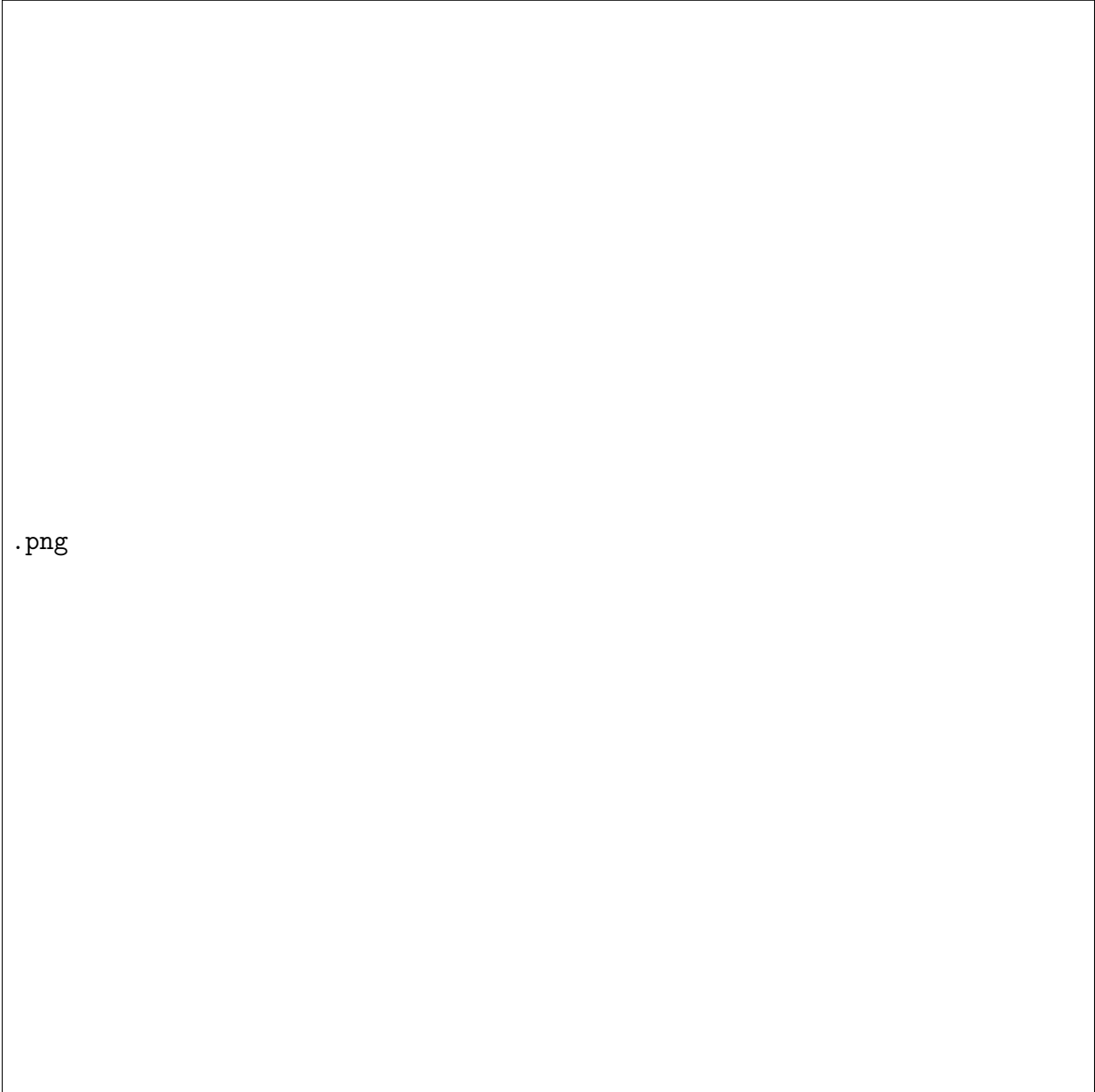
.png

Figure 3.15: The instability growth rate for linear chromaticity on the stability of a stable beam (blue) and a beam unstable to TMCI (orange). Chromaticity is expressed in nonstandard units, see section **??**
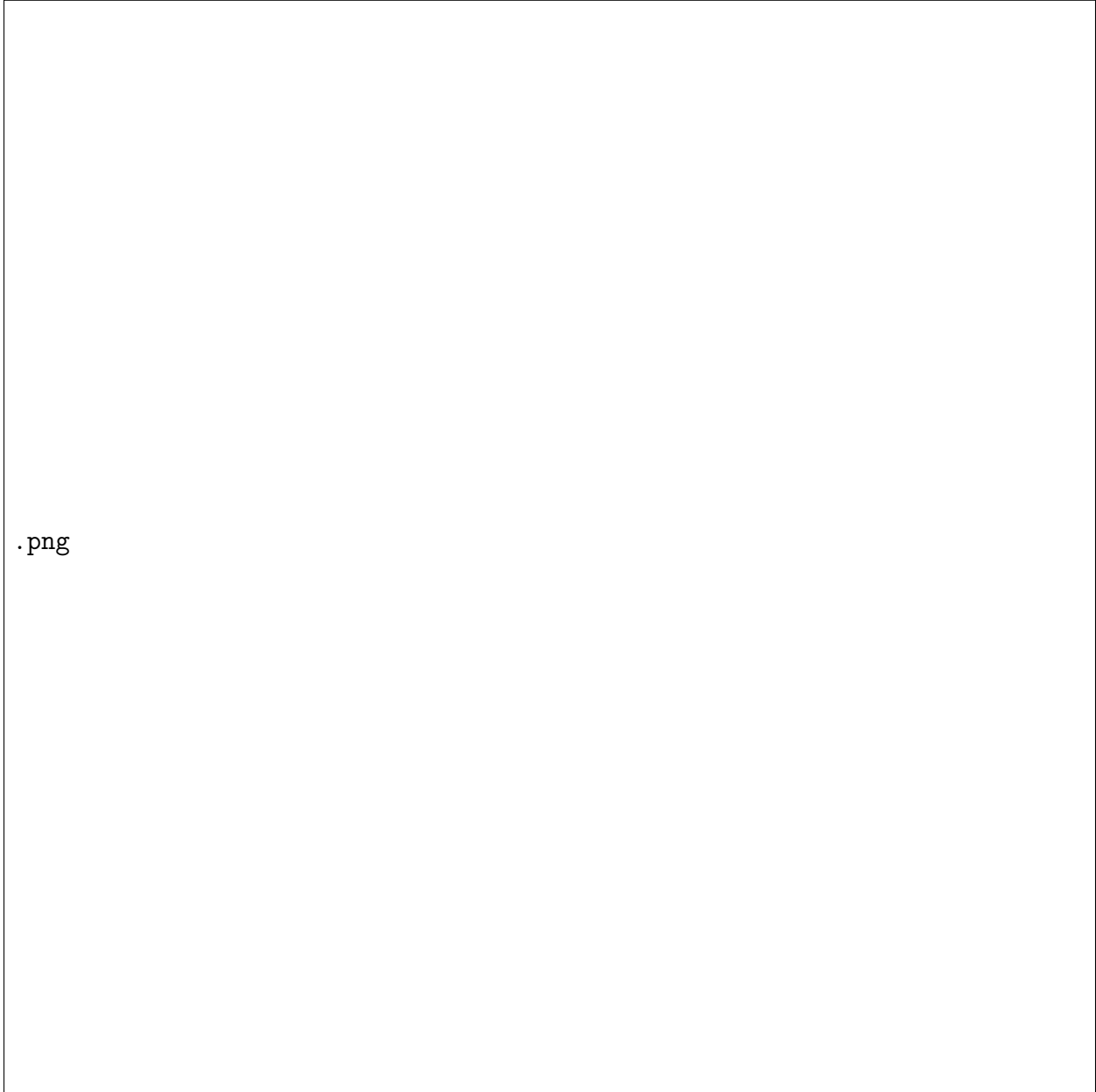
Figure 3.16: Growth rate $-Im(\Delta Q_x)$ of a hollow beam with a constant wake function and a broad band resonator for varying chromaticity. Similarities can be observed between our model, and that quoted in [?]
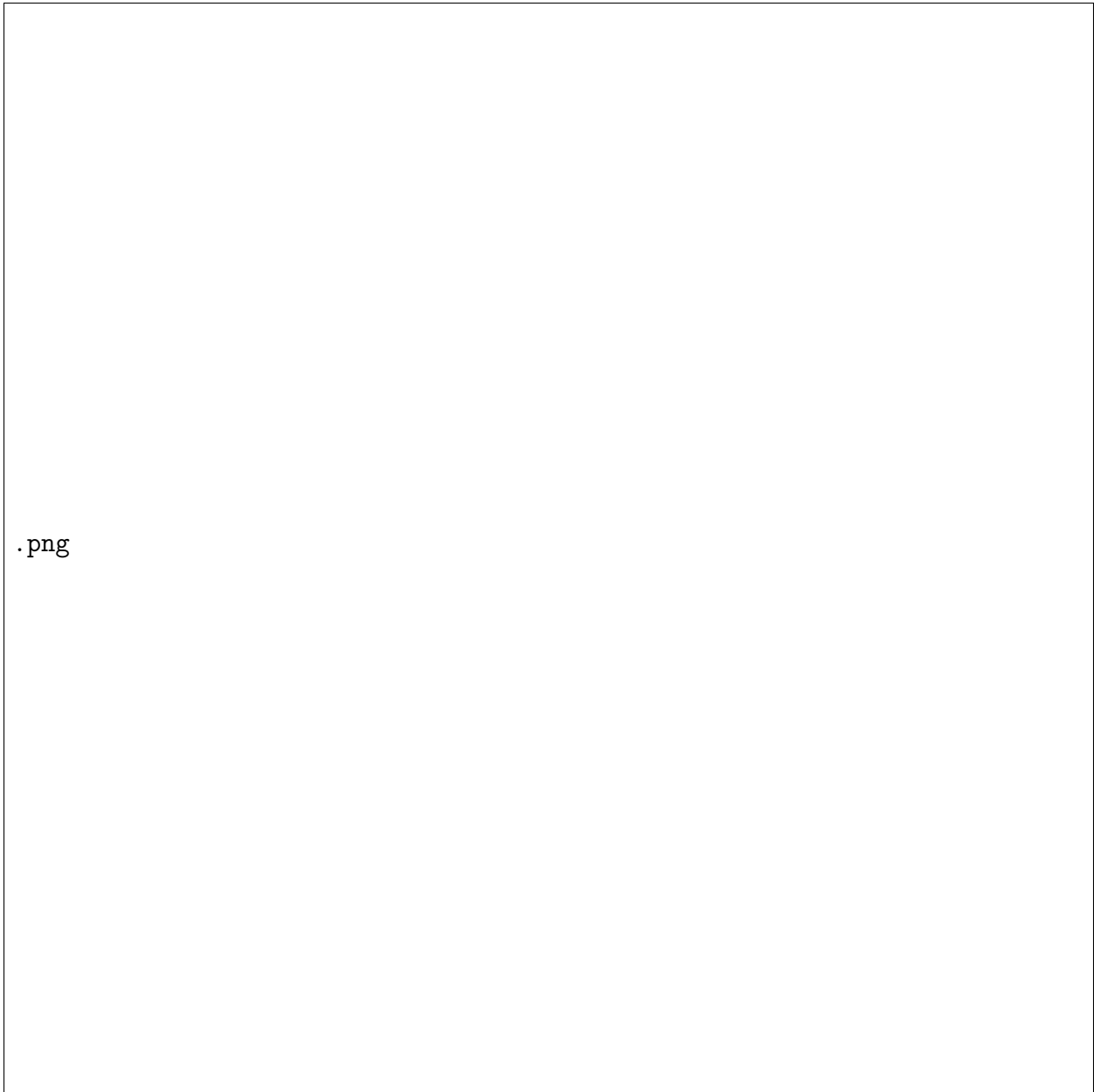
`.png`

Figure 3.17: Frequency spectra of a Gaussian beam with nonlinear cosine sinusoidal chromaticity.

3.5   Wake Impedances

Up to this point, we have focused on constant wake functions and exponential decaying wakes, since this mode, known as the rigid mode, is dominant for diffuse wakes. Over a short bunch, the wake can accumulate, but has little time to decay or evolve on its own making it approximately constant. However this is not the complete picture. Since growth can be exponential, it can also have an imaginary exponential term in it.

This means that we must also be concerned about oscillatory wake functions. These oscillatory wakes are in principle applicable to resonant structures like cavities whose high quality factor allows them to 'ring' for a long time before the fields decay. However, since cavities are localized impedance sources they will behave properly in the MLSW which assumes diffuse wakes.

Understanding these oscillatory wakes is important to determining the modes of highly unstable modes and will be the main topic for this section.

3.5.1   Tune Shifts of Oscillating Wakes

For oscillatory wake functions, we know the basics from the single square well case. Wakes with a similar pitch to the synchrotron sidebands will make it possible to drive modes beyond the zero mode. The sideband modes are more difficult to excite compared to the fundamental by about a factor of three. Since all the sidebands can be driven with similar ease, this implies that with a high enough frequency impedance it may be possible to create instabilities with arbitrarily large sideband mode numbers. This isn't realistic as we know there is some natural limit to sideband modes.

This is no longer true when we migrate to the multiloop case. Fig. **??** shows the instability

92

thresholds for mode coupling wakes, and that higher order modes are suppressed. This much more realistically limits modes to near the fundamental and is in stark comparison to the SWM. The MLSW results demonstrate that there is no need to worry about TMCI driven by some exotic high frequency phenomena.

3.5.2 Space Charge with Oscillating Wakes

Now let us move to consider a system that includes both oscillating wakes and significant space charge effects. Space charge effects depress the tunes of the system while a wake will shift a single mode or two. This shows why space charge can dampen instabilities–it shifts modes away from the mode that they would naturally couple to. This is why a negative wake constant w_l is so unstable to TMCI, with both space charge and the wake pushing coupling modes together.

There may be certain certain oscillatory wakes where space charge is no longer helpful for generating TMCI. Since oscillatory wakes shift which modes they couple to, it is possible that shifting some combination of modes may either not be helpful to damp TMCI, or even have a destabilizing effect upon the bunch. In Fig. **??**, we show the TMCI threshold for a peaked distribution.

We can validate our solutions with the code BIMBIM [**?**]. This code has some structural similarities to the MLSW as the longitudinal dynamics are approximated as well a bunch of loops of current that are then split into subdomains, but is not self consistent with regard to space charge effects and so should give at least somewhat different results. Fig. from [**?**] shows the TMCI threshold for BIMBIM. The equivalent using the MLSW is shown in Fig 3.18 and 3.19. Unlike the single square well where the thresholds for sideband wakes are close to constant, approximating the bunch with multiple loops has the threshold for the
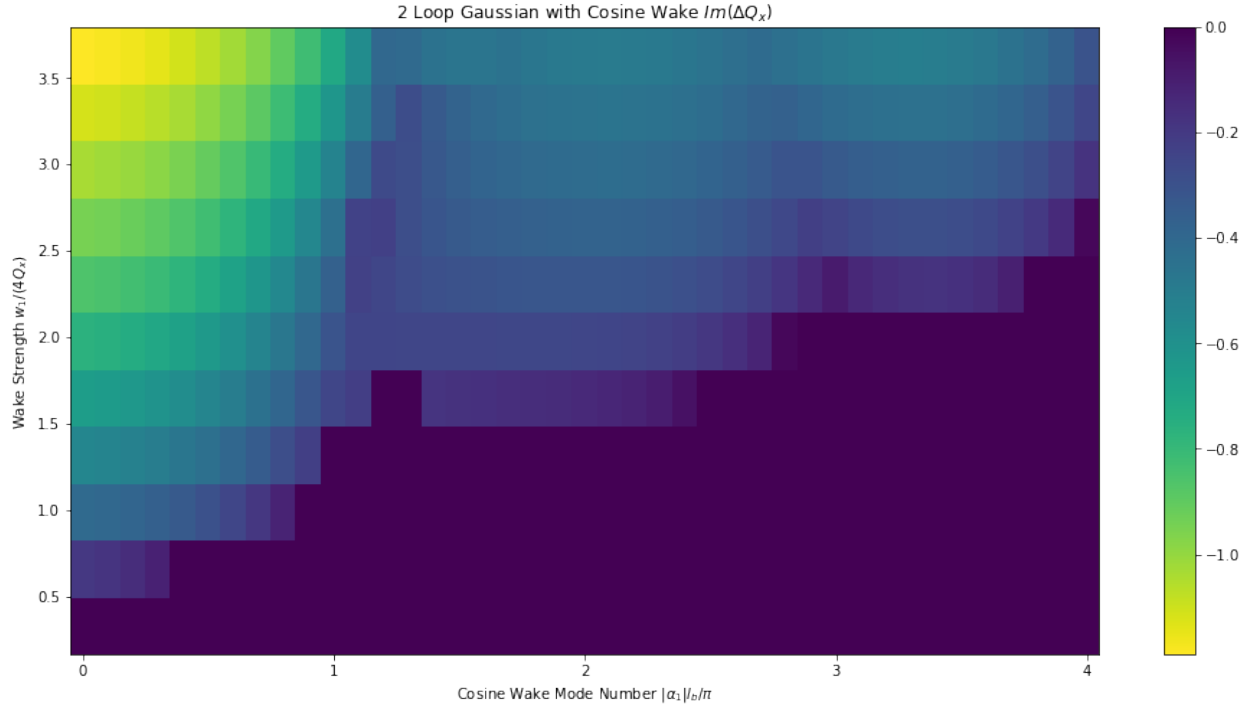
Figure 3.18: TMCI thresholds for an $N = 2$ MLSW. Note that these have good agreement with the bunches shown in similar BIMBIM simulations**??**. The two well version of this model has a slightly smaller threshold compared to the three well one.

sidebands increase linearly with sideband number.

3.5.3   Nonlinearity of Wake Functions

A key question is how many wakes are required to approximate the necessary coupling physics.

If the modes were linear this would be simple enough, as we only care about some number of physically relevant modes. If the frequency response of a wake function was linear, this could be approximated by single frequency kicks. We could integrate over the the total wake function and get the total response as a combination of individual coherent modes. However, these modes are not linear and responses change as the bunch deforms due to the input wake. Therefore, another approach will have to be taken.
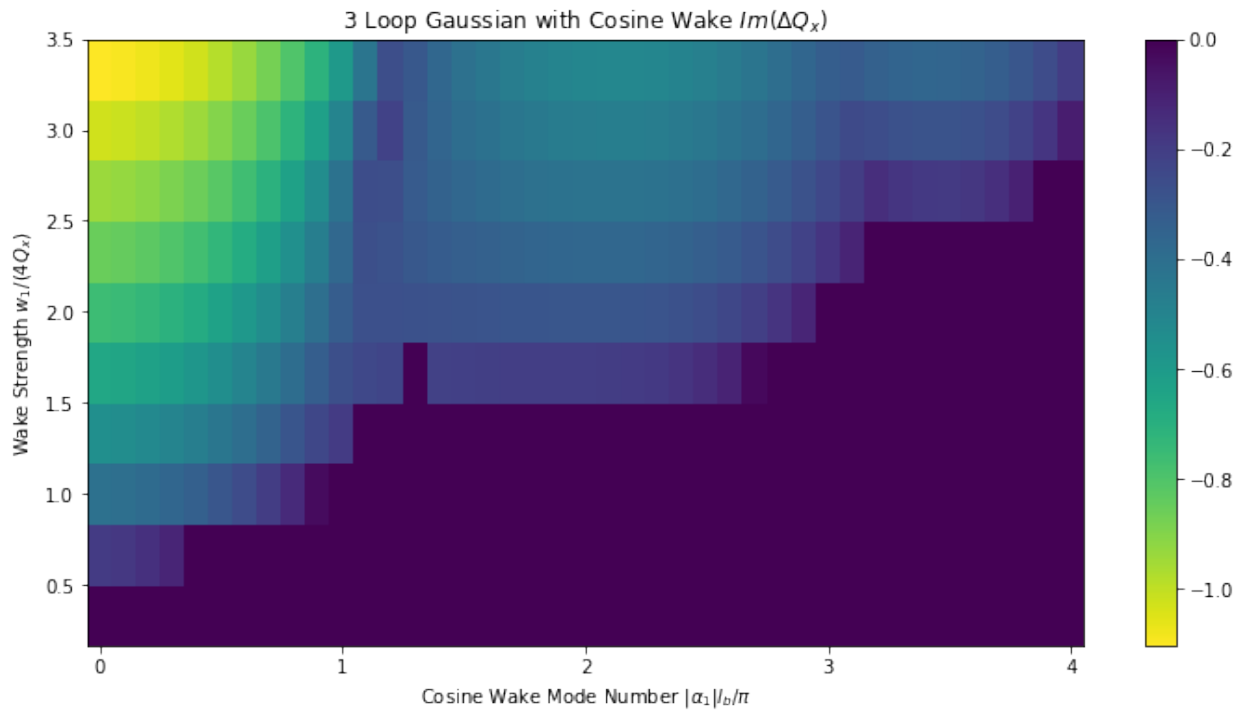
94

Figure 3.19: TMCI thresholds for an $N = 3$ MLSW. Note that these have good agreement with the bunches shown in similar BIMBIM simulations**??**. The three well version of this model has a slightly larger threshold compared to the two well one.

This is not to say that the forces aren't linear–they obviously are since wakes are electromagnetic in nature. However the total response to these forces also perturbs the bunch distribution leading to nonlinearities. Also nonlinearity tends to be accentuated by mode coupling unless the modes are orthogonal. If by prior knowledge one already knows which modes will couple, one can focus on expressing this portion of the wake physics rather than the taking a Fourier series. In Blaskiewicz[**?**] it is stated that a wake function can be approximated by three wakes in the single well case, but the applicability of this is unclear.

3.6   Nonlinear Longitudinal Motion

3.6.1   Higher Order RF Harmonics

Nonlinear terms appear naturally as higher order Taylor expansions of RF fields. If these become significant the outer loops and inner loops will have different synchrotron tunes. Beyond the natural nonlinearity, higher order harmonics can be used to deform the shape of the input distribution to something more desirable. Often this is used to decrease the peak space charge tune shift of a bunch. This flattening of a bunch is shown in Fig. **??**

3.6.2   Landau Cavity

A Landau cavity is a harmonic cavity designed to cancel out the quadratic potential terms for a given beam. Operating at full power the cavity cancels the linear term of the original sinusoid term and makes this oscillator strictly a nonlinear one. If at less than full power there will still be a linear component that weakens as the Landau cavity is energized. Because of this nonlinearity the tune will be significantly different from what one would expect in
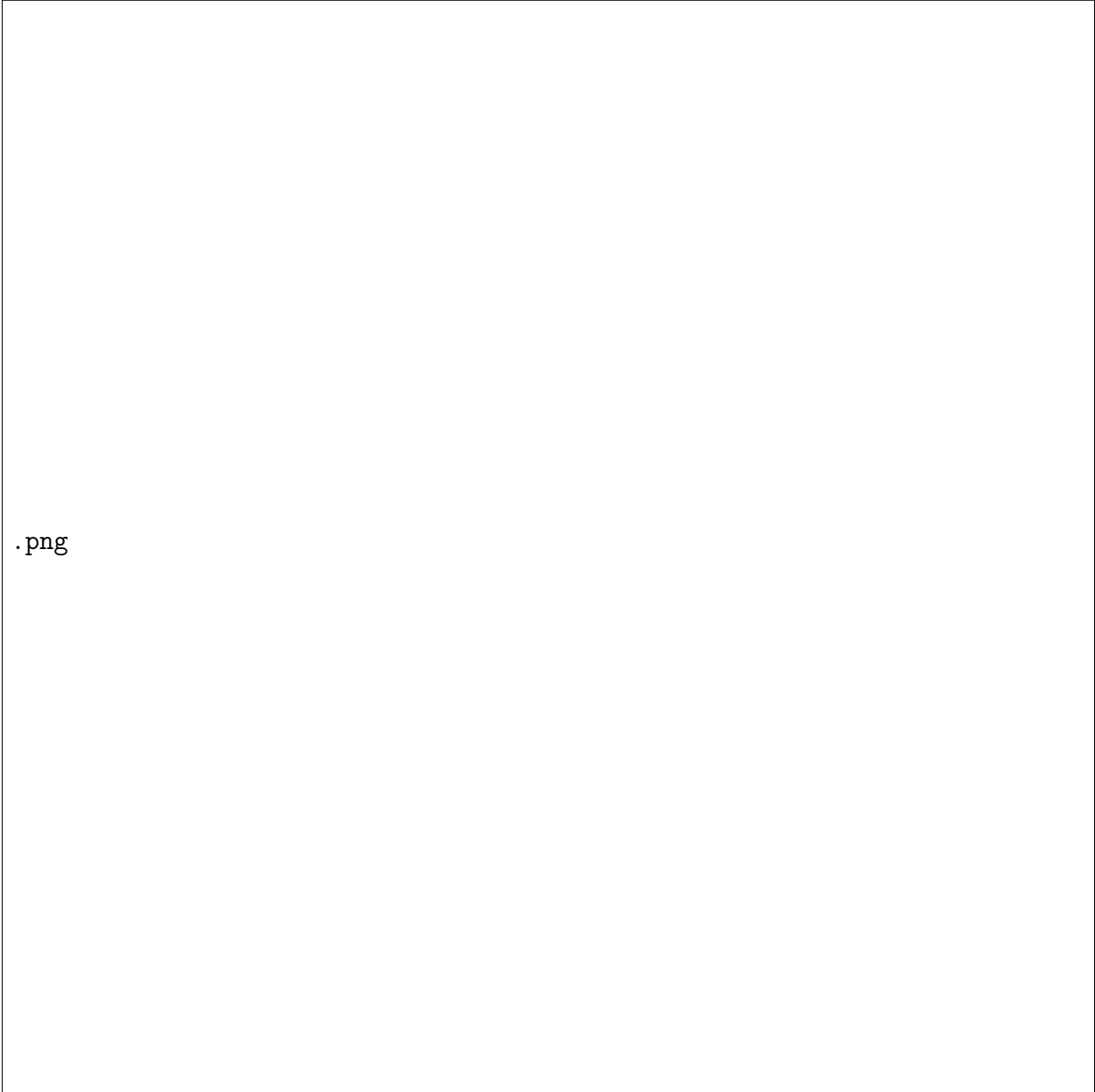
.png

Figure 3.20: This figure shows the approximated distribution function of Gaussian bunch with nonlinearity flattening the particles in the bunch due to this nonlinearity the nonlinearity is slowly and adiabatically turned on.
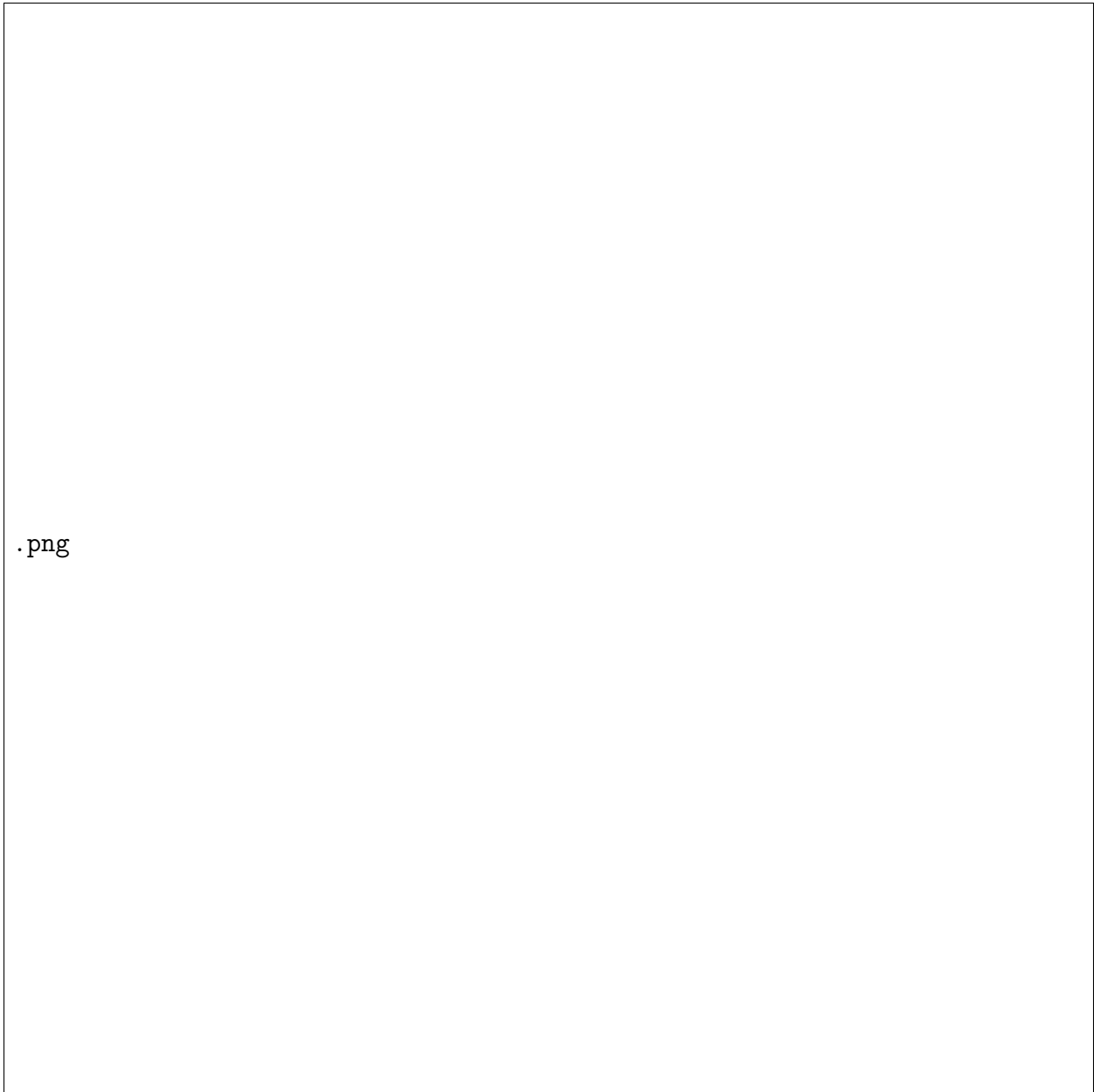
`.png`

Figure 3.21: The stability diagram with nonlinear longitudinal motion. Slight stabilization observed over the original single harmonic form.

the linear case. This cavity is normally used to induce nonlinearity and facilitate Landau Damping [**?**].

Let us consider a Landau cavity system that is unstable to TMCI when the Landau cavity is off. When the cavity is turned on slowly and adiabatically, the distribution will deform to follow the new distribution's equipotential lines. The Landau cavity will squeeze the coherent modes closer together, while dampening instabilities. If this were a linear case, smaller synchrotron modes would generally be considered less stable, so this nonlinearity will have a significant effect on the TMCI. This is due to Landau Damping within the bunch.

3.7 Damping Instabilities

3.7.1 Shifting Bunch Center

Convective motion seems to set an additional limit on the stable parameter space for mode coupling instabilities. It has been suggested that like TMCI, changing the RF and bunch shape may have a positive effect on convective motion as well. With this difficulty in mind we must ask whether there is there a bunch shape that does not give the convective motion enough space to propagate and amplify. Shifting the peak of the distribution towards either the front of back of the bunch may interfere with the growth. Fig. **??** shows the head tail amplification of a given beam with a shifted potential and a preserved betatron tune.

3.8 Coupled Bunch Modes

In the regime where wakes decay slowly compared to the distance between bunches, we must focus on how the wakes driven by one bunch effect the others. Let us consider a bunch train
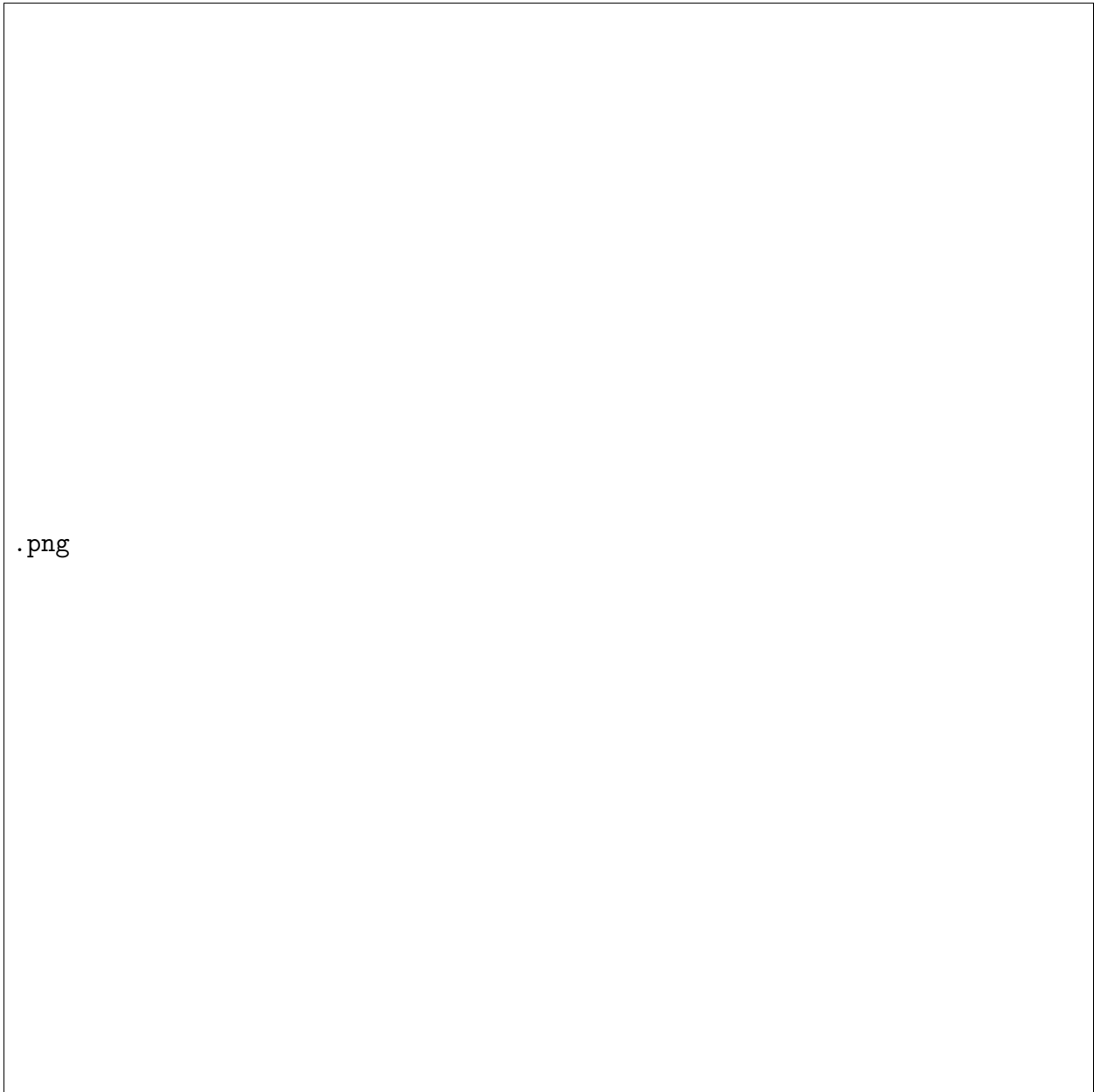
99

.png

Figure 3.22: The stability diagram for a bunch with a landau cavity. As the strength of the cavity increases, instabilities are stabilized due to nonlinear longitudinal motion.

of T total bunches that form a complete cycle around the accelerator. The coupled bunch mode number B is essentially the phase offset of the next bunch. This is a mode just like the sideband we have previously focused on for single bunch TMCI. The total evolution of the bunch will be a weighted sum of these coupled bunch modes. Therefore, if any of these coupled bunches make the bunch unstable, particle loss will occur.

Bunch trains in certain machines such as the planned EIC**??** have interbunch distances that are comparable to the length of the bunch itself. As pointed out in section **??** tracking has difficulty studying coupled bunch modes over long time periods, making this an attractive area to apply our method.

3.8.1 Short Bunch Limit

In order to test coupled bunch modes of the system, let us consider the limit where the bunch is very small compared to the distance between bunches. The results should be equivalent to that of methods where individual bunches are treated as single macroparticles.

3.8.2 Bunch Motion for EIC Parameters

With this method benchmarked, it is interesting to consider instabilities in the future EIC. Using the preconceptual design report**??**, we can model a system that is analogous to the EIC. Specifically we are interested in the fill, which takes tens of minutes, so it is possible that even small instabilities could balloon into particle loss.

Chapter 4

Experimental Verification of MLSW

It is important to verify the results of the MLSW model experimentally, but it can be difficult to do so in a meaningful way. There is a large parameter space that can be studied, but a given accelerator may not be able to access the portion of the space necessary to confirm the model.

The wake impedances are particularly difficult in this respect. The accelerator structures define the impedance and therefore the wakes making this physics more or less intrinsic to the machine itself. That is, unless wakes are created artificially with some device–a kicker.

4.1   Recycler Waker Experiment

A kicker is essentially a beam pickup with a electrode operating based off of the pickup signal. Kickers are normally designed to provide negative feedback and dampen coherent motion of the bunch. With positive feedback the kicker functions much like a wake itself, except that this wake has a resolution and function determined by the electronics rather than the accelerator structure.

Such an artificial wake makes it possible to tune parameters and drive instabilities not normally present in an accelerator, and while there are still natural wakes in the system, they can be neglected if small enough, or incorporated into the model if not.

The Fermilab Recycler Ring (RR) is a proton synchrotron that has a highly tunable

'Waker' kicker feedback system. This waker is used to drive various mode coupling insta-bilities and study them. In February 2023, an experiment was performed at the kicker to observe TMCI and Convective instabilities in the accelerator.

4.1.1 Recycler Ring Parameters

The Recycler Ring is injected to from the Fermilab Booster and was originally used as an accumulator and cooler for the antiprotons**??**. Currently, the ring accumulates protons into a more intense beam which it sends into the main injector which it shares a tunnel with. In the future it will provide an input beam used to generate muons for the g-2 experiment.

Parameter		Value
Synchrotron tune	Q_s	0.0005
Chromaticity	ξ_x, ξ_y	$-0.75, -0.16$
Betatrone tune	Q_x, Q_y	$25.42, 20.44$
Emittance	$\epsilon_{N,rms}$	2.5π mm mrad
Energy	E	8 GeV
Radius	R	528 m

Table 4.1: Parameter list for Recycler Ring from [**?**]

4.1.2 Waker Feedback System

The Waker is essentially made up of four main parts [**?**]. First is the pickup, made up of two BPMs which are at a $82°$ phase advance in order to get most of the position and momenta information. Next is the feedback system which takes the pickup data and transforms it. Then come the amplifiers which drive the kicker itself. Finally, the kicker which is a stripline that mimics a wakefield and has a bandwidth of 200 MHz. In order to obtain a good time resolution for the bunch, it must be long compared to what is resolvable by the pickup
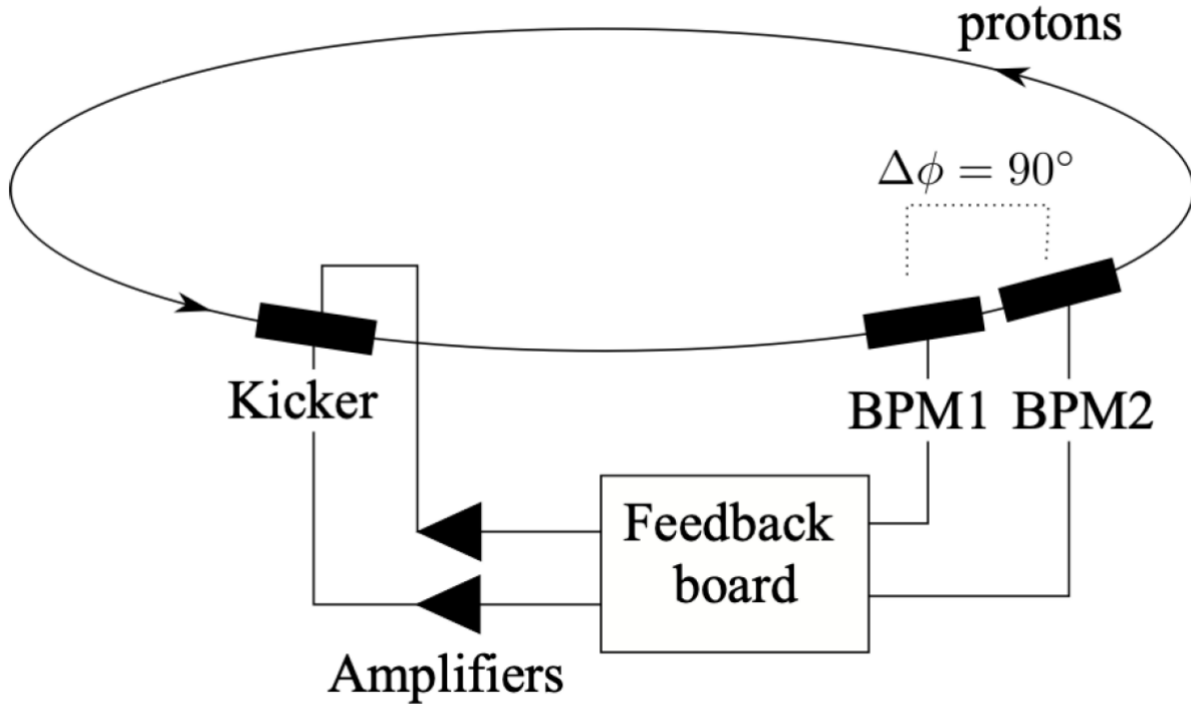
Figure 4.1: Diagram of the Waker at the Fermilab Recycler from [?]

and the kicker. The length of the bunch is around 150 ns, making the pickup and kicker resolutions sufficient.

4.1.3 Beam Position and Intensity

The BPMs and a stripline record the response of the bunch and have a sufficient time resolution to resolve bunch motion. Since these are both capacitive pickups they act as differentiators and must be integrated to give the dipole signals. These signals have two channels, the sum channel which detects beam intensity and a difference channel which detects the total bunch moment. These provide high time resolution transverse bunch information.

There are also DC Current Transformers (DCCT) which can measure the intensity of the Waker over many turns. This provides high resolution intensity measurements of the entire bunch but cannot resolve the finer structure within the bunch itself. Using this makes it

obvious whether a resonance has been crossed and particles lost, compared to the stripline and BPM measurements where it can often be difficult to determine the exact onset of particle loss.

4.2   Observing Instabilities

The objective of these experiments is to study both TMCI and Convective motion. Since these are both dipole instabilities is possible to detect them using a dipole pickup such as a BPM or the stripline. Both the BPM and stripline give similar data which is complementary to one other.

4.2.1   Coherent Modes

We known that the motion of the bunch is essentially a sum of coherent sidebands that are separated at low intensity by approximately one synchrotron tune. Nonlinearity will spread out these values, but these moments should still be resolvable. This can be performed with a normal FFT or some other more advanced method such as NAFF [?] to determine the coherent modes of the bunch.

Since we know that certain modes dominate different portions of the bunch, it is possible to enhance these signals by averaging signals from the portion of the bunch that is more heavily driven by a certain mode.

Since sideband modes can shift into one another when modes are perturbed by collective effects, a large number of turns are necessary, To obtain a finer resolution than Q_s, more than $1/Q_s$ turns are necessary. This is not however sufficient to resolve the modes or their shifts. In the run-up to this experiment, the spectrum of a 20000 turn experiment shown in
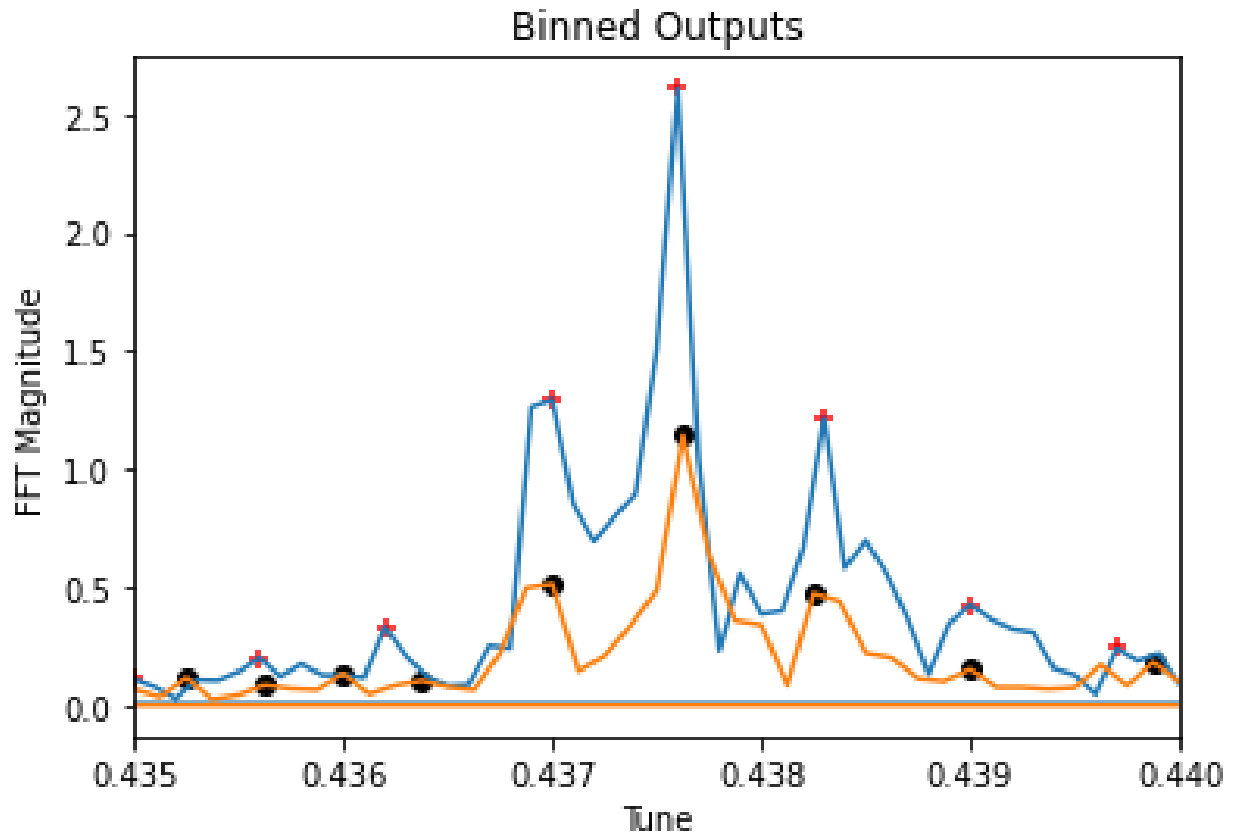
Figure 4.2: Synchro-Betatron modes of a stable beam. The orange lines show the modes before the Waker was actived, blue lines correspond to the coherent Modes after. Activating the waker should shift the center mode, but there does not seem to be a high enough resolution to observe this effect.

Fig. 4.2 shows that it is possible to resolve these modes, but additional turns are needed to improve these results.

4.2.2 Head Tail Amplification

With high time resolution measurements of the bunch along the detectors, one can determine the total dipole moment along the bunch for a given turn. If there is significant growth from head to tail, it is possible that this bunch is convective. However, this is not sufficient to prove that this is a convective mode. In certain cases, such as those outlined by Metral, et al. in [?], it is possible that a sum of normal coherent modes can interfere with one another and create something that looks convective for a short time, but isn't actually due to the convective instability.

The best way to distinguish between convective motion and a sum of coherent but non-convective motion is to ensure that these convective elements oscillate together. If these are actually different modes interfering with one another, there should be some time when the head tail growth of the bunch will reverse into tail head amplification. If the motion does not dephase like this, then this the system is undergoing convective motion.

4.2.3 Tracing TMCI Thresholds

If looking at an instability with a sharp threshold (TMCI has a sharp threshold unlike Convective Instability), it is possible to follow the surface of the instability threshold itself. This relies on the ability to carefully cross the TMCI threshold, which is not particularly difficult in negative wakes, but becomes more difficult to accomplish for positive/natural wakes due to the structure of higher loop TMCI.

4.3 Experimental Results

The experiment performed at the Recycler Waker had the following setup. The individual experiments consisted of $30,000$ turn shots, $10,000$ turns with the Waker off to begin and $20,000$ turns afterwards with the Waker on. The wakes were of the form $w_1\Theta(z-z')$ where Θ is the Heavyside Theta function and w_1 is the wake constant.

4.3.1 Non-Equilibirium Longitudinal Distributions

In order for the results to be valid, the longitudinal distribution must be an equilibrium distribution. If this is not the case, the distribution itself will oscillate. The bunch oscillation would prevent the bunch from converging to its final state, and because the bunch never converges the coherent modes will spread out.

4.3.2 Non-Convective Observations

During a number of the experimenal runs, the Recycler Ring exhibited significant oscillations of the longitudinal distribution which is shown in Fig. 4.3. This meant that we were unable to resolve the coherent modes with sufficient accuracy.

TMCI was observed in several of the experiments, most notably when the wakes became damping such as in Fig. 4.5. These did not exhibit head tail growth, but still cause loss due to exponential growth of the entire mode.

4.3.3 Convective Instability Observations

Finally we shall conclude with observations of the Convective Instability driven by the Waker. Several of these Instabilities were observed but the cleanest one is shown in Fig. **??**. This
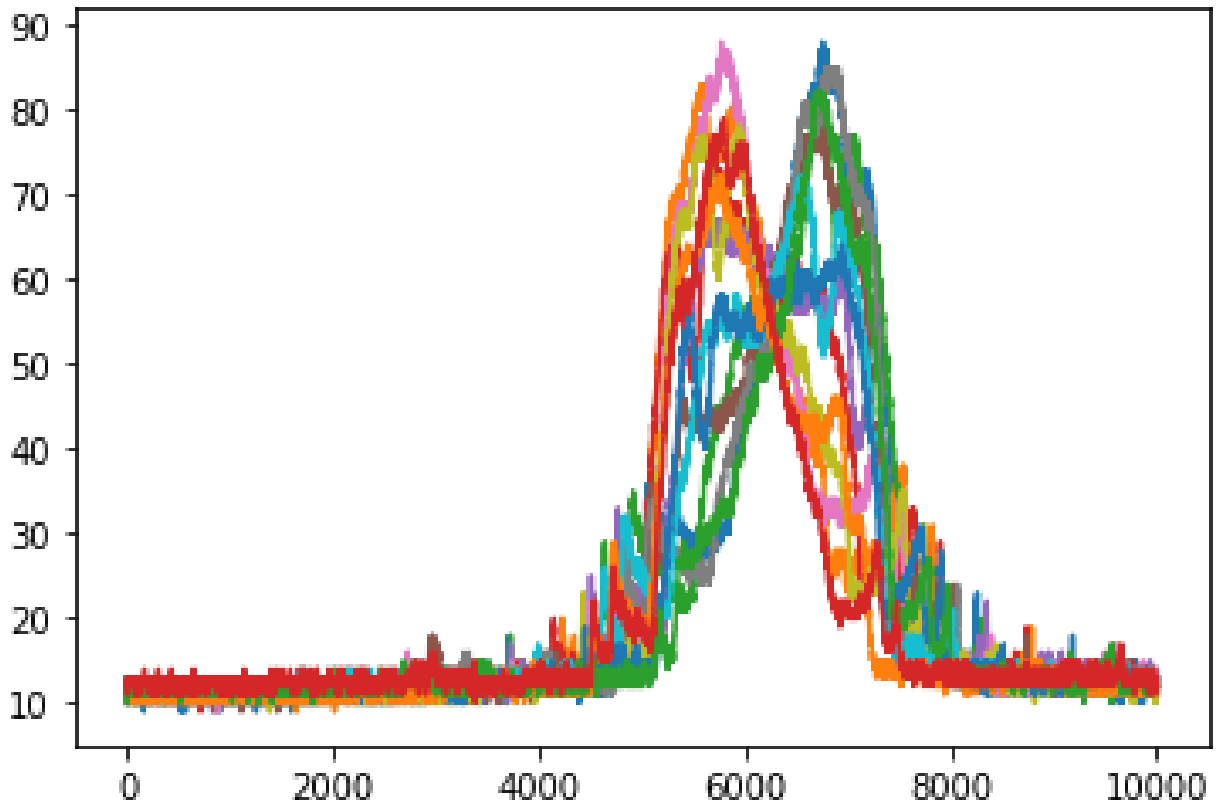
Figure 4.3: The beam intensity obtained with BPM at different turns. The head of the bunch begins at around 3000 with the tail near to contemporaneous with the edge of the measurement.
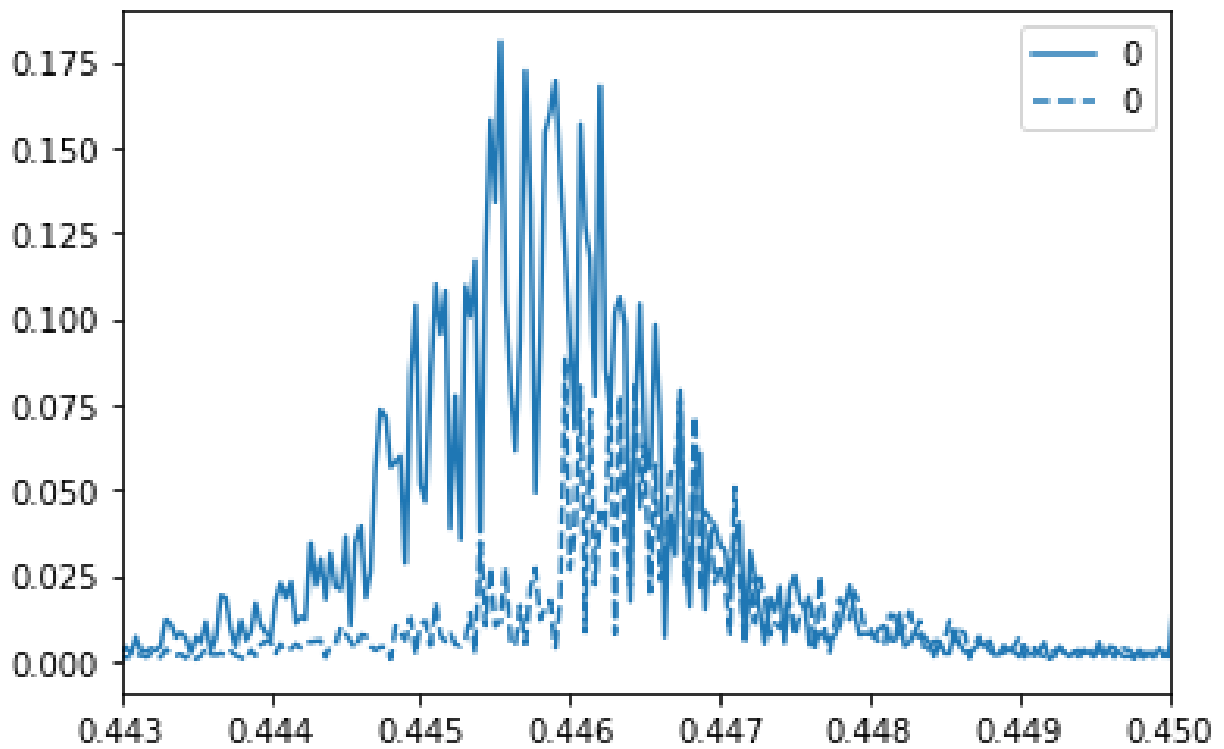
Figure 4.4: FFT spectrum of a Waker experiment. As can be seen, coherent modes cannot be resolved with accuracy. This is due to the non-equilibrium longitudinal distribution. The two colors corresponds to before the waker was turned on (blue dotted) and after it was (blue solid).

Figure 4.5: TMCI Instability observed for a damping kicker wake. A wake is considered damping when $w_k < 0$.

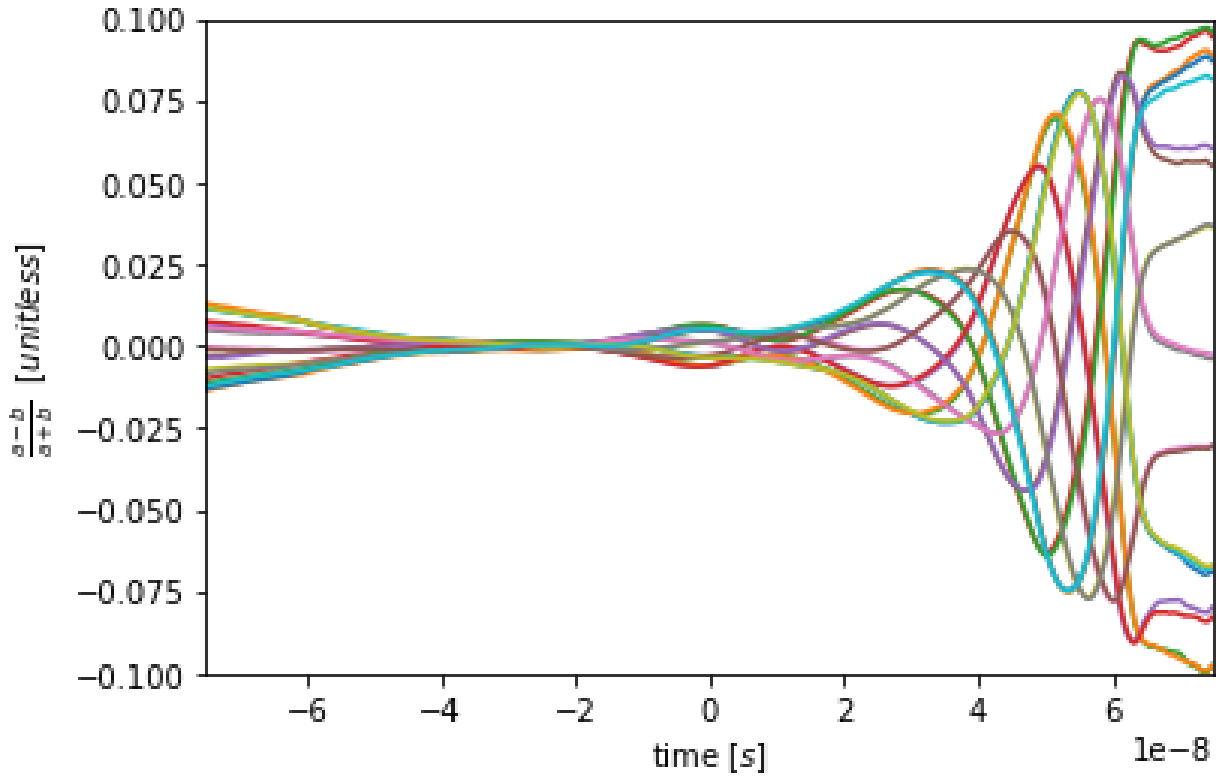Figure 4.6: Stroboscopic plot of Convective Instability observed using the Waker. Head Tail amplification of this mode is significant–around a factor of 10.

mode is convective as at no time does the system shift form Head Tail Amplificaiton to Tail Head amplification as one would expect if these were from adjacent modes moving out of phase.

This is in close agreement with the prediction for convective instabilities in **??**.

Chapter 5

Periodic Resonance at the Alternating Gradient Synchrotron

Space charge phenomena have a significant effect on more than just coherent instabilities. Resonant particle loss, essentially particle loss due to resonances between a particle's tune nonlinear optics will be changed by the presence of intense space charge effects. In order to study one example of this known as Periodic Resonance, experiments were performed at the Alternating Gradient Synchrotron (AGS) during March and April of Run 22.

The AGS is a synchrotron in the Brookhaven National Laboratory (BNL) Collider Accelerator Complex which injects into the Relativistic Heavy Ion Collider (RHIC). It has two partial Siberian Snakes?? to preserve the polarization of ions and has a 1 Hz acceleration cycle. After the EIC (Electron Ion Collider) is completed, the AGS will instead inject into the EIC ion ring. The bunch is injected into the ring at 144 ms (0 ms is the bottom of the AGS ramp) and will remain at this low energy before being later accelerated. Space charge effects are expected to be most significant during this initial injection period. Due to the rapid repetition rate, experiments must be performed in single rep snapshots rather than by sweeping parameters.

5.1 Space Charge Driven Resonance Crossings

High intensity resonance crossings operate somewhat differently from low intensity ones. Essentially this is whether we can consider the bunch as approximately point-like in tune space, or whether nonlinearity and space charge are strong enough to form a large tune footprint. The high intensity regime is indicated when the width of the resonance is smaller than the the bunch's tune shift. This structure is often referred to as the space charge 'necktie', the characteristic footprint of the bunch in tune space. An example of multiple space charge neckties is shown in Fig. 5.1. The particles on or close to a resonance line will interact with this resonance and cause an emittance growth and/or particle loss. The large size of the tune footprint means that it is more difficult to choose a working point for the beam that won't be resonantly excited. The space charge necktie has a loose correspondence to its location within the bunch–the maximum tune shift is situated at the maximum particle density of the bunch, while the edges of the bunch oscillate at what is essentially the single particle lattice tune.

The strength of a given resonance can be explained in a couple of ways. This derivation utilizes what is known as a driving term integral[**?**]. The driving term integral is the strength of a given multipole (in this case a sextupole) and a phase factor:

$$G_{0,3,l}e^{-i\xi_{0,3,l}} = \frac{\sqrt{2}}{24\pi} \oint \beta_y^{3/2} K_2(s) e^{-i[3\psi_y(s)-2\pi(3Q_y-l)s/C]} ds \tag{5.1}$$

$$G_{\pm2,1,l}e^{-i\xi_{\pm2,1,l}} = \frac{\sqrt{2}}{8\pi} \oint \beta_x^{1/2}\beta_y K_2(s) e^{-i[3\psi_y(s)\pm2\psi_x(s)-2\pi(Q_y\pm2Q_x-l)s/C]} ds \tag{5.2}$$

Where K_2 is the magnetic field strength of the sextupole field, β is the betatron function, ψ

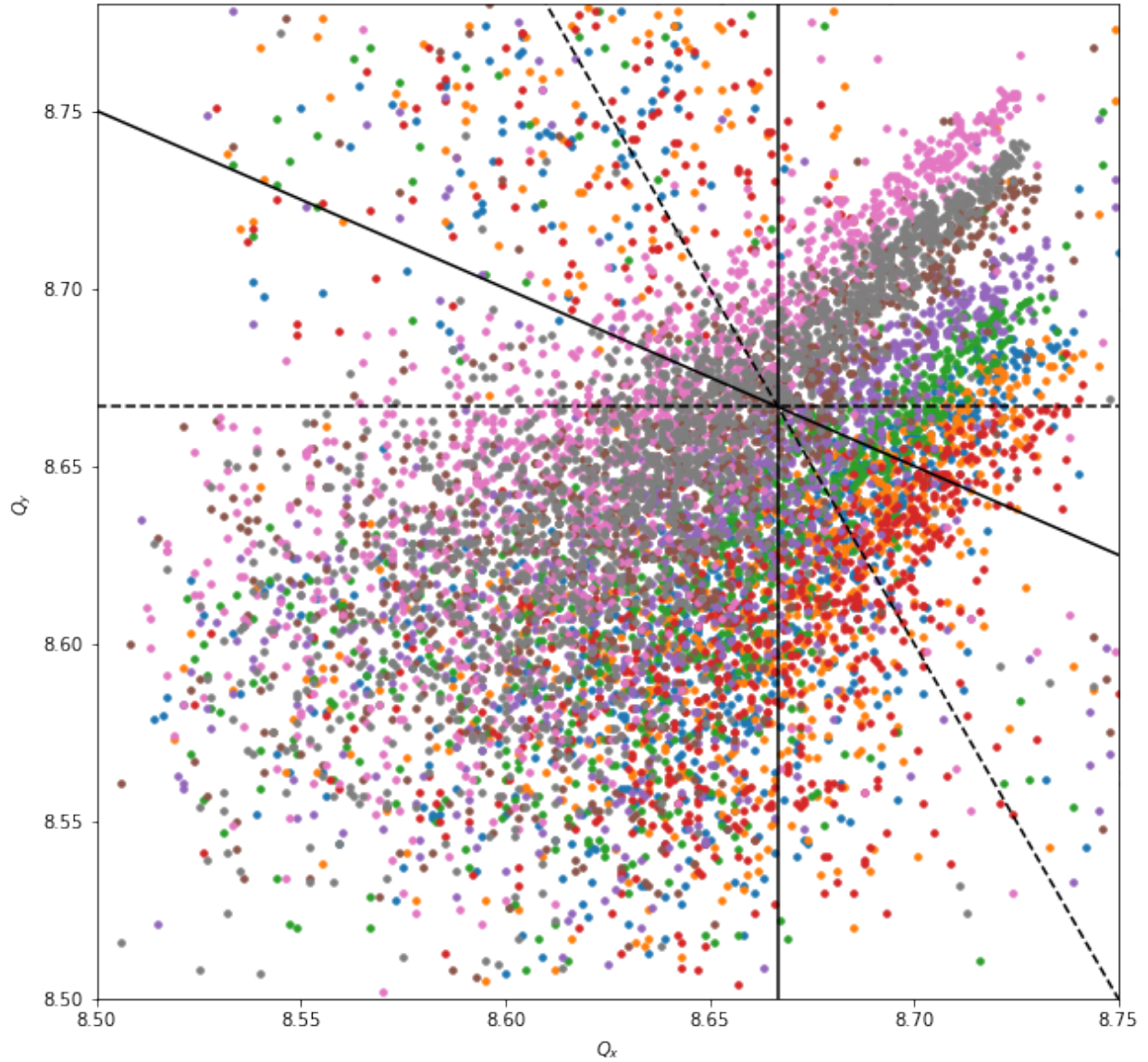Figure 5.1: Simulated tune footprint at AGS injection using PyORBIT. The solid black lines are resonances, with the dashed lines $3Q_y = 26$ and $2Q_x + Q_y = 26$ corresponding to the exited resonances of interest. At this ΔQ_{sc}, resonance crossing would be significant even for initial conditions where bunch growth or particle loss was not observed, implying that the AGS tune shift at injection is smaller than this.

is the betatron phase, ξ is some accompanying phase factor, and l is the integer resonance. Physically we can think of this driving term as a kick. Over one turn there is some total kick to the bunch. If this kick is in resonance with the tune oscillations, this leads to greater excitation with each revolution. If not on resonance these kicks will average out.

5.1.1 Periodic Resonance

Periodic Resonances are a special type of space charge-driven resonances where the tune footprint of a bunch crosses a resonance line. Particles undergoing synchrotron motion will cross these resonances repeatedly over the space of multiple synchrotron periods leading to a large total kick.

This class of resonance is naturally self-stabilizing. Both emittance growth and particle loss can decrease the space charge effect and contract the system's tune footprint. With enough emittance growth or particle loss, a bunch may no longer cross such resonances.

There are two main types of Periodic Resonances that we can expect to observe. These are the Trapping and Scattering resonance regimes.

5.1.2 Adiabaticity Parameter T

It is possible to differentiate between these regimes with a so-called Adiabaticity Parameter. which is defined in Franchetti, et al. [?] as:

$$T = \frac{1}{Q_{isl}\Delta_L}\frac{\partial L_{fp}}{\partial n} \tag{5.3}$$

where Q_{isl} is the tune of the islands, Δ_L is the size of the islands in phase space, and L_{fp} is the location of the fixed points of the bunch. For small T we are in the adiabatic regime and

particles will be trapped on stable islands if the islands are large enough. Particles in these islands will not experience substantial loss or emittance growth and we can expect that the bunch shape will not be significantly shortened since the particles are evenly distributed in the longitudinal direction. Alternately, if the parameter T is large we are in the non-adiabatic regime, and we expect bunch shortening due to particles scattered by the resonance crossing. Particles with large oscillatory amplitude in z are excited as they cross this resonance multiple times per synchrotron period. Without islands of stability, these particles will be lost. This will continue until particle loss and emittance growth move the tune shift above the resonance.

5.2   Electron Ionization Profile Monitors

Ionization Profile Monitors (IPMs) are beam diagnostic devices designed to project the transverse distribution onto a detector, effectively imaging the beam. The operation of such a device can be described as follows:

The beam passes through a residual neutral gas, ionizing some of the gas into a plasma of electrons and ions. The charged particles are accelerated to electrodes with either the ions or the electrons impacting a readout detector known as a Microchannel Plate (MCP). The MCP is segmented into multiple channels (AGS eIPMs have 64) which each detect and amplify input signals. Because of the segmentation of the system, the transverse projection is separated into bins by the hardware itself.

5.2.1 Electron IPMs

It is in principle possible to collect either electrons or ions on an MCP, with an electron IPM called an eIPM. Since electrons are much lighter than the residual gas ions, electrons will have a much more rapid time response bit worse space charge effects deforming the projected profile. The more rapid time response makes it possible to obtain turn by turn profile measurements. Our resonances of interest will be quite rapid, so eIPMs are necessary to observe the growth as it happens.

Such eIPM measurements are useless if free space charge effects perturb the results too strongly. Although it is possible to use the binned events to simulate the ionizing beam[**?**], space effects can be countered by including a magnetic field oriented normal to the MCP. This field constraints particles to a radius that is $\propto mv_\perp/B$ where $v_\perp$ is the velocity perpendicular to the field and B is the magnitude of the magnetic field. If the radius of the field is smaller than the MCP bins, this will give a similar signal to that of a space charge less eIPM. It should be noted that this magnetic field will perturb the beam itself, but is small enough to not significantly interfere with it.

Two eIPMs are installed in AGS straight sections, one in the horizontal plane at D5 and the other in the vertical plane at D15.

5.2.2 Calibrating AGS eIPMs

The performance and collection efficiency profile of eIPMs can change over time. Without frequent calibration, the drift in eIPM performance can make results unrealistic. Calibration of the eIPMs is performed by sweeping an already characterized beam across the eIPM and correcting the responses correspondingly. The bin corrections are a constant offset as well
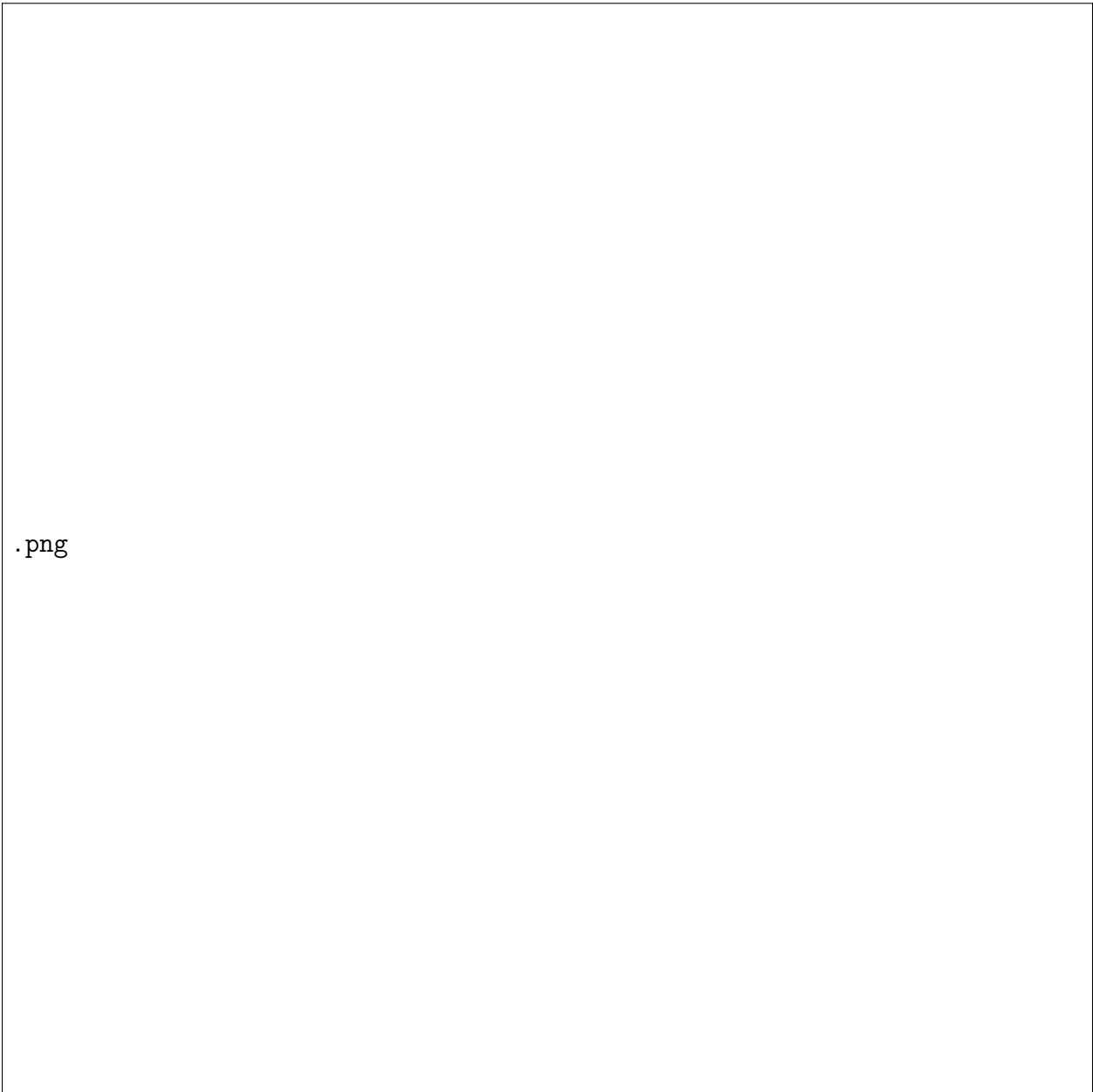
.png

Figure 5.2: Diagram of the AGS.

as a linear factor adjustment. Higher order terms may exist for especially intense beams but are not specifically corrected for.

Unlike AGS ion IPMs, AGS eIPMs can take turn by turn measurements. These can be averaged over a number of turns to decrease statistical error. Since ionization and counting are stochastic processes with comparatively few events, this statistical error is significant. Due to degrading eIPM performance, systematic errors cannot easily be quantified. For these experiments the error in bin measurement will be defined as the standard deviation of the counts.

5.2.3   'Dead' Bin Signals

If a beam bin gives results which are obviously erroneous, that bin is excluded and set to a zero sensitivity. This is not optimal however. This cutout from the distribution can make it difficult to fit a characteristic distribution to the bunch or calculate the emittance. This can be solved somewhat by averaging the adjacent bins to get an estimated value. With this, bunch size can be measured using the full width half maximum (FWHM) or another method. Our interest is primarily in relative bunch growth so this method will be sufficient. It should be noted that because the Periodic Resonances may deform the bunch shape, it is not advisable to use an assumed distribution to calculate the emittance in this case.

Not all 'Dead' bins are caught by the calibration step. It was observed that during the experiment certain bins had anomalous behavior. On alternate turns these bins registered anomalously large signals followed by signals of the correct order but uncorrelated with beam intensity. Since these signals were not automatically excluded from the analysis, this led to spikes in the observed emittance as shown in Fig. 5.3. These bins were identified and removed during post processing to eliminate these spikes.
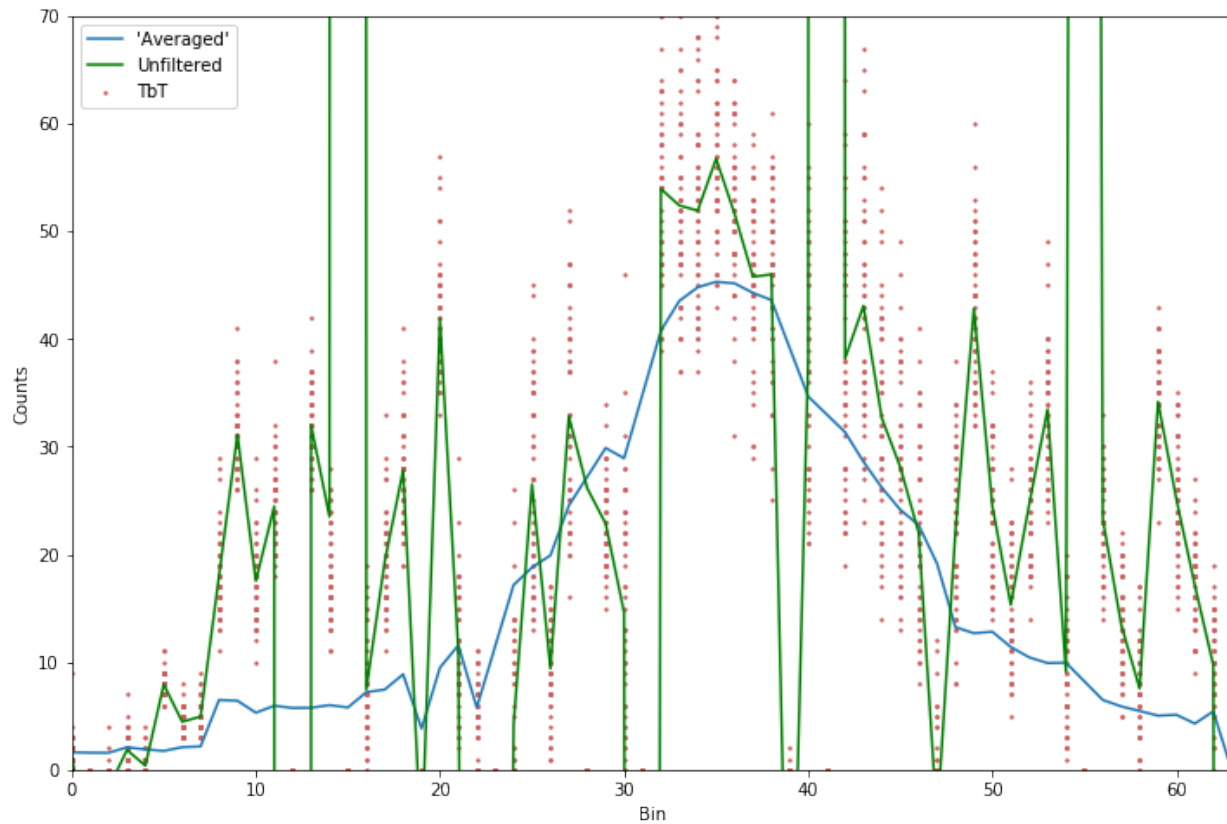
Figure 5.3: Example of eIPM calibration for 50 turns taken at injection (144 ms), The initial signals (red dots) are averaged to give the original signal which are averaged (green line). The calibration correction is applied. Dead bins are then removed with smoothed signals put in their place.

The source of these dead bins was not identified, but several observations can be made. eIPM performance can degrade from long-term damage to the system, but not all degradation in signals is permanent. Limiting eIPM use may regenerate some of the original performance of the device. And because the functioning of these bins can be intermittent, calibration may misidentify these as properly functioning bins. As a note, RF does not appear to correlate with eIPM dysfunction, exhibiting the same dead bins when RF is off..

5.2.4 eIPMs as Intensity Monitors

There are dedicated monitors in the AGS to quantify the bunch intensity. The wall current transformer (WCT) has a robust response with the ability to determine the peak of a given resonance as well as the saturated intensity after resonant beam loss. Because eIPM events scale with intensity, it is possible to use them in a mode where they also act as bunch intensity monitors. This is useful to double check the WCT data and to act as a backup if the WCT is offline. The other advantage of an eIPM is that it provides a true statistical measure of the count errors (which is not available with the WCT). This gives true turn by turn data, however the window size limits the ability to identify beam loss as it occurs. Using this method, the relative intensity of a bunch is proportional to the number of calibrated events per time, while the average survival rate for a particle from one time to another is the ratio of the final over initial intensities.

An eIPM used in this way can be expected to display some systemic errors. Mainly, these are calibration errors and errors due to dead wires. Each bin has its own calibration and its own error. The error of a bin at some initial time will be correlated with the error at some later time. Because of this, there is a correlation between the shape of the bunch (which bins it is divided into) and the associated error. This effectively increases the contribution of

these errors to the total calculated current. Because of this, as the bunch grows one expects to observe errors when using the eIPM to determine bunch intensity.

Other systematic errors can be encountered when using an eIPM. The main problem is the calibration of the bunch itself. Since the AGS calibration is calculated from an input test beam, that places an initial limit on the accuracy of such a model. More important is the eIPM model itself. There is also a chance to undercount at high intensity when many events are happening at once[?]. Higher order intensity corrections may be needed to correct for this if a bunch shape changes significantly. This may lead to observed intensity changes from eIPMs that are not physical.

5.2.5   eIPMs at the Relativistic Heavy Ion Collider

Although this experiment was only concerned with the AGS, it is worth performing a study at the Relativistic Heavy Ion Collider (RHIC). Since the dead bins have been identified as the source of error we can perform a similar search of historical data from RHIC.

As can be seen in Fig. **??**, RHIC does not exhibit the anomalous dead bins seen in the AGS. This is not surprising as the performance of RHIC eIPMs seem to be more stable than the AGS devices. As with the AGS case, each bin has a varying sensitivity yielding striations for each individual bin.

5.3   Periodic Resonance at AGS Run 22

With continued high intensity operations at the AGS there is interest in studying resonances at strong space charge, primarily 3rd order resonances. The single particle tune during AGS run 22 is $Q_y \sim 8.8$ two of the nearest accessible third order resonances are $3Q_y = 26$ and
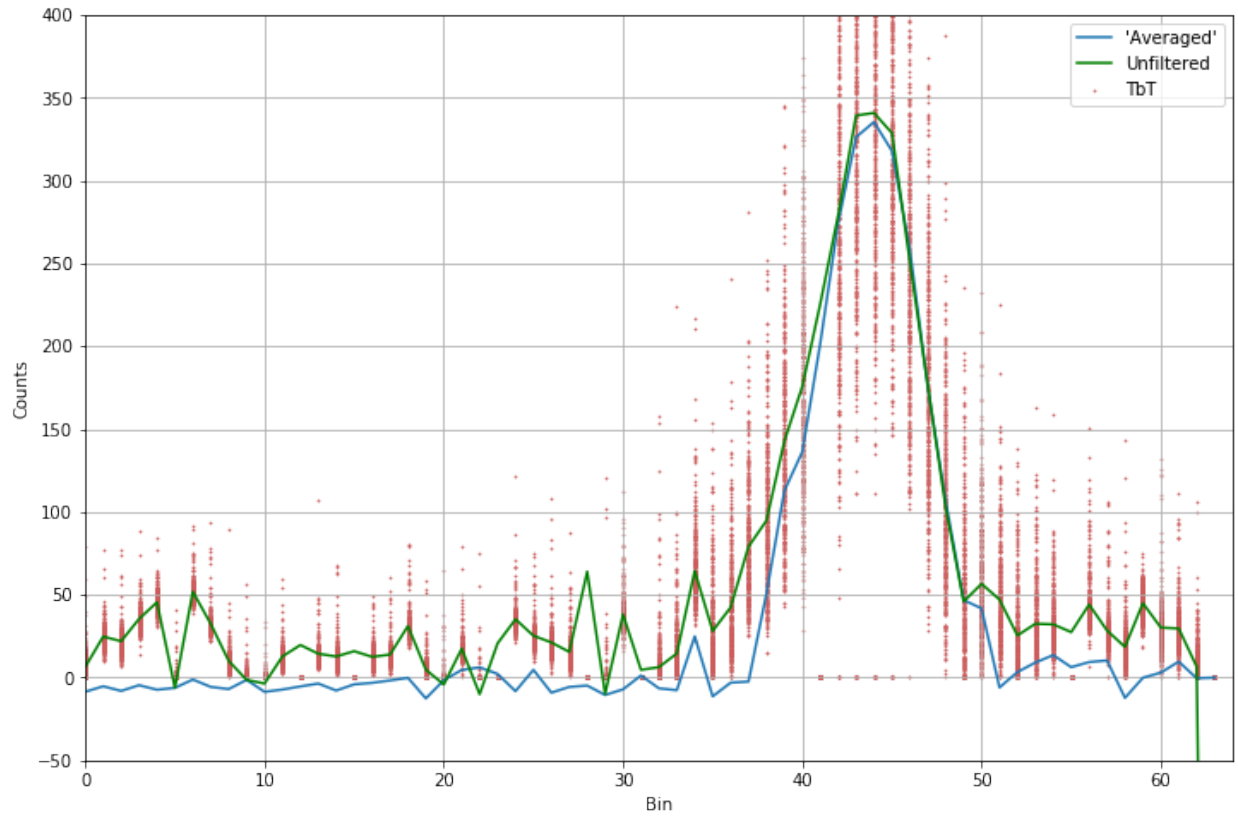
Figure 5.4: eIPM at RHIC, note that less corrections are needed for RHIC bins. There seem to be no missing/dead bins.

$2Q_x + Q_y = 26$. Before the introduction of the partial snakes, these resonances had been studied at low intensity[**?**] and corrected with sextupole families. Current AGS settings have shifted to a tune further away from the third order resonances, but at high intensity they may still be a concern. Therefore, our focus was to drive periodic resonances over a series of initial lattice tunes–beginning directly on resonance and slowly increasing the vertical tune Q_y until effects from the resonance crossing are no longer observed.

The experiment was conducted as follows. First the vertical tune was brought near to the resonance line $Q_y = 26/3$. This vertical resonance was chosen as the vertical eIPMs at the AGS are less noisy than their horizontal counterparts. This can be done in the current AGS configuration, but this tune will not preserve polarization of the bunch. Since polarization is not important in this experiment, its loss will not be missed. Three main devices were employed to study resonant effects. First, the eIPM which was discussed in detail in section 5.2. This provided bunch size and emittance measurements along with intensity calculations at 1 ms increments starting at 144 ms (the injection). Secondly there was the Wall Current Transformer, which gives the total intensity of the bunch over a longer time scale than the eIPM is capable of. Finally, there was the Wall Current Monitor, which gives the intensity of the bunch in z over a very short time scale. This makes it possible to resolve changes in the longitudinal bunch projection as particles are lost, and observe 'bunch shortening'.

5.3.1 Resonance Driving Term Adjustments

At the nominal settings for the AGS, the loss due to the periodic resonance was not easily resolved. With enough time, even a small resonance could lead to loss, however the acceleration cycle of the AGS made long time studies of such weaker resonances impossible. Instead it was decided to strengthen the 3rd order nonlinear driving term to make the resonance

detectable. This was originally performed with two sextupoles that were spaced such that they have an additive contribution to the driving term, but no effect on the chromaticity. However, the currents necessary to produce such an effect on the beam were not achievable in the AGS. Instead, it was decided to use the sextupole corrector family originally designed to dampen this resonance. By purposefully adjusting this sextupole family, it was possible to strengthen the driving term and make the resonances correspondingly stronger.

With the adjusted driving term significant resonant particle loss was observed, indicating that the resonance was able to interact strongly with the input beam and cause loss and emittance growth.

5.3.2 Experimental Observations

With the Enhanced resonance strength, emittance growth and particle loss can be observed at injection before quickly saturating on the order of a few milliseconds. As the bunch crosses the resonance (Fig. **??** left to right) we note that initially the emittance grows, then these excited particles are lost to the walls of the beam pipe and are registered on the Wall Current Transformer. This implies that emittance of resonant particles will grow until they either saturate the instability, or are lost. Once particles are lost, the emittance decreases as the driving resonant force is proportional to $J^{3/2}$. Therefore, once edge particles are lost, the emittance decreases and only central particles survive.

It is worth discussing the particle loss in more detail. The eIPM counts observe a local particle loss minima before the main resonance. This is not theoretically expected as emmittance growth should precede particle loss (and dampen the emittance growth peak) since particles must grow transversely to be lost by this mechanism. Since no other loss mechanism or resonance can be identified for this minima and further because the WCT in
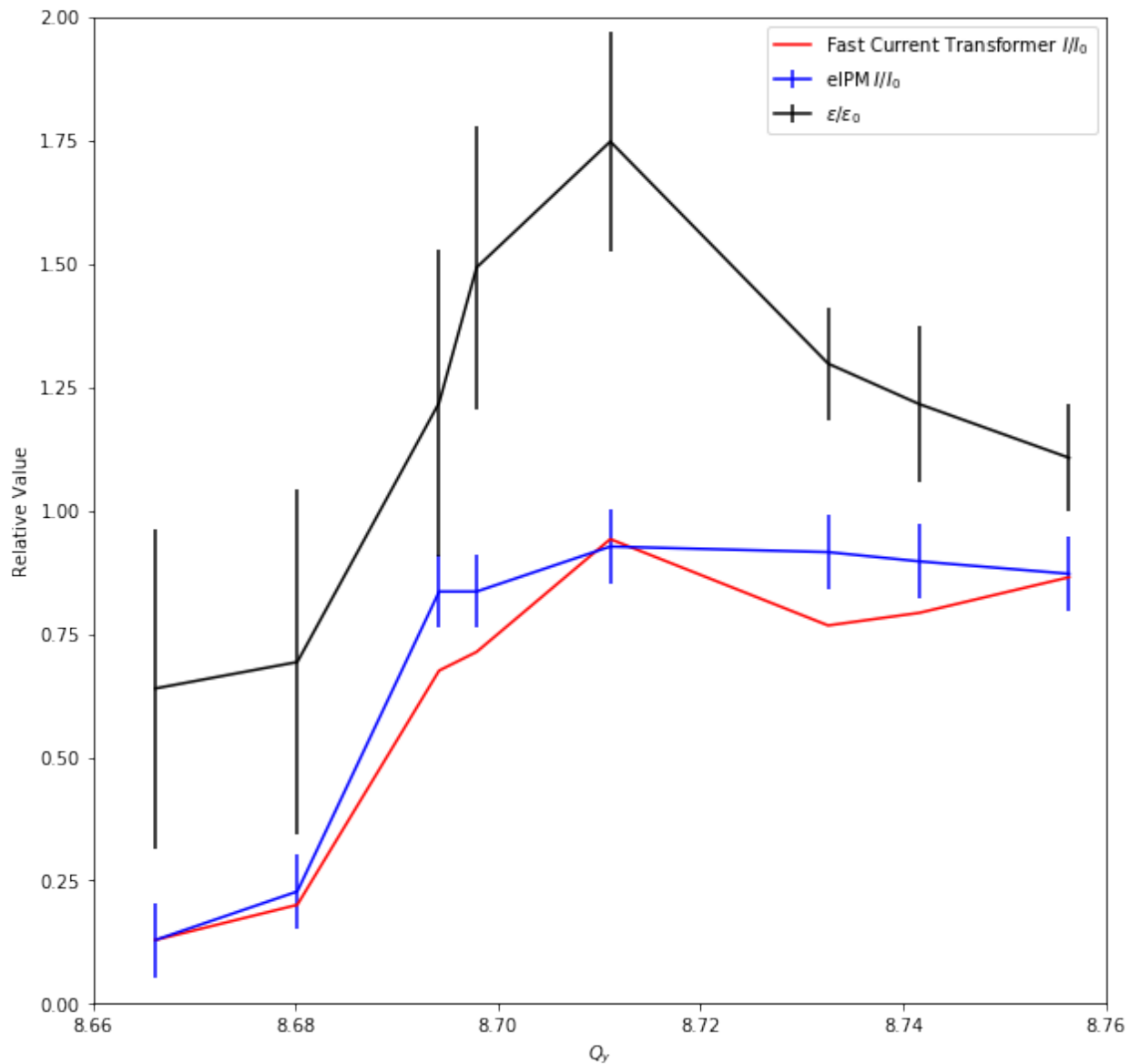
Figure 5.5: Periodic Resonance at injection. Emittance growth and bunch survival consistant with work from Franchetti, et al. cite franchettiPS cite franchettiGSI. Note the slight deviation in survival rates between the two methods, specifically the local minimum observed in the eIPM at $Q_y = 8.73$. This disagreement seems to be due to a systemic error in the eIPM survival rate.

Fig. **??** does not reproduce this behavior, we must conclude that this is erroneous. This is not unexpected as correlations between bin signals could create significant error for beams growing transversely.

Finally the Wall Current Monitor should also be mentioned. The original longitudinal projection does not change shape significantly for any of the resonance crossings tested.

The lack of bunch shortening makes it difficult to classify this periodic resonance as either adiabatic rregime trapping or the non-adiabatic regime scattering. Bunch shortening is normally a sign that the machine is in the adiabatic regime, but it is possible that noise in the RF could have flattened the bunch profile of the non-adiabatic scattering regime. Future experiments are likely needed to conclusively prove one or the other conjecture.

APPENDIX

Transverse Moments

Normalization Moment, $\dot{\psi}$

$$\dot{\psi} = \frac{d}{dt}\psi(t, y, p_y, z, \dot{z}) \tag{4}$$

ψ along with the other moments does not depend on x or p_x (as those terms were integrated away). Therefore,

$$\dot{\psi} = \psi(t, y, p_y, z, \dot{z}) \int dx \int dp_x \frac{df}{dt} = \int dx \int dp_x [\frac{\partial f}{\partial t} + \sum_{i \neq x}(\dot{q}_i \frac{\partial f}{\partial q_i} + \dot{p}_i \frac{\partial f}{\partial p_i})] \tag{5}$$

Which is zero by eq. 2.7. Thus the x projection of the distribution function ψ, does not vary in time.

$$\dot{\psi} = 0 \tag{6}$$

Position Moment, $\dot{X}$

$$\frac{dX}{dt} = \frac{\partial X}{\partial t} + \sum_{i=1}^{3} (\dot{q}_i \frac{\partial X}{\partial q_i} + \dot{p}_i \frac{\partial X}{\partial p_i}) \tag{7}$$

$$\frac{\partial X}{\partial t} = \frac{1}{\psi} \frac{\partial}{\partial t} \int dx x \int dp_x f = \frac{1}{\psi} \int dx x \int dp_x \frac{\partial f}{\partial t} \tag{8}$$

The explicit time dependence can be substituted into the Vlasov equation. This makes the convective derivative d/dt [?] a sum of terms of the form $\dot{u}\frac{\partial f}{\partial u} \int dx x \int dp_x - \int dx x \int dp_x \dot{u}\frac{\partial f}{\partial u}$.

$$\begin{aligned}
\dot{X} = -\frac{1}{\psi}[&\int dx x \int dp_x p_x \frac{\partial f}{\partial x} - \int dx x \int dp_x F_x \frac{\partial f}{\partial p_x} + \int dx x \int dp_x p_y \frac{\partial f}{\partial y} \\
&- \int dx x \int dp_x F_y \frac{\partial f}{\partial p_y} + \int dx x \int dp_x p_z \frac{\partial f}{\partial z} - \int dx x \int dp_x \frac{dU}{dz} \frac{\partial f}{\partial p_z}] \\
&+ p_x \frac{\partial X}{\partial x} - F_x \frac{\partial X}{\partial p_x} + p_y \frac{\partial X}{\partial y} - F_y \frac{\partial X}{\partial p_y} + p_z \frac{\partial X}{\partial z} - \frac{dU}{dz} \frac{\partial X}{\partial p_z}
\end{aligned} \tag{9}$$

Each individual integral can be evaluated on their own for clarity.

$$T_1 = -\frac{1}{\psi} \int dx x \int dp_x p_x \frac{\partial f}{\partial x} \quad T_2 = \frac{1}{\psi} \int dx x \int dp_x F_x \frac{\partial f}{\partial p_x}$$

$$T_3 = -\frac{1}{\psi} \int dx x \int dp_x p_y \frac{\partial f}{\partial y} \quad T_4 = \frac{1}{\psi} \int dx x \int dp_x F_y \frac{\partial f}{\partial p_y}$$

$$T_5 = -\frac{1}{\psi} \int dx x \int dp_x p_z \frac{\partial f}{\partial z} \quad T_6 = \frac{1}{\psi} \int dx x \int dp_x \frac{dU}{dz} \frac{\partial f}{\partial p_z}$$

$$T_7 = p_x \frac{\partial X}{\partial x} \qquad\qquad T_8 = -F_x \frac{\partial X}{\partial p_x}$$

$$T_9 = p_y \frac{\partial X}{\partial y} \qquad\qquad T_{10} = -F_y \frac{\partial X}{\partial p_y}$$

$$T_{11} = p_z \frac{\partial X}{\partial z} \qquad\qquad T_{12} = -\frac{dU}{dz} \frac{\partial X}{\partial p_z}$$

This allows us to express the integral $\dot{X}$ as a finite sum of integrals.

$$\frac{\partial X}{\partial \theta} = \Sigma_{i=1}^{6} T_i \tag{10}$$

$$\dot{X} = \frac{dX}{d\theta} = \Sigma_{i=1}^{12} T_i \tag{11}$$

We shall now evaluate terms T_1 through T_{12} sequentially in the following sections.

T_1

$$T_1 = -\frac{1}{\psi} \int dx x \int dp_x p_x \frac{\partial f}{\partial x} = -\frac{1}{\psi} \int dp_x p_x (x f|_{x=-\infty}^{\infty} - \int dx f) = 0 + P \tag{12}$$

$$T_1 = P \tag{13}$$

T_2

$$T_2 = \frac{1}{\psi} \int dx x \int dp_x F_x \frac{\partial f}{\partial p_x} = \frac{1}{\psi} \int dx x F_x \int dp_x \frac{\partial f}{\partial p_x} \tag{14}$$
$$= \frac{1}{\psi} \int dx x F_x f|_{p_x=-\infty}^{\infty}$$

Evaluating the limits

$$T_2 = 0 \tag{15}$$

T_3

$$T_3 = -\frac{1}{\psi} \int dx x \int dp_x p_y \frac{\partial f}{\partial y} = -\frac{p_y}{\psi} \frac{\partial}{\partial y} \int dx x \int dp_x f \tag{16}$$

$$T_3 = -\frac{p_y}{\psi}\frac{\partial X}{\partial y} \tag{17}$$

T_4

$$T_4 = \frac{1}{\psi}\int dx x \int dp_x F_y \frac{\partial f}{\partial p_y} = \frac{1}{\psi}\frac{\partial}{\partial p_y}\int dx x F_y \int dp_x f \tag{18}$$

If F_y is a function of x this cannot be further simplified.

$$T_4 = \frac{1}{\psi}\frac{\partial}{\partial p_y}\int dx x F_y \int dp_x f \tag{19}$$

If F_y is not an function of x then the x dynamics are not coupled in to the other transverse direction making further simplification possible.

$$T_4 = \frac{F_y}{\psi}\frac{\partial X}{\partial p_y} \tag{20}$$

T_5

$$T_5 = -\frac{1}{\psi}\int dx x \int dp_x p_z \frac{\partial f}{\partial z} = -\frac{p_z}{\psi}\frac{\partial}{\partial z}\int dx x \int dp_x p_z f \tag{21}$$

$$T_5 = -\frac{p_z}{\psi}\frac{\partial X}{\partial z} \tag{22}$$

133

T_6

$$T_6 = \frac{1}{\psi} \int dx x \int dp_x \frac{dU}{dz} \frac{\partial f}{\partial p_z} = \frac{1}{\psi} \frac{dU}{dz} \frac{\partial}{\partial p_z} \int x f dx dp_x \tag{23}$$

$$T_6 = \frac{1}{\psi} \frac{dU}{dz} \frac{\partial X}{\partial p_z} \tag{24}$$

T_7

$$T_7 = p_x \frac{\partial X}{\partial x} = \frac{p_x}{\psi} \frac{\partial}{\partial x} \int x f dx dp_x \tag{25}$$

We then apply the power rule.

$$\begin{aligned} T_7 &= \frac{p_x}{\psi} [\int dx dp_x f + \int x \frac{\partial f}{\partial x} dx dp_x] \\ &= \frac{p_x}{\psi} [\psi + \int dp_x x f|_{x=-\infty}^{\infty} - \int dp_x \frac{\partial f}{\partial x}] \\ &= \frac{p_x}{\psi} [\psi - \psi + \int dp_x (x f_{x=-\infty}^{\infty})] \end{aligned} \tag{26}$$

$$T_7 = 0 \tag{27}$$

T_8

$$\begin{aligned} T_8 &= -\frac{F_x}{\psi} \frac{\partial X}{\partial p_x} = -\frac{F_x}{\psi} \int dx x \int dp_x \frac{\partial f}{\partial p_x} \\ &= -\frac{F_x}{\psi} \int dx x f_{p_x=-\infty}^{\infty} \end{aligned} \tag{28}$$

134

$$T_8 = 0 \tag{29}$$

T_9 through T_{12}

$$T_9 = p_y \frac{\partial X}{\partial y} \tag{30}$$

There is no need to simplify any further as it cancels with T_3.

$$T_{10} = -F_y \frac{\partial X}{\partial p_y} \tag{31}$$

There is no need to simplify any further as it cancels with T_4.

$$T_{11} = p_z \frac{\partial X}{\partial z} \tag{32}$$

There is no need to simplify any further as it cancels with T_5.

$$T_{12} = -\frac{dU}{dz} \frac{\partial X}{\partial p_z} \tag{33}$$

There is no need to simplify these terms any further. The total time derivative of the spatial moment is therefore:

$$\dot{X} = \sum_{i=1}^{12} T_i = P - F_y \frac{\partial X}{\partial p_y} + \int dx\, x F_y \int dp_x\, f \tag{34}$$

And if F_y is not a function of x,

$$\dot{X} = \sum_{i=1}^{12} T_i = P \tag{35}$$

Momentum Moment, $\dot{P}$

$$\frac{dP}{dt} = \frac{\partial P}{\partial t} + \sum_{i=1}^{3}(\dot{q}_i\frac{\partial P}{\partial q_i} + \dot{p}_i\frac{\partial P}{\partial p_i}) \tag{36}$$

$$\frac{\partial P}{\partial t} = \frac{1}{\psi}\frac{\partial}{\partial t}\int dx\, x \int dp_x f = \frac{1}{\psi}\int dx\, x \int dp_x \frac{\partial f}{\partial t} \tag{37}$$

The explicit time dependence can be substituted int the Vlasov equation. This makes the convective derivative d/dt [?] a sum of terms of the form $\dot{u}\frac{\partial f}{\partial u}\int dx\, x \int dp_x - \int dx\, x \int dp_x \dot{u}\frac{\partial f}{\partial u}$.

$$\begin{aligned}
\dot{P} = -\frac{1}{\psi}[&\int dx \int dp_x p_x^2\frac{\partial f}{\partial x} - \int dx \int dp_x p_x F_x\frac{\partial f}{\partial p_x} + \int dx \int dp_x p_x p_y\frac{\partial f}{\partial y} \\
&- \int dx \int dp_x p_x F_y\frac{\partial f}{\partial p_y} + \int dx \int dp_x p_x p_z\frac{\partial f}{\partial z} - \int dx \int dp_x p_x\frac{dU}{dz}\frac{\partial f}{\partial p_z}] \\
&+ p_x\frac{\partial P}{\partial x} - F_x\frac{\partial P}{\partial p_x} + p_y\frac{\partial P}{\partial y} - F_y\frac{\partial P}{\partial p_y} + p_z\frac{\partial P}{\partial z} - \frac{dU}{dz}\frac{\partial P}{\partial p_z}
\end{aligned} \tag{38}$$

Once again we will evaluate each individual integral.

$$T_{13} = -\frac{1}{\psi} \int dx \int dp_x p_x^2 \frac{\partial f}{\partial x} \qquad T_{14} = \frac{1}{\psi} \int dx \int dp_x p_x F_x \frac{\partial f}{\partial p_x}$$

$$T_{15} = -\frac{1}{\psi} \int dx \int dp_x p_x p_y \frac{\partial f}{\partial y} \qquad T_{16} = \frac{1}{\psi} \int dx x \int dp_x p_x F_y \frac{\partial f}{\partial p_y}$$

$$T_{17} = -\frac{1}{\psi} \int dx \int dp_x p_x p_z \frac{\partial f}{\partial z} \qquad T_{18} = \frac{1}{\psi} \int dx \int dp_x p_x \frac{dU}{dz} \frac{\partial f}{\partial p_z}$$

$$T_{19} = p_x \frac{\partial P}{\partial x} \qquad\qquad T_{20} = -F_x \frac{\partial P}{\partial p_x}$$

$$T_{21} = p_y \frac{\partial P}{\partial y} \qquad\qquad T_{22} = -F_y \frac{\partial P}{\partial p_y}$$

$$T_{23} = p_z \frac{\partial P}{\partial z} \qquad\qquad T_{24} = -\frac{dU}{dz} \frac{\partial P}{\partial p_z}$$

This allows us to express the integral $\dot{P}$ as a finite sum of integrals.

$$\frac{\partial P}{\partial \theta} = \Sigma_{i=13}^{18} T_i \qquad (39)$$

$$\dot{P} = \frac{dP}{d\theta} = \Sigma_{i=13}^{24} T_i \qquad (40)$$

T_{13}

$$T_{13} = -\frac{1}{\psi} \int dx \int dp_x p_x^2 \frac{\partial f}{\partial x} = -\frac{1}{\psi} \int dp_x p_x^2 f|_{x=-\infty}^{\infty} = 0 \qquad (41)$$

$$T_{13} = 0 \qquad (42)$$

T_{14}

$$T_{14} = \frac{1}{\psi} \int dx \int dp_x F_x \frac{\partial f}{\partial p_x} = \frac{1}{\psi} \int dx F_x \int dp_x p_x \frac{\partial f}{\partial p_x} \qquad (43)$$

$$= \frac{1}{\psi} \int dx F_x (p_x f|_{p_x=-\infty}^{\infty} - \int dp_x f) = -\frac{1}{\psi} \int dx F_x \int dp_x f$$

Evaluating this integral becomes exceedingly messy for incoherent space charge and other nonlinear fields. It is possible to Taylor expand the higher orders, but this leads to the additional difficulty where higher order terms must also be solved in order to get a self consistent solution. We define the Taylor expansion of the transverse force around the origin as $g_n \equiv \frac{1}{n!} \frac{d^n F_x}{dx^n} x^n |_0$.

$$T_{14} = -g_0 - g_1 X - \frac{1}{\psi} \int (F_x - g_0 - g_1 x) dx \int f dp_x \tag{44}$$

If higher order terms are sufficiently weak, the higher order terms can reasonably be neglected.

T_{15}

$$T_{15} = -\frac{1}{\psi} \int dx \int dp_x dp_x p_y \frac{\partial f}{\partial y} = -\frac{p_y}{\psi} \frac{\partial}{\partial y} \int dx \int dp_x p_x f \tag{45}$$

$$T_{15} = -p_y \frac{\partial P}{\partial y} \tag{46}$$

T_{16}

$$T_{16} = \frac{1}{\psi} \int dx x \int dp_x F_y \frac{\partial f}{\partial p_y} = \frac{1}{\psi} \frac{\partial}{\partial p_y} \int dx x F_y \int dp_x f \tag{47}$$

If F_y is a function of x this cannot be further simplified without going to a higher order.

$$T_{16} = \frac{1}{\psi}\frac{\partial}{\partial p_y}\int dx\, F_y \int dp_x p_x f \tag{48}$$

If F_y is not an function of x then the x dynamics are not coupled in to the other transverse direction making further simplification possible.

$$T_{16} = F_y \frac{\partial X}{\partial p_y} \tag{49}$$

T_{17}

$$T_{17} = -\frac{1}{\psi}\int dx \int dp_x p_x p_z \frac{\partial f}{\partial z} = -\frac{p_z}{\psi}\frac{\partial}{\partial z}\int dx \int dp_x p_x p_z f \tag{50}$$

$$T_{17} = -p_z \frac{\partial P}{\partial z} \tag{51}$$

T_{18}

$$T_{18} = \frac{1}{\psi}\int dx \int dp_x p_x \frac{dU}{dz}\frac{\partial f}{\partial p_z} = \frac{1}{\psi}\frac{dU}{dz}\frac{\partial}{\partial p_z}\int p_x f dx dp_x \tag{52}$$

$$T_{18} = \frac{dU}{dz}\frac{\partial P}{\partial p_z} \tag{53}$$

T_{19}

$$T_{19} = p_x \frac{\partial P}{\partial x} = \frac{p_x}{\psi} \int dx x \int dp_x \frac{\partial f}{\partial p_x} \tag{54}$$
$$= \frac{p_x}{\psi} \int dx x f^\infty_{p_x = -\infty}$$

$$T_{19} = 0 \tag{55}$$

T_{20}

$$T_{20} = -F_x \frac{\partial P}{\partial p_x} = -F_x \frac{\partial}{\partial p_x} \int p_x f dx dp_x \tag{56}$$

We then apply the power rule.

$$T_{20} = -\frac{F_x}{\psi} [\int dx dp_x f + \int dx dp_x p_x \frac{\partial f}{\partial p_x}]$$
$$= -\frac{F_x}{\psi} [\psi + \int dp_x p_x f|^\infty_{x=-\infty} - \int dp_x \frac{\partial f}{\partial p_x}] \tag{57}$$
$$= -\frac{F_x}{\psi} [\psi - \psi + \int dp_x (p_x f^\infty_{p+x=-\infty})]$$

$$T_{20} = 0 \tag{58}$$

T_{21} through T_{24}

$$T_{21} = p_y \frac{\partial P}{\partial y} \tag{59}$$

140

$$T_{22} = -F_y \frac{\partial P}{\partial p_y} \tag{60}$$

$$T_{23} = p_z \frac{\partial P}{\partial z} \tag{61}$$

$$T_{24} = -\frac{dU}{dz}\frac{\partial P}{\partial p_z} \tag{62}$$

There is no need to simplify any further as they are already in a usable form and mostly cancel. Summing the terms together we obtain the complete solution for $\dot{P}$.

$$
\dot{P} = \sum_{i=13}^{24} T_i = -g_0 - g_1 X - \frac{1}{\psi} \int (F_x - g_0 - g_1 x) dx \int f dp_x \tag{63}
$$
$$
+ \frac{1}{\psi}\frac{\partial}{\partial p_y} \int dx F_y \int dp_x p_x f - F_y \frac{\partial P}{\partial p_y}
$$

And if F_y is not a function of x, and the system is linear it is possible to simplify further. For external electromagnetic fields, a nonlinear system implies that F_y is a function of x, [?] but this is ultimately unimportant.

$$
\dot{P} = \sum_{i=13}^{24} T_i = -g_0 - g_1 X \tag{64}
$$

Thus for linear forces without coupling, it is possible to express the collective motion of the beam bunch as a set of coupled partial differential equations. This is not true for nonlinearities and coupling, but that is beyond the scope of this section. A discussion of the implications of nonlinearity and coupling will be presented in section ??.